Wegener Center for Climate and Global Change
University of Graz

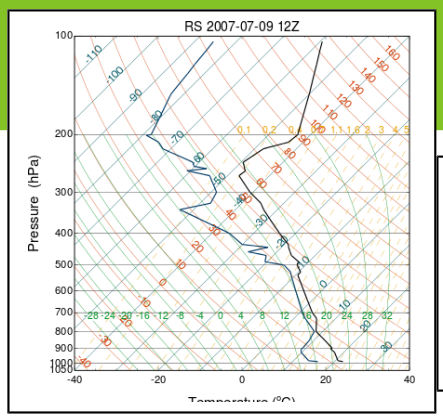

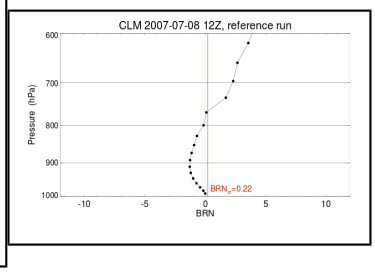

Scientific Report No. 52-2013

Turbulence Parameterization and its Effects on the Simulation of the Vertical Planetary Boundary Layer Structure in Regional Climate Models

Stefanie Peßenteiner

July 2013

Wegener Center

UNI GRAZ

The **Wegener Center for Climate and Global Change** combines as an interdisciplinary, internationally oriented research institute the competences of the University of Graz in the research area „Climate, Environmental and Global Change“. It brings together, in a dedicated building close to the University central campus, research teams and scientists from fields such as geo- and climate physics, meteorology, economics, geography, and regional sciences. At the same time close links exist and are further developed with many cooperation partners, both nationally and internationally. The research interests extend from monitoring, analysis, modeling and prediction of climate and environmental change via climate impact research to the analysis of the human dimensions of these changes, i.e., the role of humans in causing and being effected by climate and environmental change as well as in adaptation and mitigation. (more information at www.wegcenter.at)

The present report is the result of a Master thesis work completed in May 2013.

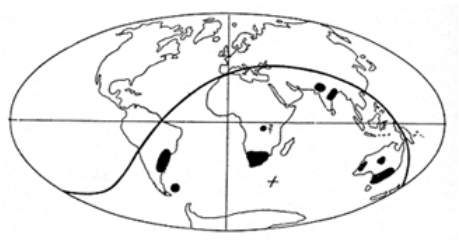

Alfred Wegener (1880-1930), after whom the Wegener Center is named, was founding holder of the University of Graz Geophysics Chair (1924-1930) and was in his work in the fields of geophysics, meteorology, and climatology a brilliant, interdisciplinary thinking and acting scientist and scholar, far ahead of his time with this style. The way of his ground-breaking research on continental drift is a shining role model — his sketch on the relationship of the continents based on traces of an ice age about 300 million years ago (left) as basis for the Wegener Center Logo is thus a continuous encouragement to explore equally innovative scientific ways: *paths emerge in that we walk them* (Motto of the Wegener Center).

Wegener Center Verlag • Graz, Austria

© 2005 All Rights Reserved.
Selected use of individual figures, tables or parts of text is permitted for non-commercial purposes, provided this report is correctly and clearly cited as the source. Publisher contact for any interests beyond such use: wegcenter@uni-graz.at.

ISBN 978-3-9503112-9-7

July 2013

Contact: Stefanie Peßenteiner.
stefanie.pessenteiner@edu.uni-graz.at

Wegener Center for Climate and Global Change
University of Graz
Brandhofgasse 5
A-8010 Graz, Austria
www.wegcenter.at

Master Thesis
to obtain the degree Magister Rerum Naturalium at the
Department of Natural Sciences, University of Graz

Turbulence Parameterization and its Effects on the Simulation of the Vertical Planetary Boundary Layer Structure in Regional Climate Models

Stefanie Peßenteiner, Bakk.rer.nat.

April 2013

Supervisor: Ass.-Prof. Mag. Dr. rer. nat. Andreas Gobiet
Co-Supervisor: Mag. Dr. rer. nat. Heimo Truhetz
Wegener Center for Climate and Global Change
University of Graz

Abstract

The planetary boundary layer (PBL) sets the stage to various weather phenomena and its evolution is closely related to severe weather events. Accurate forecasts and climate projections of the PBL are therefore of great interest. As turbulence is the dominant mechanism of the PBL, its representation presents a crucial task in climate modeling. Particularly regarding smaller-scale atmospheric processes, turbulence parameterization is of increasing importance and its accurate implementation raises expectations of improved model performance.

After giving an introduction to the PBL, this thesis approaches the question of "what is turbulence?" on a phenomenological basis. Mathematical treatment of turbulence is discussed and the fundamental equations of climate models, describing the temporal evolution of meteorological variables, are presented. Applying Reynolds averaging to these equations to account for turbulent processes not explicitly resolved leads to unknown variables. The appearance of these unknown quantities is known as turbulence closure problem which needs to be approached by parameterization. This thesis presents several closure techniques and describes turbulence parameterization schemes implemented in the COSMO climate model. To evaluate the performance of these schemes at 3 km horizontal resolution with respect to their ability to represent the vertical structure of the PBL, simulations are compared to radiosounding measurements. Two typical meteorological conditions—a gentle pressure gradient situation in July 2007 and a fog/stratus situation in January 2008—serve as case studies. The results indicate the ability of the model to generally capture the PBL conditions. Whereas the fog layer height is underestimated in the analyzed model setups, improvements from a decreased asymptotic turbulence length in the convective situation, as suggested by other studies, are to some extent confirmed in this work.

Zusammenfassung

Die planetare Grenzschicht (PGS) bildet die Voraussetzung für verschiedenste Wetterphänomene und Unwetterereignisse sind eng an ihre Entwicklung im Tagesgang gekoppelt. Präzise Voraussagen und Klimaprojektionen der PGS sind daher von großer Bedeutung. Die Abbildung von Turbulenz als dominanter Prozess der PGS stellt eine wichtige Aufgabe in der Klimamodellierung dar. Besonders kleinskalige atmosphärische Prozesse betreffend, gewinnt Turbulenzparametrisierung an Bedeutung. Ihre angemessene Implementierung in Modellen verspricht verbesserte Klimasimulationen.

Nach einer Einführung in die PGS nähert sich diese Diplomarbeit der Frage "Was ist Turbulenz?" zunächst phänomenologisch. Möglichkeiten zur mathematischen Beschreibung von Turbulenz werden erläutert und die fundamentalen Gleichungen, welche die zeitliche Entwicklung von meteorologischen Größen in Klimamodellen beschreiben, werden präsentiert. Die Anwendung der Reynoldsmittelung, die dazu dient auch nicht explizit aufgelöste turbulente Prozesse zu berücksichtigen, führt zum Auftreten unbekannter Terme in den Grundgleichungen. Das Auftauchen unbekannter Größen ist als Turbulenzschließungsproblem bekannt und erfordert Parametrisierungsansätze. In dieser Arbeit werden einige solcher Schließungsansätze vorgestellt und die Implementierung der Turbulenzparametrisierung im regionalen Klimamodell COSMO präsentiert. Um die Leistung der verschiedenen Parametrisierungen zu analysieren, werden Modellsimulationen mit Radiosondenmessungen verglichen. Dabei dienen eine gradientschwache Wetterlage im Juli 2007 und eine Nebelsituation im Januar 2008 als Fallbeispiele. Die Ergebnisse zeigen, dass das Modell in der Lage ist, die vorherrschenden Zustände in der PGS zu erfassen. Während die Höhe der Nebelschicht in den analysierten Modellkonfigurationen unterschätzt wird, bestätigt die vorliegende Arbeit nur in gewissem Ausmaß die in anderen Studien erzielte Verbesserung durch Reduzierung der asymptotischen Turbulenzlänge.

Acknowledgments

First of all, I want to thank my supervisors Andreas Gobiet and Heimo Truhetz for giving me the possibility to write my thesis in the research group ReLoClim at the Wegener Center for Climate and Global Change. I am thankful for the financial support of this thesis through the Wegener Center and the possibility of an own work place with the whole office infrastructure.

Thanks to Martin Suklitsch for providing model output used in the case studies of this thesis. I also want to acknowledge the Austrian Weather Service ZAMG for providing their meteorological data. The radiosounding data by courtesy of the University of Wyoming and the weather maps provided by the German Wetterzentrale proved as very useful for my case studies. Thanks also to Michael Pock who provided the LaTeX framework used for this thesis.

I also want to thank my colleagues of the working group and the other special people I met at the Wegener Center. Special thanks goes to Raimund Klingler for his company through all the years of studying and to Therese Rieckh, not only for sharing chocolate and having lunch together but also forging plans for traveling and hiking tours, which enlightened long office-days. I want to thank Florian Ladstädter for his technical support and never-ending enthusiasm in teaching computer related and organizing stuff. Thank you also for proof-reading this thesis and useful comments as well as for the sunny mountain tops outside working life.

Furthermore I want to mention Jörg Ofner and Irene Herzog whom I want to thank for their friendship and positive attitude. Without the financial support of my parents this thesis and my studies would not have been possible. More important to me however is their constant honest encouragement to find my way in life. I really want to thank you for that.

Contents

Abstract iii

Zusammenfassung v

Acknowledgments vii

List of Figures xi

List of Tables xiii

1 Introduction 1
1.1 Planetary Boundary Layer . . . 1

2 Turbulence 5
2.1 What is Turbulence? . . . 5
2.1.1 Phenomenological Approach . . . 5
2.1.2 Origins of Turbulence . . . 7
2.2 Mathematical Treatment of Turbulence . . . 8
2.2.1 Reynolds Decomposition . . . 8
2.3 Variances and Turbulent Fluxes . . . 10
2.3.1 Variance, Covariance and Correlation . . . 10
2.3.2 Fluxes . . . 12
2.3.3 Reynolds Stress . . . 13
2.4 Scales of Turbulent Motion . . . 15
2.4.1 Richardson Cascade . . . 15
2.4.2 Kolmogorov's Local Similarity Theory . . . 16

3 Turbulence in Regional Climate Models 19
3.1 The Climate System . . . 19
3.2 Introduction to Climate Modeling . . . 20
3.3 Basic Set of Atmospheric Equations . . . 22
3.4 Reynolds Averaged Fundamental Equations . . . 26
3.5 Reynolds Averaged Momentum Equation . . . 27
3.6 The Closure Problem . . . 29

3.7 Turbulence Kinetic Energy . . . 32
3.8 Parameterization . . . 33
3.9 Turbulence Closure . . . 34
3.9.1 Local Closures . . . 34
3.9.2 Non-Local Closures . . . 38

4 Turbulence Parameterization in COSMO-CLM 41
4.1 The COSMO-Model . . . 41
4.2 Turbulence Closure in COSMO-CLM . . . 43
4.3 1D TKE-based Turbulence Scheme . . . 43
4.4 3D TKE-based Turbulence Scheme . . . 44
4.5 Additional Remarks on the Turbulence Schemes . . . 46

5 Case Studies 49
5.1 Data . . . 49
5.1.1 COSMO-CLM Data . . . 49
5.1.2 Radiosounding Data . . . 50
5.2 Methods . . . 51
5.2.1 Skew-T Log-P Diagram . . . 51
5.2.2 Stability . . . 53
5.2.3 Convective Available Potential Energy . . . 54
5.2.4 Bulk Richardson Number . . . 54
5.3 Test Cases . . . 56
5.3.1 Test Case 1: July 8, 2007 . . . 56
5.3.2 Test Case 2: July 9, 2007 . . . 63
5.3.3 Test Case 3: January 11, 2008 . . . 66

6 Discussion and Outlook 71

Acronyms 73

Bibliography 75

List of Figures

1.1 Schematic view of the vertical atmospheric structure. 2

2.1 Reynolds Experiment - Transition from laminar to turbulent flow. 6
2.2 Time series of observed wind velocity, temperature and absolute humidity fluctuations. 9
2.3 Reynolds decomposition of a fluctuating variable. 9
2.4 Idealization of the eddy mixing process (left) and time series of w', θ' and $w'\,\theta'$ (right). 13
2.5 Deformation of fluid parcels due to Reynolds stress. 14
2.6 Turbulent jets at low and high Reynolds number. 17

3.1 Schematic view of the components of the climate system, their processes and interactions. 20
3.2 RCM model domain nested in a global domain. 21
3.3 Mixing length theory: Vertical profiles of mean moisture and mean velocity. 36
3.4 Transilient turbulence theory: Non-local mixing across finite layers. 39

5.1 Model domains for the simulations conducted in the NHCM-1 study. 51
5.2 Plain Skew-T diagram. 52
5.3 Synoptic situation on July 8, 2007. 57
5.4 Global radiation, 2m temperature and wind speed at Vienna Hohe Warte from July 7 to July 9, 2007. 58
5.5 Skew-T diagrams of the radiosounding and the corresponding model runs on July 8, 2007 at 00Z. 59
5.6 Skew-T diagrams of the radiosounding and the corresponding model runs on July 8, 2007 at 12Z. 60
5.7 Comparison of radiosounding and CLM wind profiles from July 8, 2007 00Z. 61
5.8 Comparison of radiosounding and CLM wind profiles from July 8, 2007 12Z. 62
5.9 Profile of the Bulk Richardson Number for the radiosounding at 12Z on July 8, 2007. 63
5.10 Comparison of simulated Bulk Richardson Numbers calculated with $\theta_{v2\mathrm{m}}$ and θ_v at the lowest model level for July 8, 2007. 64

5.11 Skew-T diagrams of the radiosounding and the corresponding model runs on July 9, 2007 at 12Z. 65
5.12 Comparison of measured and simulated Bulk Richardson Numbers (calculated with θ_v at the lowest model level) for July 9, 2007 at 12Z. 66
5.13 Comparison of measured precipitation (climate station) and CLM precipitation amounts for July 9, 2007. 67
5.14 Synoptic situation on January 11, 2008. 67
5.15 Fog layer in a zoomed-in skewed temperature profile for January 11, 2008. 68
5.16 Comparison of radiosounding and CLM wind profiles on January 11, 2008 12Z. 69

List of Tables

1.1 Comparison of boundary layer and free atmosphere characteristics. 3

3.1 Prognostic equations for the first statistical moments of the momentum equation and associated unknowns. 35
3.2 Correlation triangles of unknowns for the momentum equation. 35

5.1 Interpretation of the Bulk Richardson Number. 55

1 Introduction

Climate change is a highly topical and political, environmental, and scientific issue. Investigating how our climate transforms, provides the basis for taking positive actions against climate change. Climate modeling plays an important role in improving our understanding of the climate system and predicting its behavior. With increasing capacity of computational resources and the related increased resolution of climate models Planetary Boundary Layer (PBL) parameterization schemes are attracting more and more attention. Turbulence, intrinsically tied to the PBL, is a very complex topic and still far from being completely understood. Improving our knowledge about turbulence is essential for properly representing turbulent processes in climate models. Enhanced representations of turbulence and turbulent mixing bear expectations of improved model performance, better understanding of the processes in the PBL and climate models in general.

1.1 Planetary Boundary Layer

The PBL is that part of the atmosphere where we spend most of our lives. Since it is the coupling link between the Earth's surface and the rest of the atmosphere it plays a key role not only in the exchange of heat and water but also in the dissipation of kinetic energy, the redistribution of pollutants and the modulation of weather. The PBL is the scene where weather phenomena like fog occur and it sets the stage to others like deep convection and tornadoes. According to Stull (1988) the Atmospheric Boundary Layer (ABL), synonym to PBL, is defined as *"that part of the troposphere that is directly influenced by the presence of the Earth's surface, and responds to surface forcings with a timescale of about an hour or less."* The remaining part of the troposphere is loosely referred to as free atmosphere (Figure 1.1). As far as climate modeling and the boundary layer are concerned one could ask whether the PBL has an effect on climate and how it in turn is affected by climate change (cf. Garratt 1992). By controlling the evaporation and redistribution of water into the atmosphere the ABL affects the cloud distribution which then in turn influences the ABL through modified radiative fluxes or cloud-induced circulations. Changes of the land surface lead to altered albedo and evapotranspiration which can influence the structure of the ABL and thus the regional climate. These are only a few examples underlining the fact that the PBL takes an important role in regional climate change. On the other hand one can infer that an increase in temperature affects for example evaporation and thereby the energy balance and the entire PBL. From these

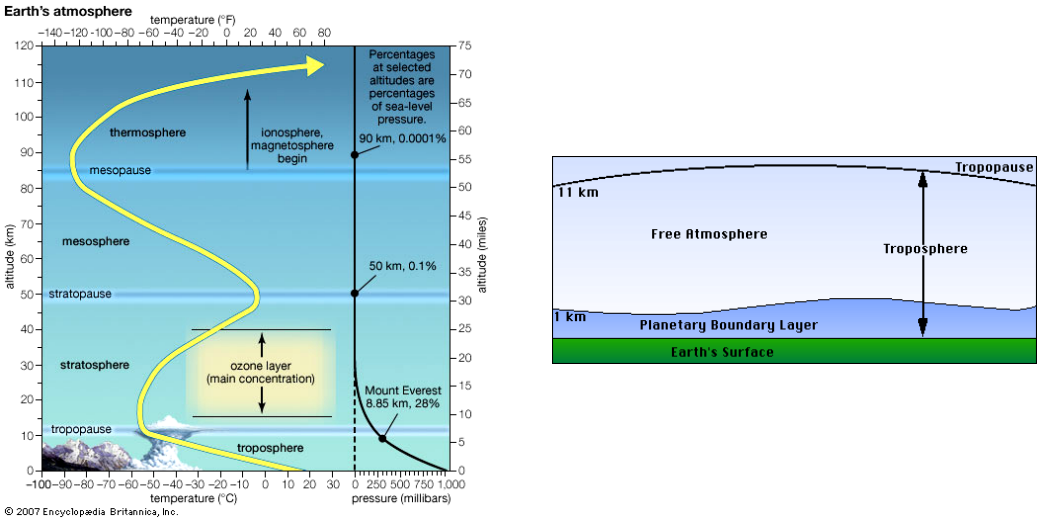

Figure 1.1: Schematic view of the vertical atmospheric structure (Encyclopaedia Britannica 2007) (left) and its lowest layer, the PBL (Lee 1996) (right).

considerations it becomes clear, that a realistic representation of the PBL and its major physical processes is essential in climate modeling.

Figure 1.1 gives a schematic view of the vertical structure of the atmosphere (left) and its lowest layer, the PBL (right). The PBL has a mean depth of 1 km but it is quite variable in time and space (Stull 1988). The PBL-height is dependent on the rate of cooling/heating of the surface, on the topography, on winds, synoptic systems and other factors. In general its evolution follows the net radiation of the sun at the surface, i.e. the diurnal cycle. After sunrise on a clear day, the heating of the land surface leads to an increasing depth of the PBL by thermal mixing. Before radiative cooling causes a suppression of the turbulent mixing process and the shrinking alongside, the boundary layer depth reaches its maximum in the late afternoon. Table 1.1 gives a compact comparison of boundary layer and free atmosphere characteristics. Since turbulence is the dominant feature it is sometimes even used to define the PBL. Usually the top of the PBL is specified as the level where turbulence disappears or becomes insignificant (Arya 2001). A closer look on turbulence as *the* characteristic of the PBL will be given in Chapter 2.

Property	**Boundary Layer**	**Free Atmosphere**
Turbulence	Almost continuously turbulent over whole depth.	Turbulence e.g. in convective clouds.
Friction	Strong drag against Earth's surface. Large energy dissipation.	Small viscous dissipation.
Dispersion	Rapid turbulent mixing in the vertical and horizontal.	Small molecular diffusion. Often rapid horizontal transport by mean wind.
Thickness	Variations in time and space (100 m to 2 km). Diurnal oscillations over land.	Less variable. 8 km to 18 km. Slow time variations.

Table 1.1: Comparison of boundary layer and free atmosphere characteristics, adapted from Stull (1988).

2 Turbulence

2.1 What is Turbulence?

When beginning to study turbulence it soon becomes clear that it is an exciting and controversially discussed topic, constituting to be one of the outstanding problems of the physical sciences (Davidson et al. 2011). "Giants of modern physics" are quoted (Hillebrandt and Kupka 2009), like Werner Heisenberg asking god "Why relativity? And why turbulence? I really believe he will have an answer for the first"[1], and Richard Feynman calling it "the most important unsolved problem of classical physics." Although turbulence is all around us—in the disordered behavior of chimney plumes, in wind gusts and in waterfalls, or when we mix milk in our coffee—there is still surprisingly little to predict with relative certainty and the understanding of it is quite limited (cf. Davidson 2004). Some might consider this quite discouraging, others will follow a more enthusiastic road, like a colleague cited by Wyngaard (2010) calling turbulence a beautiful mistress you cannot stay away from, no matter how badly she treats you.

2.1.1 Phenomenological Approach

A thorough definition of turbulence is quite difficult. A turbulent flow exhibits disordered behavior in time and space. Arya (2001) for example introduces turbulence by referring to the chaotic nature of many flows, "which is manifested in the form of irregular, almost random fluctuations in velocity, temperature, and scalar concentrations around their mean values in time and space." This approach will be picked up later in the mathematical treatment of turbulence (Section 2.2). In an attempt to define turbulence, many textbooks choose a route of listing characteristics of turbulent flows (e.g. Tennekes and Lumley 1972). One of these characteristics is the fact that turbulence always occurs at **large Reynolds numbers**. The Reynolds experiment gives a very vivid picture of turbulence and can serve to draw a first important conclusion about turbulence: A turbulent flow is not laminar. At the end of the 19th century Osborne Reynolds studied flows of varying fluids in pipes of different radii in order to investigate the transition from laminar to turbulent flows.

Figure 2.1 shows the flow transition during a Reynolds experiment in which a filament of dye is introduced in a flow of water through a pipe. The flow rate can be adjusted with a valve. At low flow velocities the dye filament forms a straight line through the

[1] Even though this citation is also attributed to Horace Lamb (Weisstein 1996–2007).

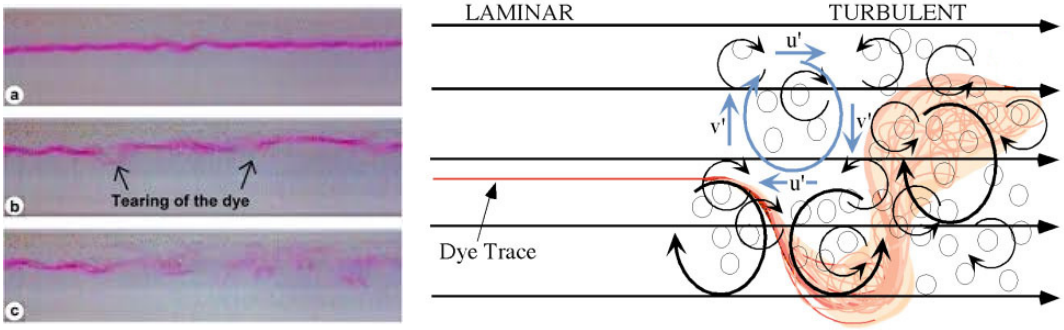

Figure 2.1: Reynolds Experiment - Transition from laminar to turbulent flow (left: Wagner et al. (2002), right: Ware (2002)). On the right picture the superposition of eddies (irregular swirls of motion) of different sizes in the turbulent flow is indicated by curved arrows.

length of the tube. With increasing velocity the filament becomes wavy which indicates the transition of the flow. If the velocity is further increased the dye thread breaks up and diffuses—the flow has become turbulent. The hypothesis of Reynolds experiments was to show that the transition from laminar to turbulent flow depends on the ratio between external forces acting on the fluid and internal (viscous) forces and led to the concept of the Reynolds number (Rotach and Schmidli 2011):

$$\mathrm{Re} =: \frac{\text{inertial forces}}{\text{viscous forces}} = \frac{\rho U^2/L}{\mu U/L^2} = \frac{U\,L}{\nu}. \tag{2.1}$$

In (2.1) a characteristic velocity U and length scale L are introduced, in the example of the pipe flow L is for example the diameter. ν is the kinematic viscosity of the fluid—a property which can be measured. At large Reynolds numbers, the inertial forces are large compared to the viscous forces so that rapid random fluctuations are no longer suppressed. At small Reynolds numbers viscous can overcome inertial forces and the flow stays laminar. At the *critical* Reynolds number (Re_{cr}) the flow becomes turbulent (a value often found in literature is $\mathrm{Re}_{cr} = 2300$). The characteristic length scale is not always as easy to determine as in the case of a flow through a pipe, but usually it is a limiting scale. As far as the Planetary Boundary Layer (PBL) is concerned such a scale ranges from 100 m to a few thousand meters (vertical extent). With $\nu_a = 1.5 \cdot 10^{-5}\mathrm{m}^2/\mathrm{s}$ (Rotach and Schmidli 2011) for air at typical environmental temperatures it can easily be shown that the Reynolds number always exceeds the critical value by far—the PBL is dominated by turbulence. One thing that follows from considerations about the Reynolds experiment is the fact that turbulence is a **property of the flow** and not of the fluid. Even if viscosity—a material property—plays a role in how easily a turbulent state can be obtained, the environmental (boundary) conditions are essential. Without movement (U) turbulence could not exist. Other characteristics of the turbulence phenomenon

are **irregularity** and **diffusivity**, causing mixing of heat and momentum as well as mass transfer. The irregularity makes turbulent motion almost unpredictable even if the flow is determined by deterministic conservation equations—deterministic chaos is predictable but only for a short time. Each realization of the flow is different and very sensitive to the initial conditions. The mixing-property (diffusivity) is essential for the PBL where exchanges of momentum, heat, water vapor and pollutants between the Earth's surface and the atmosphere occur. Molecular diffusion is quite inefficient compared to turbulent diffusion (roughly 10^{-6} times compared to turbulence (Rotach and Schmidli 2011)). The atmosphere receives all the water vapor through turbulent transfer processes at the surface, we owe our air quality to the mixing capability and, by spreading dust and aerosols, it helps providing condensation nuclei which are needed in precipitation or fog formation processes. Turbulence is **rotational** ($\nabla \times \vec{F} \neq 0$) and three-dimensional[2]. It is characterized by **high levels of fluctuating vorticity** ($\vec{\omega} = \nabla \times \vec{F}$) (Tennekes and Lumley 1972). An attractive way to treat turbulent flows is by regarding it as superposition of eddies[3] of different spatial scales. Another essential characteristic of turbulence is its **dissipative** nature. The kinetic energy of turbulence is transformed into heat by viscous shear stresses which perform deformation work. Without continuous energy supply turbulence decays quickly. Small scale turbulence is responsible for the permanent dissipation of kinetic energy in the atmosphere. Even if the PBL comprises less than 2 % of the atmosphere's total kinetic energy, its loss within the PBL accounts for almost one half on an annual basis (Arya 2001). Turbulence is a **continuum** phenomenon, governed by the equations of fluid mechanics (Tennekes and Lumley 1972). In a fully turbulent flow eddies of all spatial scales can be found (even if there might be a preferred eddy size induced by the configuration of the flow). The smallest scales of atmospheric turbulence ($\sim 10^{-3}$ m) are by far larger than the mean free path length ($\sim 10^{-7}$ m) for air (Rotach and Schmidli 2011). The superposition of all scales of eddy motion can be displayed in an energy spectrum with the total kinetic energy represented by the area under the curve. It shows the amount of total turbulence kinetic energy associated with each eddy scale. The energy cascade will be discussed in Section 2.4.

2.1.2 Origins of Turbulence

Turbulence can only persist with a constant input of energy. It is generated mechanically, thermally and inertially. These excitation mechanisms shall be discussed in the following

[2] A discussion about two-dimensional turbulence can be found for example in Davidson (2004). Small scale atmospheric phenomena are clearly three-dimensional.

[3] An eddy is a more or less loose concept of complex three-dimensional structures, mostly connected to irregular swirls of motion; Davidson (2004) for example refers to "a longstanding tradition in turbulence of studiously avoiding any formal definition of what is meant by a turbulent eddy", he further formulates the idea of an eddy as "blob of vorticity". Velocity, length and time scales can be assigned to eddies.

(Wallace and Hobbs 2006):

- **Mechanical:** Wind shear is the most important source of disturbance. Mechanical turbulence is also known as forced convection[4] (predominantly vertical motion resulting in transport/mixing of atmospheric properties). The shear can be caused by frictional drag to the surface, obstacles (wake turbulence swirling behind buildings, trees or even islands) or be simply free shear (away from solid surfaces).
- **Thermal:** If the vertical motion is caused by buoyancy forces one speaks of thermal turbulence or free convection. It is triggered by differential heating of the ground (e.g. due to clouds). Over a sunlit surface energy is transferred from the ground to the air molecules by conduction. As the warm air rises and expands, cooler air from nearby is drawn in and replaces the raising air. These movements result in parcels of buoyant air called thermals.
- **Inertial:** Inertial turbulence is a special form of shear turbulence where small eddies are generated along the edges of larger ones. The inertial energy of the larger eddies is transferred and lost to smaller eddies, resulting in an energy cascade. A further description will be given in Subsection 2.4.1.

2.2 Mathematical Treatment of Turbulence

The non-linear nature of turbulent fluid dynamics makes a deterministic description very difficult. A statistical treatment is inevitable and leads to averaged or expected measures of turbulent motion. If turbulence is understood as "the effect of groups of eddies of different size" (Jacobson 1999), one is interested in the description of the net effect of those. When a field variable like velocity or temperature is measured at a fixed point, it is observed, that the signal fluctuates in time (Figure 2.2). This is caused by eddies of various size passing the sensor.

Due to the irregular variation of the variables in time and space it is common to describe them as sums of a mean and a fluctuating (turbulent) part. As will be discussed in section Section 3.4, mean and turbulent parts can be seen analogous to spatially resolved and unresolved components of a climate model. Since it was first proposed by Reynolds (1894), the decomposition of a variable into a mean and a fluctuating part is called "Reynolds decomposition".

2.2.1 Reynolds Decomposition

The separation of a quantity into an average and a fluctuation part is given by:

$$u(\vec{x},t) = \overline{u}(\vec{x}) + u'(\vec{x},t). \tag{2.2}$$

[4] Forced convection also occurs if topographical barriers or weather fronts force the air to rise.

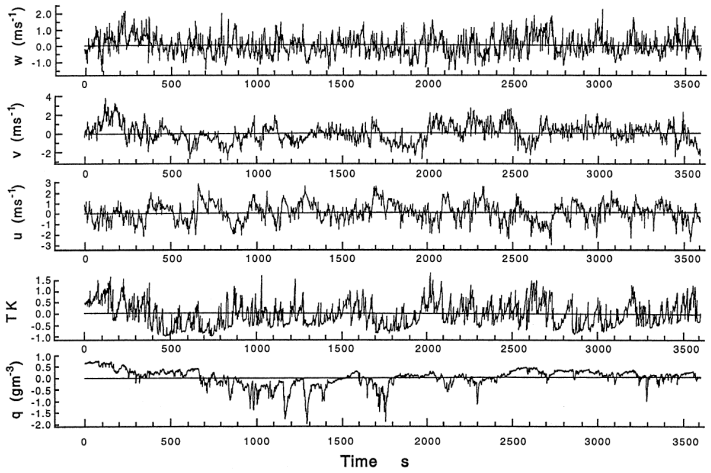

Figure 2.2: Time series of observed wind velocity, temperature and absolute humidity fluctuations in the surface layer (27.4 m above ground) at a suburban site in Vancouver, Canada (Roth 1991).

The left-hand side of (2.2) represents the instantaneous variable whereas the right-hand side gives the sum of mean and fluctuating turbulent part. The turbulent part is defined as the difference between the mean value and the instantaneous value ($u' = u - \overline{u}$). There are several ways of averaging. In the case of (2.2) $\overline{u}$ denotes the time mean ($\overline{u} = \frac{1}{T}\int_0^T u(\vec{x},t)dt$), the arithmetic average of all values during a certain period T. Figure 2.3 shows the temporal behavior of u, $\overline{u}$ and u'.

Other averaging techniques are the spatial and the ensemble average. Spatial averaging makes use of the mean value over a covered space of e.g. SOnic Detection And Ranging (SODAR) observations. In an ensemble average the mean over a large number of identical

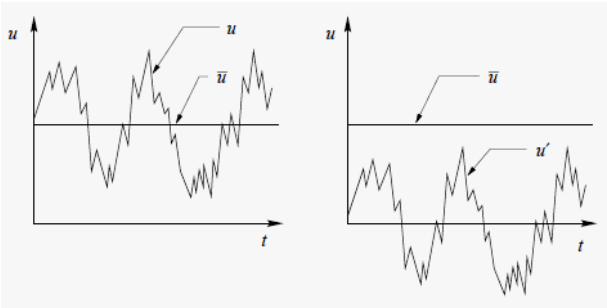

Figure 2.3: A fluctuating variable with its decomposition in a mean and turbulent part (McDonough 2007).

experiments is taken. Under the varying weather conditions in the atmosphere this average can not be used. As will be discussed later (Section 3.4) the ensemble mean will be replaced by averaging over a model time interval and a grid-cell volume. The ergodic hypothesis for homogeneous and stationary turbulence implies that the discussed averages are all the same. It is often used to "make the turbulence problem more tractable" (Stull 1988). From the definition of the time average ($\overline{u} = \frac{1}{T}\int_0^T u(\vec{x},t)dt$) several rules of averaging can be deduced (assuming a and b being time dependent Reynolds decomposed variables and c being constant):

$$\overline{c} = c \tag{2.3}$$

$$\overline{(c\,a)} = c\,\overline{a} \tag{2.4}$$

$$\overline{(\overline{a})} = \overline{a} \tag{2.5}$$

$$\overline{(\overline{a}\,b)} = \overline{a}\,\overline{b} \tag{2.6}$$

$$\overline{(a+b)} = \overline{a} + \overline{b} \tag{2.7}$$

$$\overline{\left(\frac{da}{dt}\right)} = \frac{d\overline{a}}{dt}. \tag{2.8}$$

The derivation of equations (2.3)–(2.8) can be found in Stull (1988). A formal discussion in which cases equations (2.3)–(2.8) hold[5] is given for example in Randall (2009). Further use of these averaging rules will be made in the following chapters.

2.3 Variances and Turbulent Fluxes

Several statistical measures are used to analyze the turbulence structure. Before turbulent fluxes and the eddy flux concept are introduced in a later section, the basic turbulence statistics shall be presented in the following.

2.3.1 Variance, Covariance and Correlation

The biased variance—showing the variation from the average—is given by ($a = \overline{a} + a'$):

$$\sigma_a^2 = \frac{1}{N}\sum_{i=0}^{N-1}(a_i - \overline{a})^2\,. \tag{2.9}$$

With the fluctuating part in Reynolds decomposition given by $a' = a - \overline{a}$ this leads to:

$$\sigma_a^2 = \frac{1}{N}\sum_{i=0}^{N-1} a_i'^2 = \overline{a'^2}, \tag{2.10}$$

[5] These properties are also referred to as "Reynolds conditions".

and the standard deviation:

$$\sigma_a = \sqrt{\left(\overline{a'^2}\right)}. \tag{2.11}$$

One can interpret the ratio of standard deviations of velocity fluctuations to mean wind speed as turbulence intensity I:

$$I \equiv \frac{v'}{\overline{v}} \tag{2.12}$$

with

$$v' = \sqrt{\frac{1}{3}\left(v_x'^2 + v_y'^2 + v_z'^2\right)} \tag{2.13}$$

$$\overline{v} = \sqrt{\overline{v_x}^2 + \overline{v_y}^2 + \overline{v_z}^2}. \tag{2.14}$$

In (2.12)–(2.14) v' denotes the root-mean-square of turbulent velocity fluctuations in the spatial directions x, y and z and $\overline{v}$ the mean velocity.

The covariance between two variables $a = \overline{a} + a'$ and $b = \overline{b} + b'$, providing a measure of the strength of correlation between them, is defined as:

$$\begin{aligned} \mathrm{covar}(a,b) &\equiv \frac{1}{N}\sum_{i=0}^{N-1}(a_i - \overline{a})\cdot(b_i - \overline{b}) \\ &= \frac{1}{N}\sum_{i=0}^{N-1} a_i'\, b_i' = \overline{a'\, b'}. \end{aligned} \tag{2.15}$$

The most important covariances which appear when Reynolds decomposition is applied to the conservation equations (Section 3.4) are those associated with the vertical velocity component w (Rotach and Schmidli 2011) $\overline{w'\theta'}$, $\overline{w'q'}$, and $\overline{u'w'}$. The primed variables denote the fluctuations from specific humidity q, potential temperature θ, and the wind components u, v, w. The covariances are related to heat and momentum fluxes. As an example the conditions on a hot summer day over land can be considered (cf. Stull 1988). Let $T = \overline{T} + T'$ be the temperature and $w = \overline{w} + w'$ the vertical wind component. Air which is warmer than average (positive T', positive w') is expected to rise, cooler than average air (negative T', negative w') is expected to sink. On the average the product $w'\,T'$ will thus be positive, indicating that the temperature and the vertical wind speed vary together. The correlation coefficient r_{ab} gives a measure of how the two variables a and b are correlated:

$$r_{ab} \equiv \frac{\overline{a'\, b'}}{\sigma_a\, \sigma_b}. \tag{2.16}$$

If the two variables vary together (i.e. are perfectly correlated) then $r = 1$. A value of $r = -1$ gives a perfectly negative correlation—the variables vary oppositely. If r yields 0 is no correlation between the variables is implied.

2.3.2 Fluxes

Transport of physical properties can be described as the product of a velocity and the transported quantity. A flux is defined as the transfer of a quantity per unit area per unit time. In the PBL fluxes of mass, heat, moisture and momentum are of great importance. When "divided by the average air density (or in the case of heat flux, divided by the product of air density times specific heat of air at constant pressure)" (Glickman 2012) they are called kinematic fluxes and can be measured directly. Fluxes of mass, moisture, heat and pollutants are vectors, the momentum flux is a second order tensor. Let us consider Reynolds averaging[6] for the mean vertical flux ($\overline{F}$) of a scalar quantity c (this could be for example the specific humidity q):

$$\overline{F} = \overline{w\,c} = \overline{(\overline{w} + w')(\overline{c} + c')} = \overline{w}\,\overline{c} + \overline{w'\,c'}. \tag{2.17}$$

Equation (2.17) states that the mean scalar flux is represented by the sum of a mean transport and a turbulent covariance transport. $\overline{w}$ is close to zero throughout huge parts of the PBL (Stull 1988)—the vertical turbulent flux $\overline{c'\,w'}$ takes the dominant transporting part.

Eddy Flux Concept

The turbulent part of the flux is also referred to as eddy flux. It describes the "rate of transfer of a conservative fluid property through a surface by turbulent eddies" (Glickman 2012). Following Stull (1988) and Rotach and Schmidli (2011) a small idealized eddy near the ground should be examined.

The left side of Figure 2.4 illustrates an idealized eddy mixing process. Imagining an eddy as swirl of motion one can examine the situation on a hot summer day (sitation (a) in Figure 2.4). The lapse rate of the potential temperature $\overline{\theta}$ indicates a statically unstable environment (Subsection 5.2.2). While some air from position 1 ($w' < 0$) is mixed downward, some air from position 2 will mix up ($w' > 0$). In the time average the positive and negative fluctuations balance each other per definition: $\overline{w'} = 0$—turbulence is not causing an average motion. Here it is important to note that this lack of net transport of mass does not automatically imply that turbulence can not cause a net transport of a quantity! In fact in our example (Figure 2.4 (a)) it causes an upward heat flux. As the downward ($w' < 0$) moving air parcel (assuming the potential temperature θ is conserved) ends up being cooler than the ambient environment, θ' is negative leading to a positive instantaneous covariance $w'\,\theta'$. For the upward movement (position 2) in this process the quantities are exactly the other way round ($w', \theta' > 0$), again leading to a positive $w'\,\theta'$. The average kinematic flux $\overline{w'\,\theta'}$ is thus in situation (a) (Figure 2.5) positive, leading to an upward transport of heat. In a stable situation, like during

[6] The averaging technique related to Reynolds decomposition. Rules of averaging are given by equations (2.3)–(2.8).

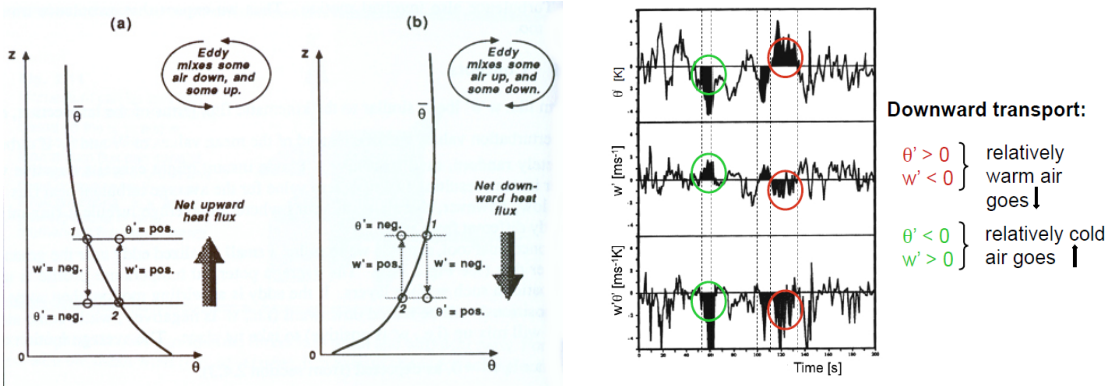

Figure 2.4: Left: Idealization of the eddy mixing process. (a) Net upward turbulent heat flux in a statically unstable environment, (b) net downward turbulent heat flux in a stable environment [Springer and Kluwer Academic Publishers: An Introduction to Boundary Layer Meteorology, by Roland B. Stull, Fig. 2.12, p.52. Copyright 1988. With kind permission from Springer Science+Business Media B.V.]. Right: Time series of w', θ' and the instantaneous $w'\,\theta'$ (Rotach and Schmidli 2011). The red and green circles resemble the small downward arrows from position 1 in (a) and (b).

night, the net effect of the small eddy (sitation (b) in Figure 2.4) is a downward heat transport. Turbulence in the atmosphere usually consists of many different eddies and thus different values of instantaneous fluxes, so that the net flux $\overline{w'\theta'}$ only becomes apparent after averaging (Stull 1988). As will be of importance and discussed in more detail in (Section 3.9) eddy flux is often treated analogous to molecular diffusion so that the mixing of properties like heat etc. is referred to as eddy diffusion.

2.3.3 Reynolds Stress

Turbulent fluxes of momentum, described by covariances of velocity components like $\overline{u'\,u'}$ or $\overline{u'\,v'}$, shall be discussed separately. In general stress is a surface force which tends to produce deformation in a body. Since turbulent eddies act like stresses, turbulent momentum flux is called Reynolds stress. The momentum fluxes are elements of the Reynolds stress tensor:

$$\hat{R} = \begin{pmatrix} \overline{u'u'} & \overline{u'v'} & \overline{u'w'} \\ \overline{v'u'} & \overline{v'v'} & \overline{v'w'} \\ \overline{w'u'} & \overline{w'v'} & \overline{w'w'} \end{pmatrix}. \tag{2.18}$$

Until now we have treated mean *kinematic* fluxes, multiplication with the density ρ leads to the fluxes. The elements of $\hat{R}$ in (2.18) are then often written in tensor notation:

$$\tau_{ij} = -\rho\,\overline{u_i' u_j'}. \tag{2.19}$$

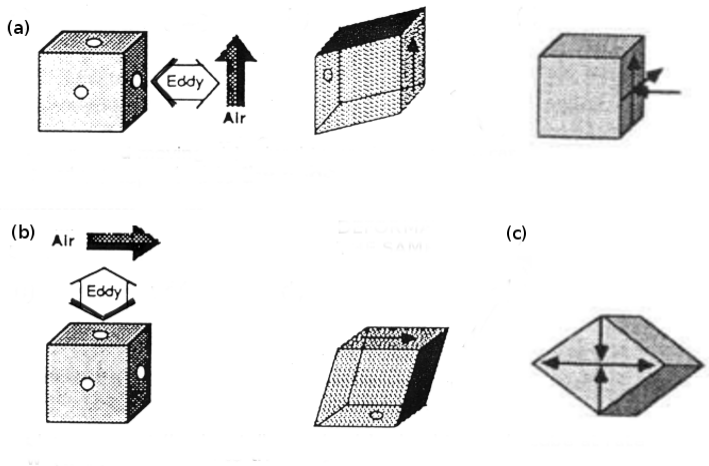

Figure 2.5: Deformation of fluid parcels due to Reynolds stress (turbulent momentum flux). Deformations (middle panel) resulting from $\overline{u'w'}$ (a) are the same as those caused by $\overline{w'u'}$ (b), both resulting in (c). Figure extracted from [Springer and Kluwer Academic Publishers: An Introduction to Boundary Layer Meteorology, by Roland B. Stull, Fig. 2.16, p.64. Copyright 1988. With kind permission from Springer Science+Business Media B.V.].

The indices i and j give the three spatial directions, where j indicates the transported quantity, and i indicates the transporting quantity. Figure 2.5 shows the effect of eddy mixing. The mixing of the j by the i component leads to a velocity difference between the faces of the cube and thus to a deformation. The negative sign in (2.19) ensures that $\tau_{13} = \overline{u'w'}$ is positive (Rotach and Schmidli 2011). As a result of surface friction the profile of mean wind speed obeys $\frac{\partial \overline{u}}{\partial z} > 0$. At the surface the mean wind vanishes.

As can be seen in Figure 2.5 the deforming effect of u' mixing w' into the cube is the same as w' mixing u' (just the relative orientation is different). When neglecting the rotational aspect it follows that $\overline{u'w'} = \overline{w'u'}$ and in consequence that $\hat{R}$ is symmetric. As will be shown in chapter Section 3.6 it is possible to gain predictive equations for $\overline{u'w'}$ by averaging the *momentum equations*. In doing so unknown terms of higher order emerge leading to the *closure problem of turbulence*.

Turbulence Kinetic Energy

Being a measure of turbulence intensity, an important quantity in the study of the PBL is mean Turbulence Kinetic Energy (TKE) which is given per unit mass:

$$\mathrm{TKE} = \frac{1}{2}\left(\overline{u'^2} + \overline{v'^2} + \overline{w'^2}\right). \tag{2.20}$$

Following this definition it can be obtained by taking the trace of the Reynolds tensor $\hat{R}$ (2.18). In a later section (Section 3.7) a budget equation will be written for (2.20) in

which production and loss terms can be balanced. In general TKE follows a diurnal cycle, days with strong surface heating and strong winds are characterized by high values of TKE. As will become clear in the following (Section 2.4) there is continuous dissipation of TKE due to viscosity.

2.4 Scales of Turbulent Motion

Scaling laws and dimensional analyses are practical tools often used in the study of turbulence and the atmosphere in general. As far as atmospheric length and time scales are concerned, turbulence forms the lower end with a typical time scale from seconds to minutes and a typical length scale from millimeters to a few hundred meters. In Subsection 2.1.1 it was already stated that a turbulent flow covers a wide range of length and time scales. With increasing Reynolds number of the mean flow, the range of eddy sizes increases (Arya 2001). Some of those scales are well suited to analyze and describe the flow. They shall in the following be introduced. The upper-bound scale is determined by geometry and dimensions of the flow field, the lower bound by molecular viscosity. The larger (upper-bound) eddy scales were introduced in Subsection 2.1.1 with the definition of the Reynolds number. These scales are the characteristic length L, given by the physical domain, and the characteristic velocity U, the mean velocity of the flow. The large eddies are referred to as "energy-containing eddies"[7]. Typically, an energy transfer from the largest to the smallest eddies takes place on a timescale of about one large-eddy turnover (Glickman 2012). The idea of an energy cascade was proposed by Lewis Richardson first.

2.4.1 Richardson Cascade

In 1922 *Lewis Richardson* suggested that energy is transferred from large to small scales where it is finally dissipated by viscous action (Richardson 1922). This hypothesis is referred to as energy cascade and was originally formulated in a parodic rhyme:

> Big whorls have little whorls
> That feed on their velocity,
> And little whorls have lesser whorls
> And so on to viscosity.

In the energy cascade's picture eddies are continuously forming and breaking up in smaller ones. The largest eddies are produced by mechanisms producing turbulence itself (Subsection 2.1.2), namely mean flow shear and thermal convection. The smaller eddies undergo another break-up process and transfer their energy to even smaller scales. This

[7] From the energy spectra it can be deduced that the larger eddies are in general those containing the greatest share of turbulent energy.

process continues until the eddies become stable at a sufficiently small Reynolds number where molecular viscosity becomes effective and the energy is dissipated (Pope 2000). This picture places dissipation at the end of a row of succeeding processes—it illustrates that the rate of dissipation ε of TKE is related to the first process in the cascade—the energy transfer from the largest eddies. The actual process of energy transfer and quantitative considerations linked to it are quite complex. The transfer mechanisms are thought to be associated with vortex stretching[8]. "But even if the energy cascade and vortex stretching go hand-in-hand", as Mathieu and Scott (2000) state, "a precise relationship between them is far from clear in developed turbulence".

2.4.2 Kolmogorov's Local Similarity Theory

Based on Richardson's ideas Andrej Nikolaevic Kolmogorov developed a famous theory of locally isotropic turbulence. Since he published his papers (Kolmogorov 1941b,a) on that then groundbreaking conceptual framework in 1941 it is often referred to as *K41-theory*. Kolmogorov's approach combined ideas of statistical physics, dimensional analysis and scaling as well as their application to fluid mechanics. In the present thesis the basic concepts of Kolmogorov's turbulence theory should be presented in a very compact form, mainly following the explanations in Pope (2000).

Turbulent flows at the same integral scale (that of the larger eddies) but with different Reynolds numbers show a great difference in the size of the smallest eddies (which become smaller and smaller as the Reynolds number increases, Figure 2.6). One of Kolmogorov's merits was to identify the smallest scales of the energy cascade—the scales which are responsible for the dissipation of energy. He also gave an answer to the question of how characteristic velocity and time scale vary as the eddy size l varies. Kolmogorov's hypothesis of local isotropy states that *at sufficiently high Reynolds numbers small scale turbulent motions ($l \ll l_0$)[9] are statistically isotropic.* He argues that there are many steps in the energy cascade from large, most energetic, eddies to the small scale motions and during the successive break-downs the memory of the large-scale processes (which are affected by the geometric properties of the flow and therefore depending on direction) is continuously lost. In this sense the term *local* refers to the range of the dissipating eddy motions—it means isotropy at small scales. Similarity refers to the postulate that the statistics of the small-scale motions have similar (universal) characteristics in all turbulent flows of large Reynolds numbers. As an incidental remark it should be noted, that the condition of sufficiently high Reynolds numbers are well satisfied in the

[8] Vorticity is the curl of velocity ($\vec{\omega} = \vec{\nabla} \times \vec{U}$). "When a moving portion of fluid also rotates transversally to its motion an increase in speed causes it to rotate faster, a phenomenon called vortex stretching. This causes that portion of fluid to become thinner and elongated, and fold and intertwine with other such portions. This is an intrinsically three-dimensional mechanism which plays a fundamental role in turbulence and is associated with large fluctuations in the vorticity field." (Rosa 2006).

[9] l_0 is the length scale of the largest size eddies. It is comparable to the flow scale L. The characteristic velocity $u_0(l_0)$ is in order of the root mean square turbulence intensity (2.12).

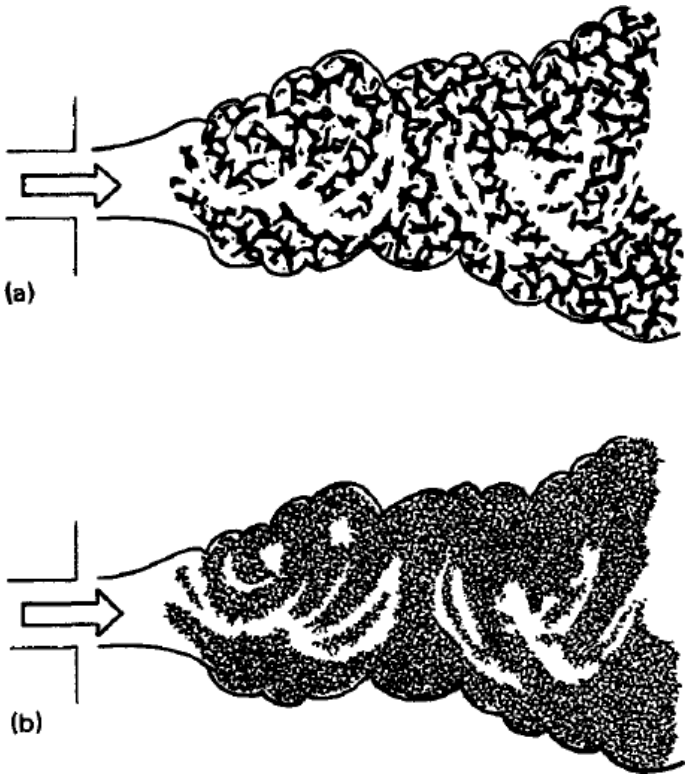

Figure 2.6: Turbulent jets at (a) a relatively low and (b) a relatively high Reynolds number (Tennekes and Lumley 1972).

atmosphere (Arya 2001), so that Kolmogorov's concept is found to be quite useful for our considerations. In order to distinguish between anisotropic large scales and isotropic small scales three length scale areas can be defined as follows:

1. A length scale l_{EI} which is a kind of demarcation scale, is introduced.[10]
2. Anisotropic large eddies are given by $l > l_{EI}$.
3. Isotropic small eddies have a length scale of $l < l_{EI}$.

Now the question arises on which parameters the statistically universal state of local isotropy depends. It was Kolmogorov's outstanding idea that the determining quantity was the rate of energy transfer between the large and small scales of motion which is approximately equal to the second dominant process in the energy cascade - the viscous dissipation[11]. There must exist a range of eddy size for which turbulence structure is in a statistical equilibrium and whose motion is only determined by the parameters ε (energy transfer, or equivalently energy dissipation) and ν (kinematic viscosity). This is the essence of Kolmogorov's first similarity thesis (Pope 2000): *In every turbulent flow at sufficiently high Reynolds number, the statistics of the small scale motions ($l < l_{EI}$) has a universal form that is uniquely determined by ε and ν.* The scale range $l < l_{EI}$ in which the time scales $\frac{l}{u(l)}$ are small compared to $\frac{l_0}{u_0}$ is called universal equilibrium range. Small eddies can adapt quickly in order to maintain a dynamic equilibrium with the transfer rate. Dimensional considerations lead then to unique length, velocity and time scales—*the Kolmogorov scales* formed with the determining parameters ε and ν:

$$\eta \equiv \left(\frac{\nu^3}{\varepsilon}\right)^{\frac{1}{4}} \tag{2.21}$$

$$u_\eta \equiv (\varepsilon\nu)^{\frac{1}{4}} \tag{2.22}$$

$$\tau_\eta \equiv \left(\frac{\nu}{\varepsilon}\right)^{\frac{1}{2}}. \tag{2.23}$$

η is interpreted as the length at which viscous effects gain importance—the Reynolds number becomes 1 as formed with Kolmogorov's scales ($\frac{\eta u_\eta}{\nu} = 1$). This indicates, that the equations above characterize the smallest scales, the scales at which energy is dissipated. Since the energy input determined by the domain size takes place at the other end of the energy spectrum, η and L characterize the energy cascade. At large Reynolds numbers the two scales can differ from each other by some orders of magnitude.

[10] According to Pope (2000) it is approximately given by $l_{EI} \approx \frac{1}{6} l_0$.

[11] One can plausibilize that for large eddies viscous stresses and dissipation are small. Correspondingly their decay time is relatively large. A statistically steady state which is only the case for a balance between energy transfer and energy dissipation can then be assumed.

3 Turbulence in Regional Climate Models

The previous sections gave an introduction to turbulence and its mathematical treatment. Prior to investigating how regional climate models deal with turbulence an introduction to the climate system and climate modeling with its basic equations will be given in the following.

3.1 The Climate System

Earth's climate system is composed of several spheres connected to and interacting with each other. Each of the spheres possesses a specific time scale on which characteristic processes take place. The components of the climate system are atmosphere, hydrosphere (liquid water in oceans, seas, rivers etc.), cryosphere (land ice including glaciers and ice shelves), biosphere (all life on the planet) and lithosphere (the solid earth). Sometimes the influence of humans (through cultural and technological activities) is highlighted by introducing another component, namely the anthroposphere.

Figure 3.1 shows the components of the climate system and some of the important processes in them. The amount of energy entering the Earth-atmosphere system determines its climatic state. All the energy received by the system stems from the shortwave radiation of the sun. In order to keep the system stable, incoming shortwave energy and outgoing longwave energy (infrared radiation, emitted by the Earth's surface), balance each other. Radiative, convective and dynamical processes determine the circulation of the atmosphere. Heat, momentum and water exchange between atmosphere and ocean are depicted in Figure 3.1 as well as human influences which become manifest in altered albedo (for example through changes in land use) or changes in the composition of the atmosphere (through anthropogenic emissions of greenhouse gases). The presence of snow and ice covers modifies transfers of mass and momentum at the Earth's surface and impacts the radiative budget since it lessens absorption. These are just some of the interactions between the various components of the climate system. Climate models which are able to incorporate more and more of the essential processes due to an increase of computational capacities are an important tool to study these interdependencies and gain more knowledge about the physical principles behind them.

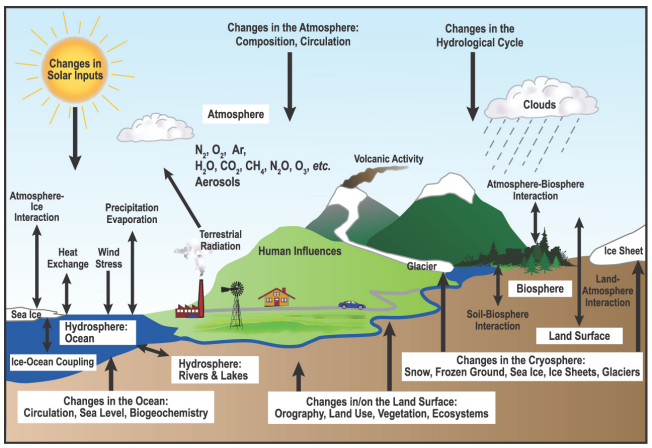

Figure 3.1: Schematic view of the components of the climate system, their processes and interactions taken from Somerville et al. (2007, p. 104).

3.2 Introduction to Climate Modeling

A climate model is a mathematical model of the climate system with the purpose to understand and predict its behavior. The core of a climate model is built up by systems of differential equations which stem from basic laws of physics, chemistry and fluid motion. In order to solve the equations describing atmospheric and oceanic physical and chemical processes one is reliant on super computing systems. For this purpose the Earth is covered with an imaginary three-dimensional grid where the equations are solved on each grid point, see Figure 3.2. The equation in each box of the grid is dependent on the values of adjacent boxes: Horizontal exchange takes place between grid columns, vertical exchange between grid levels. Due to limited computer and time resources the size of the grid is not arbitrary. A larger number of grid cells corresponds to a finer resolution and needs computers of larger capacity to perform the simulations. Whereas General Circulation Models (GCMs)[1], addressing large-scale climate properties as general circulation of atmosphere and ocean, have a typical horizontal resolution of a few hundred kilometers, Regional Climate Models (RCMs) can afford to have a smaller grid size by only covering a certain region of the Earth. At the present time typical RCM grids for climate projections are in the range of 10 km or larger (e.g. Suklitsch et al. (2011)). Due to this finer resolution RCMs can provide climate information on a more regional or even local scale. Regionalization techniques can be divided into two main categories: Statistical and dynamical downscaling (e.g. Rummukainen (2010)). Statistical downscaling tries to gain finer-scale climate information via statistical relationships between large

[1] GCM is also used to abbreviate Global Climate Model. In most of the cases the terms can be used interchangeably.

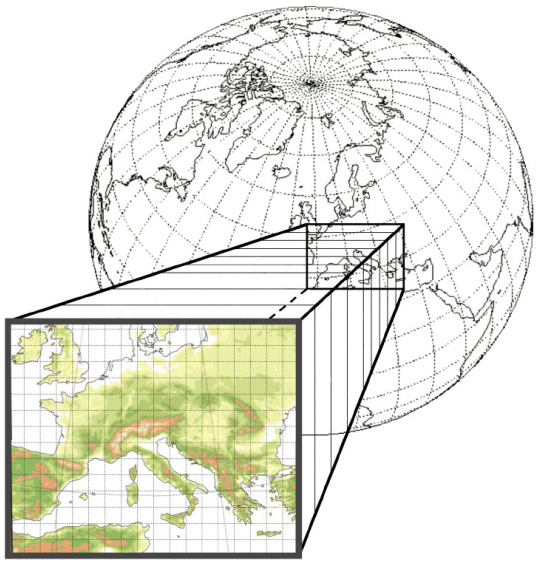

Figure 3.2: RCM-domain nested (embedded) in a global domain to provide the boundary and initial conditions (Rotach and Schmidli 2011).

scale and local climate variables. Dynamical downscaling refers to generating locally relevant data via the same physical-dynamical principles as GCMs. Usually this is done by nesting a RCM in an existing GCM (Figure 3.2). The time-dependent large-scale atmospheric fields of temperature, winds and moisture then serve as lateral boundary conditions (e.g. Giorgi and Mearns 1999). The boundary data can also be provided by re-analyzed observed data like for simulations of the past climate as in the case studies of this thesis (Chapter 5). Hand in hand with spatial discretization time is also divided into discrete slices. The choice of the time step is not arbitrary since one has to consider numerical stability criteria: The finer the resolution the shorter the time step (for RCMs typically 5 minutes or less, for GCMs typically 30 minutes). As a consequence from solving the equations on a grid with a certain size there are two kinds of processes within climate models. Processes with scales larger than the grid scale can be explicitly resolved. Other processes, like clouds, being of sub-grid scale, remain unresolved and have to be parameterized. Thus parameterization means describing sub-scale processes and their impacts through scale parameters (large-scale resolved fields) which are better accessible (e.g. Kraus 2008). Before addressing the question of parameterization and turbulence parameterization in particular, the fundamental equations shall be presented.

3.3 Basic Set of Atmospheric Equations

There are five basic physical principles forming the foundation of climate models (e.g. Stull (1988), Pielke (2002)), namely conservation of mass, heat, motion, water and conservation of other gaseous and aerosol materials. The fundamental equations expressing these laws can be derived by analyzing the budgets of energy, mass and momentum for an infinitesimal box of fluid (control volume). The equation of state of an ideal gas serves as additional law, relating the parameters used in the other equations. By solving the set of equations the primary meteorological variables wind speed and wind direction, air temperature, air density, air pressure and water content (cf. Jacobson 1999) can be simulated. The following equations will be presented in tensor notation for which the Einstein summation convention for repeated indices holds.

Ideal Gas Law—Equation of State

The ideal gas law, describing the equation of state of a hypothetical ideal gas, is given by

$$p = \rho\, R\, T_v. \tag{3.1}$$

It relates pressure p, density of moist air ρ, virtual temperature T_v and the gas constant for dry air R. T_v is the temperature that dry air must have to equal the density of moist air at the same pressure (Stull 1988). It can be approximated by $T_v = (1 + 0.608\, w)\, T$ with the mixing ratio w.

At this point it is also convenient to introduce the potential temperature and the virtual potential temperature which are important meteorological concepts used throughout this thesis. Potential temperature θ is defined as

$$\theta \equiv T \left(\frac{p_0}{p}\right)^{\kappa}, \tag{3.2}$$

with the reference pressure p_0 (often assumed to be $p_0 = 1000\,\mathrm{hPa}$) and the Poisson constant κ given by the ratio of gas constant to specific heat $\kappa = \frac{R}{c_p}$. θ is the temperature an unsaturated parcel of dry air would attain if it was brought adiabatically (without exchange of heat with the environment; changes in internal energy for systems of fixed mass are solely a consequence of work) from a pressure p to a pressure p_0. (3.2) is called *Poisson's equation*. Virtual potential temperature[2] is defined in a similar way

$$\theta_v \equiv T\,(1 + 0.608\, w) \left(\frac{p_0}{p}\right)^{\kappa} = T_v \left(\frac{p_0}{p}\right)^{\kappa}. \tag{3.3}$$

[2] A proper definition would distinguish between virtual potential temperature and potential virtual temperature. Since the difference is small enough, (3.3) can be used for both in many cases. See e.g. Jacobson (1999).

Conservation of Mass—Continuity Equation

It is assumed that there are no sinks or sources for mass in the Earth's atmosphere[3] (Pielke 2002). Since entering (leaving) of mass in (out of) a control volume yields an increase (decrease) of mass within, conservation of mass is also known as continuity equation. With mass expressed as density times volume and factoring the volume out (in the limit of the box volume going to zero), the continuity equation is written as:

$$\frac{\partial \rho}{\partial t} + \frac{\partial (\rho\, u_j)}{\partial x_j} = 0. \tag{3.4}$$

For smaller than mesoscale motions ($< 200\,\mathrm{m}$) (Stull 1988) the incompressibility approximation holds leading to a reduction of (3.4):

$$\frac{\partial u_j}{\partial x_j} = 0. \tag{3.5}$$

Water and sea ice can in general be assumed incompressible.

Conservation of Momentum

Newton's second law expresses conservation of motion. The change of the rate of momentum is proportional to the net force exerted on a body. Since Earth is rotating, Coriolis forces have to be taken into account. Other *external* forces result from pressure gradients and gravity. *Internal* forces are caused by fluid interactions with itself (Pielke 2002). They account for dissipation by molecules. The momentum equation is then given by

$$\underbrace{\frac{\partial u_i}{\partial t}}_{\mathrm{I}} + \underbrace{u_j \frac{\partial u_i}{\partial x_j}}_{\mathrm{II}} = \underbrace{-\delta_{i3} g}_{\mathrm{III}} - \underbrace{2\,\epsilon_{ijk}\,\Omega_j\,u_k}_{\mathrm{IV}} - \underbrace{\frac{1}{\rho}\frac{\partial p}{\partial x_i}}_{\mathrm{V}} + \underbrace{\frac{1}{\rho}\frac{\partial \tau_{ij}}{\partial x_j}}_{\mathrm{VI}}. \tag{3.6}$$

The braced terms represent (Stull 1988):

I storage of momentum (inertia)

II advection

III gravitational force

IV Coriolis effects

V pressure-gradient forces

[3] The effect of gases and aerosols transferred in and out of land and water bodies or thermal escape are neglected.

VI influence of viscous stress

Assuming the air behaves like a Newtonian fluid, and applying the incompressibility approximation, term VI reduces to $\nu \frac{\partial^2 u_i}{\partial x_j^2}$ with the kinematic viscosity ν (Stull 1988). Term IV can be rewritten using the Coriolis parameter $f_c = 2\,\omega \sin\phi$ with a typical mid-latitude value of the order of $1 \times 10^{-4}\,\mathrm{s}^{-1}$. ω denotes the angular velocity of the Earth, ϕ the latitude. The momentum equation is then often written as:

$$\frac{\partial u_i}{\partial t} + u_j \frac{\partial u_i}{\partial x_j} = -\delta_{i3} g + f_c\, \epsilon_{ij3}\, u_j - \frac{1}{\rho}\frac{\partial p}{\partial x_i} + \nu \frac{\partial^2 u_i}{\partial x_j^2}. \tag{3.7}$$

Conservation of Water

If q_T represents the mass of water in all phases per unit mass of moist air, i.e. q_T is the total specific humidity, the conservation equation of water substance can be written as

$$\frac{\partial q_T}{\partial t} + u_j \frac{\partial q_T}{\partial x_j} = \nu_q \frac{\partial^2 q}{\partial x_j^2} + \frac{S_{q_T}}{\rho}. \tag{3.8}$$

Incompressibility was again assumed. ν_q is the molecular diffusivity for water vapor in the air. S_{q_T} stands for a (source minus sink) term for water (body source term affecting whole volume, not just boundaries). In general it includes phase changes and chemical reactions. The latter can be neglected in many applications. Following Stull (1988) total humidity is split into vapor (q) and non-vapor parts (q_L). Together with $S_{q_T} = S_q + S_{q_L}$ (3.8) leads to two coupled equations:

$$\frac{\partial q}{\partial t} + u_j \frac{\partial q}{\partial x_j} = \nu_q \frac{\partial^2 q}{\partial x_j^2} + \frac{S_q}{\rho} + \frac{E}{\rho} \tag{3.9}$$

$$\underbrace{\frac{\partial q_L}{\partial t}}_{\mathrm{I}} + \underbrace{u_j \frac{\partial q_L}{\partial x_j}}_{\mathrm{II}} = \underbrace{}_{\mathrm{VI}} + \underbrace{\frac{S_{q_L}}{\rho}}_{\mathrm{VII}} + \underbrace{\frac{E}{\rho}}_{\mathrm{VIII}}, \tag{3.10}$$

with E representing the mass of water vapor created by a phase change from liquid or solid. Molecular diffusion has been assumed to have a negligible effect on liquid or solid particles (missing term VI in Equation 3.10). Terms I, II and VI can be seen analogous to the terms in (3.6), VII is a net moisture source term (sources minus sinks) and VIII a conversion (solid/liquid to vapor) term.

Conservation of Heat–First Law of Thermodynamics

"The first law of thermodynamics relates the change in temperature of a gas to energy transfer between the gas and its environment and work done by or on the gas." (Jacobson 1999). It serves as starting point for the thermodynamic equation.

$$dQ = dW + dI, \tag{3.11}$$

where dQ denotes a differential heat exchange, dW the differential work and dI a differential increase in internal energy. When air expands, work is done by the air: $dW = p\,dV$. The change in volume can also be expressed via the inverse density α. If additionally the change in internal energy is expressed in the change by temperature multiplied by the energy required for the change, i.e. via the specific heat, (3.11) can be rewritten in terms of virtual temperature:

$$dQ = c_p\,dT_v - \alpha dp. \tag{3.12}$$

c_p is the specific heat at constant pressure and α the specific volume of air (the inverse density). More thorough derivations of (3.12) can be found in Jacobson (1999) or in a slightly different form in Pielke (2002). The heat equation or thermodynamic energy equation can now be obtained by differentiating (3.12) with respect to time:

$$\frac{dT_v}{dt} = \frac{1}{c_p}\frac{dQ}{dt} + \frac{1}{c_p\,\rho}\frac{dp}{dt}. \tag{3.13}$$

By rewriting (3.13) in terms of potential temperature the last term can be eliminated. Stull (1988) presents a form of the heat equation in terms of θ including phase change information E:

$$\underbrace{\frac{\partial\theta}{\partial t}}_{\text{I}} + \underbrace{u_j\frac{\partial\theta}{\partial x_j}}_{\text{II}} = \underbrace{\nu_\theta\frac{\partial^2\theta}{\partial x_j^2}}_{\text{VI}} - \underbrace{\frac{1}{\rho\,c_p}\left(\frac{\partial Q_j^*}{\partial x_j}\right)}_{\text{VII}} - \underbrace{\frac{L_p\,E}{\rho c_p}}_{\text{VIII}}. \tag{3.14}$$

ν_θ is the thermal diffusivity and L_p the latent heat (at 0 °C gas↔liquid: $L_v = 2.501 \times 10^6$ J kg^{-1}, liquid↔solid: $L_f = 3.337 \times 10^5$ J kg^{-1} and gas↔solid: $L_s = 2.834 \times 10^6$ J kg^{-1} (Glickman 2012)) associated with the phase change E. Q_j^* is the net radiation component in j-direction. It is essential not to neglect the moisture contribution to the specific heat in the Planetary Boundary Layer (PBL) (Stull 1988), thus c_p is that for moist air at constant pressure. The roman numbers describe the terms analogous to those in (3.6) and (3.10).

Conservation of a Scalar Quantity

If C is the concentration (mass per volume) of other (than water) gaseous and aerosol materials its conservation can be formulated as:

$$\underbrace{\frac{\partial C}{\partial t}}_{\text{I}} + \underbrace{u_j\frac{\partial C}{\partial x_j}}_{\text{II}} = \underbrace{\nu_C\frac{\partial^2 C}{\partial x_j^2}}_{\text{VI}} + \underbrace{S_c}_{\text{VII}}. \tag{3.15}$$

ν_c denotes the molecular diffusivity of the constituent. S_c again is a body source term describing processes not already in the equation (e.g. chemical reactions). As above the roman numbered terms are analogous to those in (3.6) and (3.10).

Summary of the Fundamental Equations

Putting the above described equation together leads to the set of atmospheric equations which form the basis for most of the numerical weather or climate prediction models. Apart from (3.16) these are prognostic nonlinear differential equations. The term prognostic implies the predictive character of the equations, whereas diagnostic refers to equations without time derivative relating the state of variables at one point in time. Sometimes these equations are referred to as "primitive equations". If there are no simplifications made (for example by neglecting terms due to scaling arguments or approximations) this set has no general analytic solution for atmospheric flows. One relies on numerical solutions on a grid (see Section 3.2) in which the differentials $\left(\frac{\partial A}{\partial x}\right)$ are approximated by differences $\left(\frac{A_{i+1}-A_i}{\Delta x}\right)$.

$$p = \rho R T_v \tag{3.16}$$

$$\frac{\partial \rho}{\partial t} + \frac{\partial(\rho u_j)}{\partial x_j} = 0 \tag{3.17}$$

$$\frac{\partial u_i}{\partial t} + u_j \frac{\partial u_i}{\partial x_j} = -\delta_{i3} g + f_c \epsilon_{ij3} u_j - \frac{1}{\rho}\frac{\partial p}{\partial x_i} + \nu \frac{\partial^2 u_i}{\partial x_j^2} \tag{3.18}$$

$$\frac{\partial q_T}{\partial t} + u_j \frac{\partial q_T}{\partial x_j} = \nu_q \frac{\partial^2 q}{\partial x_j^2} + \frac{S_{q_T}}{\rho} \tag{3.19}$$

$$\frac{\partial \theta}{\partial t} + u_j \frac{\partial \theta}{\partial x_j} = \nu_\theta \frac{\partial^2 \theta}{\partial x_j^2} - \frac{1}{\rho c_p}\left(\frac{\partial Q_j^*}{\partial x_j}\right) - \frac{L_p E}{\rho c_p} \tag{3.20}$$

$$\frac{\partial C}{\partial t} + u_j \frac{\partial C}{\partial x_j} = \nu_C \frac{\partial^2 C}{\partial x_j^2} + S_c. \tag{3.21}$$

3.4 Reynolds Averaged Fundamental Equations

Since turbulent motions continuously cover ranges from a few millimeters up to the thickness of the entire PBL, models would need to employ extremely high resolutions in space and time to resolve them. In practical applications this can not be afforded.[4] One is therefore reliant on Reynolds Averaging (described in Subsection 2.2.1) to use reasonable grid sizes and still account for motions smaller than the size of the grid. By recalling Reynolds Averaging (Subsection 2.2.1) for a variable ψ (any of the variables in (3.16)–(3.21))

$$\psi = \overline{\psi} + \psi', \tag{3.22}$$

[4] In research applications over very limited domains resolving the whole range of spatial/temporal scales is in fact done and called direct numerical simulation (DNS). Another form of turbulence simulation somehow "lying in between" DNS and Reynolds Averaged simulations is Large Eddy Simulation (LES), which partly resolves turbulence by using a spatial filter.

one can interpret the mean part $\overline{\psi}$ in terms of the grid (Pielke 2002):

$$\overline{\psi} = \int_{t}^{t+\Delta t} \int_{x}^{x+\Delta x} \int_{y}^{y+\Delta y} \int_{z}^{z+\Delta z} \psi \; dz \; dy \, dx \; dt/(\Delta t)(\Delta x)(\Delta y)(\Delta z). \tag{3.23}$$

$\overline{\psi}$ is thus the average of ψ over the time step Δt and grid intervals Δx, Δy, Δz, and ψ' the subgrid-scale deviation from this average. In order to obtain the Reynolds averaged equations for the mean flow one applies the averaging rules (2.3)–(2.8) to the governing equations (3.16)–(3.21). Since this procedure can be quite lengthy for some of the equations Stull (1988) uses a very useful methodology, which helps to keep track of the required steps. Starting point are the primitive equations (3.16)–(3.21).

1. Expand the dependent variables into a mean and a turbulent part.
2. Apply Reynolds averaging to get equations for the mean variables.
3. Put the result into flux form by adding the continuity equation.
4. Subtract equations gained in the previous step 3 from those in step 1. This leads to equations for the turbulent parts.
5. Multiply the results of the previous step 4 by other fluctuating quantities and Reynolds average to yield prognostic equations for turbulence statistics such as Turbulence Kinetic Energy (TKE) or fluxes (Section 2.3).

As an example of applying this methodology the equation for mean momentum will be derived in Section 3.5 leading to the "famous" closure problem in turbulence in Section 3.6.

3.5 Reynolds Averaged Momentum Equation

A simplification which is often invoked when it comes to the conservation of momentum is the *Boussinesq Approximation*. According to this approximation, density is assumed constant except for the buoyancy term in the vertical velocity, where only weak density deviations can already have a huge effect. For a more detailed discussion when the Boussinesq Approximation is valid see e.g. Stull (1988). In practice it means replacing the density $\rho = \overline{\rho} + \rho'$, whenever occurring, by $\overline{\rho}$. Only in the gravity term density is replaced by $g - \frac{\theta'_v}{\overline{\theta}_v} g$. The latter part non surprisingly states that air warmer than the average air is less dense and can be derived by applying Reynolds averaging to the ideal gas law (3.1) and using the Poisson equation (c.f. Stull 1988).

As a starting point the momentum equation (3.7) is recalled for convenience:

$$\frac{\partial u_i}{\partial t} + u_j \frac{\partial u_i}{\partial x_j} = -\delta_{i3} g + f_c \, \epsilon_{ij3} \, u_j - \frac{1}{\rho} \frac{\partial p}{\partial x_i} + \nu \frac{\partial^2 u_i}{\partial x_j^2}. \tag{3.24}$$

Applying the Boussinesq Approximation yields:

$$\frac{\partial u_i}{\partial t} + u_j \frac{\partial u_i}{\partial x_j} = -\delta_{i3} \left(g - \frac{\theta_v'}{\overline{\theta_v}} g \right) + f_c \, \epsilon_{ij3} \, u_j - \frac{1}{\overline{\rho}} \frac{\partial p}{\partial x_i} + \nu \frac{\partial^2 u_i}{\partial x_j^2}. \tag{3.25}$$

Now the variables are split into mean and turbulent parts (except for the gravitational term already expanded by applying the Boussinesq Approximation):

$$\begin{aligned} \frac{\partial (\overline{u_i} + u_i')}{\partial t} + (\overline{u_j} + u_j') \frac{\partial (\overline{u_i} + u_i')}{\partial x_j} = \\ -\delta_{i3} \left(g - \frac{\theta_v'}{\overline{\theta_v}} g \right) + f_c \, \epsilon_{ij3} \, (\overline{u_j} + u_j') - \frac{1}{\overline{\rho}} \frac{\partial (\overline{p} + p')}{\partial x_i} + \nu \frac{\partial^2 (\overline{u_i} + u_i')}{\partial x_j^2}. \end{aligned} \tag{3.26}$$

Now the expanded and rearranged equation is averaged to arrive at a predictive equation for the mean flow:

$$\begin{aligned} \overline{\frac{\partial \overline{u_i}}{\partial t}} + \overline{\frac{\partial u_i'}{\partial t}} + \overline{\frac{\overline{u_j} \partial \overline{u_i}}{\partial x_j}} + \overline{\frac{\overline{u_j} \partial u_i'}{\partial x_j}} + \overline{\frac{u_j' \partial \overline{u_i}}{\partial x_j}} + \overline{\frac{u_j' \partial u_i'}{\partial x_j}} = \\ -\overline{\delta_{i3} g} + \overline{\delta_{i3} \left(\frac{\theta_v'}{\overline{\theta_v}} \right) g} + \overline{f_c \, \epsilon_{ij3} \, \overline{u_j}} + \overline{f_c \, \epsilon_{ij3} \, u_j'} - \overline{\frac{1}{\overline{\rho}} \frac{\partial \overline{p}}{\partial x_i}} + \overline{\frac{1}{\overline{\rho}} \frac{\partial p'}{\partial x_i}} + \nu \overline{\frac{\partial^2 \overline{u_i}}{\partial x_j^2}} + \nu \overline{\frac{\partial^2 u_i'}{\partial x_j^2}}. \end{aligned} \tag{3.27}$$

With the averaging rules (2.3)–(2.8) many of the terms in (3.27) become zero, leaving:

$$\frac{\partial \overline{u_i}}{\partial t} + \overline{u_j} \frac{\partial \overline{u_i}}{\partial x_j} + \overline{u_j' \frac{\partial u_i'}{\partial x_j}} = -\delta_{i3} g + f_c \epsilon_{ij3} \overline{u_j} - \frac{1}{\overline{\rho}} \frac{\partial \overline{p}}{\partial x_i} + \nu \frac{\partial^2 \overline{u_i}}{\partial x_j^2}. \tag{3.28}$$

In order to proceed further in the methodology presented in Section 3.4 some considerations about the Reynolds averaged continuity equation shall be made. Since the incompressibility approximation holds for flows in the PBL, (3.5) serves as the starting equation to be averaged:

$$\begin{aligned} \frac{\partial (\overline{u_j} + u_j')}{\partial x_j} = \frac{\partial \overline{u_j}}{\partial x_j} + \frac{\partial u_j'}{\partial x_j} = 0 \\ \overline{\frac{\partial \overline{u_j}}{\partial x_j} + \frac{\partial u_j'}{\partial x_j}} = 0. \end{aligned} \tag{3.29}$$

The averaging rules give

$$\frac{\partial \overline{u_j}}{\partial x_j} = 0 \quad \text{and} \quad \frac{\partial u_j'}{\partial x_j} = 0. \tag{3.30}$$

If the second equation in (3.30) is multiplied by u_i and averaged, the third term on the left-hand side of (3.28) can be converted to flux form. If it is then put on the right-hand side the prognostic equation for momentum becomes:

$$\underbrace{\frac{\partial \overline{u_i}}{\partial t}}_{\text{I}} + \underbrace{\overline{u_j}\frac{\partial \overline{u_i}}{\partial x_j}}_{\text{II}} = \underbrace{-\delta_{i3} g}_{\text{III}} + \underbrace{f_c \epsilon_{ij3} \overline{u_j}}_{\text{IV}} - \underbrace{\frac{1}{\overline{\rho}}\frac{\partial \overline{p}}{\partial x_i}}_{\text{V}} + \underbrace{\nu \frac{\partial^2 \overline{u_i}}{\partial x_j^2}}_{\text{VI}} - \underbrace{\frac{\partial \overline{(u_i' u_j')}}{\partial x_j}}_{\text{X}} . \tag{3.31}$$

The roman numbers I–VI are consistent with (3.6), with the only difference that they describe mean momentum. Term X is the Reynolds stress (see Subsection 2.3.3). This term underlines the importance of turbulence—its consideration is essential since it affects the mean flow! In order to predict the behavior of the mean flow this term has to be known. It can be predicted by deriving a forecast equation like above but it will eventually lead to other unknown terms. This is what is known as *turbulence closure problem*. The equations are not closed and there are always more unknown terms than equations. Before going into more detail in Section 3.6 the other equations predicting mean flow are presented for completeness.

$$\overline{p} = \overline{\rho}\, R\, \overline{T_v} \tag{3.32}$$

$$\frac{\partial \overline{u_j}}{\partial x_j} = 0 \tag{3.33}$$

$$\frac{\partial \overline{q_T}}{\partial t} + \overline{u_j}\frac{\partial \overline{q_T}}{\partial x_j} = \nu_q \frac{\partial^2 \overline{q}}{\partial x_j^2} + \frac{S_{q_T}}{\overline{\rho}} - \frac{\partial \overline{(u_j' q_T')}}{\partial x_j} \tag{3.34}$$

$$\frac{\partial \overline{\theta}}{\partial t} + \overline{u_j}\frac{\partial \overline{\theta}}{\partial x_j} = \nu_\theta \frac{\partial^2 \overline{\theta}}{\partial x_j^2} - \frac{1}{\overline{\rho}\, c_p}\left(\frac{\partial \overline{Q_j^*}}{\partial x_j}\right) - \frac{L_p\, E}{\overline{\rho} c_p} - \frac{\partial \overline{(u_j' \theta')}}{\partial x_j} \tag{3.35}$$

$$\frac{\partial \overline{C}}{\partial t} + \overline{u_j}\frac{\partial \overline{C}}{\partial x_j} = \nu_C \frac{\partial^2 \overline{C}}{\partial x_j^2} + S_C - \frac{\partial \overline{(u_j' c')}}{\partial x_j}. \tag{3.36}$$

3.6 The Closure Problem

The colored quantities in (3.31)–(3.36) represent divergences of turbulent fluxes (introduced in Subsection 2.3.2). They result as a consequence of the nonlinear terms denoted by II in (3.6), (3.10), (3.14), and (3.15). The flux terms indicate that the turbulent fluctuations cause transport of momentum, heat, and water and must be known in order to predict how the mean quantities, i.e. the variables in the grid cells, change with time. It is possible to derive predictive equations for the flux terms. Again the momentum equation should serve as example. As starting point serves a prognostic equation for the turbulent part u_i' of total wind. It can be obtained by subtracting the equation for the

mean part (3.31) from (3.26):

$$\frac{\partial u_i'}{\partial t}+\frac{\overline{u_j}\partial u_i'}{\partial x_j}+u_j'\frac{\partial \overline{u_i}}{\partial x_j}+u_j'\frac{\partial u_i'}{\partial x_j}=-\delta_{i3}\left(\frac{\theta_v'}{\overline{\theta_v}}\right)g+f_c\epsilon_{ij3}u_j'-\frac{1}{\overline{\rho}}\frac{\partial p'}{\partial x_i}+\nu\frac{\partial^2 u_i'}{\partial x_j^2}+\frac{\partial\overline{(u_i'u_j')}}{\partial x_j}. \quad (3.37)$$

Multiplying (3.37) by u_k, Reynolds averaging and interchanging the indices k and i results in:

$$\begin{aligned}\overline{u_i'\frac{\partial u_k'}{\partial t}}+\overline{u_i'\overline{u_j}\frac{\partial u_k'}{\partial x_j}}+\overline{u_i'u_j'\frac{\partial\overline{u_k}}{\partial x_j}}+\overline{u_i'u_j'\frac{\partial u_k'}{\partial x_j}}=\\ -\delta_{k3}\overline{u_i'\left(\frac{\theta_v'}{\overline{\theta_v}}\right)}g+f_c\epsilon_{kj3}\overline{u_i'u_j'}-\overline{\frac{u_i'}{\overline{\rho}}\frac{\partial p'}{\partial x_k}}+\nu\overline{u_i'\frac{\partial^2 u_k'}{\partial x_j^2}}.\end{aligned} \quad (3.38)$$

The product rule of calculus gives

$$\frac{\partial\overline{u_i'u_k'}}{\partial t}=\overline{u_i'\frac{\partial u_k'}{\partial t}}+\overline{u_k'\frac{\partial u_i'}{\partial t}}, \quad (3.39)$$

in which the first term on the right-hand side corresponds to the first term in (3.38). With interchanging the indices in (3.38) again and putting the two equations together, the moment flux budget equation results in:

$$\begin{aligned}\underbrace{\frac{\partial(\overline{u_i'u_k'})}{\partial t}}_{\text{I}}+\underbrace{\overline{u_j}\frac{\partial(\overline{u_i'u_k'})}{\partial x_j}}_{\text{II}}=\underbrace{-(\overline{u_i'u_j'})\frac{\overline{u_k}}{\partial x_j}-(\overline{u_k'u_j'})\frac{\overline{u_i}}{\partial x_j}}_{\text{III}}-\underbrace{\frac{\partial(\overline{u_i'u_j'u_k'})}{\partial x_j}}_{\text{IV}}\\ \underbrace{+\left(\frac{g}{\overline{\theta_v}}\right)\left[\delta_{k3}\overline{u_i'\theta_v'}+\delta_{i3}\overline{u_k'\theta_v'}\right]}_{\text{V}}+\underbrace{\overline{\frac{p'}{\overline{\rho}}\left(\frac{\partial u_i'}{\partial x_k}+\frac{\partial u_k'}{\partial x_i}\right)}}_{\text{VIII}}-\underbrace{2\nu\overline{\frac{\partial u_i'}{\partial x_j^2}\frac{\partial u_k'}{\partial x_j^2}}}_{\text{X}}.\end{aligned} \quad (3.40)$$

The Coriolis and pressure diffusion terms as well as the molecular diffusion term for turbulent momentum flux have been neglected based on scaling arguments suggesting that they are smaller than the other terms. For a step-by-step derivation see Stull (1988). It is important to remember that (3.40) represents 9 separate equations (reduced to 6 by symmetries as discussed in Subsection 2.3.3). The roman numbered terms have the following meanings (Stull 1988) for (3.40):

I storage of momentum flux

II advection of momentum flux by mean wind

III production of momentum flux by mean wind shears

IV transport of momentum flux by turbulent motions

V buoyant production/consumption

VIII redistribution by the return-to-isotropy term

X viscous dissipation term

Recalling the turbulence continuity equation it can be shown that term VIII does not change the total budget but tends to redistribute energy through interaction of fluctuating velocities and pressure and thereby makes turbulence more isotropic. The dissipation term X is, as implied by the name, always a loss term becoming larger with decreasing eddy size. For small eddies viscosity soon takes effect, converting motion to heat. The highlighted term IV (triple-correlation-term) illustrates what was noted before: More unknown terms appear as one tries to include a predictive equation for the turbulent fluxes in the model. If one tries to derive equations for those, quadruple-correlation-terms will appear (see also Table 3.1). This is the turbulence closure problem. It requires that the unknown terms are represented as functions of known variables. It requires parameterization. Before taking a closer look on what parameterizing means (Section 3.8, and Section 3.9) equations for the turbulent fluxes of the other fundamental variables shall be presented in a compact form.

Moisture Flux

The moisture flux budget is given by:

$$\underbrace{\frac{\partial(\overline{q'u_i'})}{\partial t}}_{\text{I}} + \underbrace{\overline{u_j}\frac{\partial(\overline{q'u_i'})}{\partial x_j}}_{\text{II}} = \underbrace{-(\overline{q'u_j'})\frac{\overline{u_i}}{\partial x_j}}_{\text{III}} \underbrace{-\frac{\partial(\overline{q'u_j'u_i'})}{\partial x_j}}_{\text{IV}}$$
$$\underbrace{+\delta_{i3}\left(\frac{\overline{q'\theta_v'}}{\overline{\theta_v}}\right)g}_{\text{V}} + \underbrace{\left(\frac{1}{\overline{\rho}}\right)\left[\overline{p'\frac{\partial q'}{\partial x_i}}\right]}_{\text{VIII}} \underbrace{-2\nu\overline{\left(\frac{\partial u_i'}{\partial x_j}\right)\left(\frac{\partial q'}{\partial x_j}\right)}}_{\text{X}} \underbrace{-\overline{u_iu_j}\frac{\partial\overline{q}}{\partial x_j}}_{\text{XI}}, \tag{3.41}$$

with I denoting storage, II advection and terms III, XI and V relating to production/ loss. Turbulent transport is numbered with IV, and term VIII refers to redistribution. Term X describes again molecular dissipation of turbulent moisture flux. In (3.41) the Coriolis term as well as the pressure and the molecular diffusion terms were neglected due to scale-considerations.

Heat Flux

The heat flux budget equation reads:

$$\underbrace{\frac{\partial(\overline{\theta' u_i'})}{\partial t}}_{\text{I}} + \underbrace{\overline{u_j}\frac{\partial(\overline{\theta' u_i'})}{\partial x_j}}_{\text{II}} = \underbrace{-(\overline{\theta' u_j'})\frac{\overline{u_i}}{\partial x_j}}_{\text{III}} \underbrace{- \frac{\partial(\overline{\theta' u_j' u_i'})}{\partial x_j}}_{\text{IV}}$$
$$\underbrace{+\delta_{i3}\left(\frac{\overline{\theta'\theta_v'}}{\overline{\theta_v}}\right)g}_{\text{V}} + \underbrace{\left(\frac{1}{\overline{\rho}}\right)\left[\overline{p'\frac{\partial\theta'}{\partial x_i}}\right]}_{\text{VIII}} \underbrace{- 2\nu\overline{\left(\frac{\partial u_i'}{\partial x_j}\right)\left(\frac{\partial\theta'}{\partial x_j}\right)}}_{\text{X}} \underbrace{- \overline{u_i' u_j'}\frac{\partial\overline{\theta}}{\partial z}}_{\text{XI}}. \tag{3.42}$$

The roman numbers describe the terms in analogy to above. Often term V is approximated by $\delta_{i3} g \frac{\overline{\theta_v'^2}}{\overline{\theta_v}}$. In (3.42), the radiation term was neglected in addition to Coriolis, pressure and molecular diffusion terms.

3.7 Turbulence Kinetic Energy

Being an important variable in the study of the PBL, TKE shall be treated separately. It serves as a measure of turbulence intensity and effectiveness (2.12) and is often used instead of the velocity fluctuations in closure schemes (Subsection 3.9.1). TKE is "produced" by shear and buoyancy and "destroyed" by dissipation (Section 2.4). It can be transported by the mean velocity in the flow. Thus the terms of a budget equation for TKE describe turbulence generating and TKE-transporting physical processes and can determine flow stability (Stull 1988). Recalling (2.20), stating that TKE $= \frac{1}{2}\overline{u_i'^2}$, a budget equation for TKE can be obtained from the prognostic equation for momentum variance. As starting point for the latter serves (3.37), multiplied by $2\,u_i$ and Reynolds averaged:

$$\frac{\partial\overline{u_i'^2}}{\partial t} + \overline{u_j}\frac{\partial\overline{u_i'^2}}{\partial x_j} + 2\overline{u_i' u_j'}\frac{\partial\overline{u_i}}{\partial x_j} + \frac{\partial(\overline{u_j' u_i'^2})}{\partial x_j} =$$
$$+2\delta_{i3}\overline{u_i'\left(\frac{\theta_v'}{\overline{\theta}_v}\right)}g + 2\,f_c\,\epsilon_{ij3}\overline{u_i' u_j'} - 2\overline{\left(\frac{u_i'}{\overline{\rho}}\right)\frac{\partial p'}{\partial x_i}} + 2\nu\overline{u_i'\frac{\partial^2 u_i'}{\partial x_j^2}}. \tag{3.43}$$

Usually this prognostic equation for the wind speed variance is simplified further for the usage in boundary layer flows (Stull 1988). With the Coriolis term becoming zero by carrying out the summation (repeated indices) and simplified dissipation and pressure terms (see Stull 1988) the simplified velocity variance budget becomes:

$$\frac{\partial\overline{u_i'^2}}{\partial t} + \overline{u_j}\frac{\partial\overline{u_i'^2}}{\partial x_j} = +2\delta_{i3}\frac{g(\overline{u_i'\theta_v'})}{\overline{\theta_v}} - 2\overline{u_i' u_j'}\frac{\partial\overline{u_i}}{\partial x_j} - \frac{\partial(\overline{u_j' u_i'^2})}{\partial x_j} - \frac{2}{\overline{\rho}}\frac{\partial\overline{(u_i' p')}}{\partial x_i} - 2\varepsilon, \tag{3.44}$$

in which ε represents viscous dissipation and is defined as $\varepsilon = \nu\overline{\left(\frac{\partial u_i'}{\partial x_j}\right)^2}$. Dividing (3.44) by two, the budget equation for TKE is obtained (TKE is denoted by $\overline{e}$ for simplification):

$$\underbrace{\frac{\partial \overline{e}}{\partial t}}_{\text{I}} + \underbrace{\overline{u_j}\frac{\partial \overline{e}}{\partial x_j}}_{\text{II}} = + \underbrace{\delta_{i3}\frac{g}{\overline{\theta_v}}\left(\overline{u_i'\theta_v'}\right)}_{\text{III}} - \underbrace{\overline{u_i'u_j'}\frac{\partial \overline{u_i}}{\partial x_j}}_{\text{IV}} - \underbrace{\frac{\partial\left(\overline{u_j'e}\right)}{\partial x_j}}_{\text{V}} - \underbrace{\frac{1}{\overline{\rho}}\frac{\partial\left(\overline{u_i'p'}\right)}{\partial x_i}}_{\text{VI}} - \underbrace{\varepsilon}_{\text{VII}} \tag{3.45}$$

In (3.45) the roman-numbered terms have the following meanings (Stull 1988):

I local storage or tendency of TKE

II advection of TKE by mean wind

III buoyant production or consumption (depending on the heat flux $\overline{u_i'\theta_v'}$ being positive, during the day over land, or negative, at night over land)

IV mechanical or shear production/loss term; usually momentum is lost downward to the ground, resulting in a positive contribution to TKE

V turbulent transport of TKE through turbulent eddies

VI pressure correlation, describing the redistribution of TKE by pressure perturbations; often associated with oscillations in the air (buoyancy or gravity waves)

VII dissipation: conversion of TKE into heat

As for TKE one can write a budget equation for the mean kinetic energy. By doing so it turns out that it also contains term IV of (3.45) but with an opposite sign, indicating, that mechanically produced turbulence extracts energy from the mean flow—turbulent eddies are created and intensified by the mean shear of the flow. (3.45) will be invoked in Chapter 4 where it forms the basis for turbulence closure.

3.8 Parameterization

Since unknown terms have entered the prognostic equations (Section 3.6) one is dependent on parameterizations to keep the set of equations closed. Parameterizing thus means finding functional relations in terms of parameters and known variables to approximate unknown quantities. Parameters are usually empirically determined constants. Stull (1988) nicely puts it to the point stating "Sometimes parameterizations are employed because the true physics has yet to be discovered. Other times, the known physics are too complicated to use for a particular application, given cost or computer limitations. Parameterization will rarely be perfect. The hope is that it will be adequate." He furthermore presents a list of important parameterization rules:

- Parameterization should be physically reasonable.
- It must have the same dimensions as the unknown term.
- It must possess the same tensor properties.
- It must have the same symmetries.
- The parameterization must be invariant under an arbitrary transformation of coordinate systems,
- and under a Galilean transformation.
- The parameterization must satisfy the same budget equations and constraints.

Before introducing how turbulence parameterization is implemented in CCLM some basic ideas of closure techniques will be presented in the following.

3.9 Turbulence Closure

The naming of the closure is based upon the highest order of prognostic equations that are retained. The term "order" (sometimes "level") refers to the statistical moment for which a predictive equation exists ($\overline{u_i}$ corresponds to the first order, $\overline{u_i' u_j'}$ to the second, $\overline{u_i' u_j' u_k'}$ to the third and so on). Thus in a second-order closure there are predictive equations for the mean variables ($\overline{u_i}$) and the covariances ($\overline{u_i' u_j'}$) whereas the triple correlation terms ($\overline{u_i' u_j' u_k'}$) are parameterized as functions of them. Table 3.1 summarizes number of equations and unknowns for the statistical moments of the momentum equation as well as their variables to be parameterized. Correlation triangles showing the unknowns associated with different orders of closure are illustrated in Table 3.2. Note that there are more unknowns when the full set of equations is examined.

There are also "non-integer" closure methods wherein only some of the equations in a moment category are used. In a 1.5-order closure for example the parameterization usually includes a prognostic equation for the variance of potential temperature ($\overline{\theta'^2}$) and TKE (which is typically used in place of the velocity variance equations, Stull (1988)). Two different approaches for closure are used in PBL-parameterization, local and non-local closure, described in the following sections.

3.9.1 Local Closures

In local closures the unknown quantity at a grid point is parameterized in terms of known quantities and/or their vertical gradients *at the same grid point* (e.g. Warner 2011). The derivatives are calculated by using adjacent grid points in the vertical. In this way local closures consider turbulence analogous to molecular diffusion (Stull 1988).

Table 3.1: Example of the prognostic equations for the first three statistical moments of the momentum equation. The table indicates the number of equations and unknowns associated with the parameterized moments. (Stull 1988)

example prognostic variable	statistical moment	equation	variable parameterized	number of equations	number of unknowns
$\overline{u_i}$	first	$\frac{\partial \overline{u_i}}{\partial t} = \ldots - \frac{\partial \overline{u_i' u_j'}}{\partial x_j}$	$\overline{u_i' u_j'}$	3	6
$\overline{u_i' u_j'}$	second	$\frac{\partial \overline{u_i' u_j'}}{\partial t} = \ldots - \frac{\partial \overline{u_i' u_j' u_k'}}{\partial x_k}$	$\overline{u_i' u_j' u_k'}$	6	10
$\overline{u_i' u_j' u_k'}$	third	$\frac{\partial \overline{u_i' u_j' u_k'}}{\partial t} = \ldots - \frac{\partial \overline{u_i' u_j' u_k' u_m'}}{\partial x_m}$	$\overline{u_i' u_j' u_k' u_m'}$	10	15

Table 3.2: Correlation triangles of unknowns for the momentum equations of three orders of closure. (Stull 1988)

order of closure	correlation									
zero				$\overline{u}$						
			$\overline{v}$			$\overline{w}$				
first				$\overline{u'u'}$						
			$\overline{u'v'}$			$\overline{u'w'}$				
		$\overline{v'v'}$		$\overline{v'w'}$			$\overline{w'w'}$			
second				$\overline{u'u'u'}$						
			$\overline{u'u'v'}$			$\overline{u'u'w'}$				
		$\overline{u'v'v'}$		$\overline{u'v'w'}$			$\overline{u'w'w'}$			
	$\overline{v'v'v'}$		$\overline{v'v'w'}$			$\overline{v'w'w'}$			$\overline{w'w'w'}$	

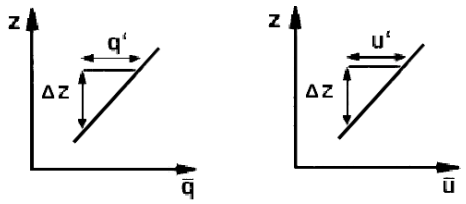

Figure 3.3: Mixing length theory: Vertical profiles of mean moisture and mean velocity. An air parcel is moved upward a distance Δz by a turbulent eddy, leading to fluctuations q' and u'.

Local First-Order Closure: K-theory

K-theory (often called gradient transport theory) is commonly used in first-order turbulence closure, relating vertical fluxes to the gradient of the mean values of the fluctuating variables. If formulated depending on local values of model variables (3.46), it belongs to the local approaches. For ψ being any of the meteorological variables with a predictive equation $\frac{\partial \overline{\psi}}{\partial t} = \ldots - \frac{\partial \overline{u_j' \psi'}}{\partial x_j}$ for the mean flow, K-theory approximates the flux $\overline{u_j' \psi'}$ to

$$\overline{u_j' \psi'} = -K \frac{\partial \overline{\psi}}{\partial x_j}, \tag{3.46}$$

where the parameter K is a scalar with units $\mathrm{m^2\,s^{-1}}$. For $K > 0$ (3.46) states that the flux occurs down the local gradient of $\overline{\psi}$. K is often referred to as eddy viscosity (analogy to molecular viscosity, indicating an increase in viscosity due to turbulent fluctuations), eddy diffusivity, or turbulent-transfer coefficient and is typically subscripted with the initial of the variable it is associated with (e.g. K_m for momentum). K-theory usually refers to vertical derivatives whereas horizontal derivatives are associated with vertical diffusion (Stensrud 2007). To specify the eddy viscosity K, Prandtl's *mixing length theory* (Prandtl 1925) is often evoked. In analogy with the mean free path of a molecule, the theory supposes that a fluid parcel, moved upward by a turbulent eddy, carries its mean properties over a characteristic distance l (the mixing length) before it mixes with its surroundings (e.g. Arya 2001). If one assumes an ideal boundary layer with linear profiles of mean humidity $\overline{q}$ and mean wind $\overline{u}$ as illustrated in Figure 3.3, the parcel thus differs from its surrounding before mixing by

$$q' = -\left(\frac{\partial \overline{q}}{\partial z}\right) \Delta z, \tag{3.47}$$

$$u' = -\left(\frac{\partial \overline{u}}{\partial z}\right) \Delta z. \tag{3.48}$$

The upward motion that is required to move the parcel over the distance Δz implies a vertical velocity component w'. If the turbulence is such that w' is proportional to u'

(Stull 1988), the vertical velocity can be expressed as:

$$w' = -cu' = c\left(\frac{\partial \overline{u}}{\partial z}\right)\Delta z, \tag{3.49}$$

with a proportionality factor c. The kinematic eddy moisture flux $\overline{w'q'}$ can now be calculated:

$$\overline{w'q'} = \overline{c\left(\frac{\partial \overline{u}}{\partial z}\right)\Delta z\left[-\left(\frac{\partial \overline{q}}{\partial z}\right)\Delta z\right]} = -c\overline{(\Delta z)^2}\left(\frac{\partial \overline{u}}{\partial z}\right)\left(\frac{\partial \overline{q}}{\partial z}\right). \tag{3.50}$$

$\overline{(\Delta z)^2}$ is the variance of parcel displacement. The mixing length l can now be defined by $l^2 = c\overline{(\Delta z)^2}$ yielding:

$$\overline{w'q'} = -l^2\left|\frac{\partial \overline{u}}{\partial z}\right|\frac{\partial \overline{q}}{\partial z}. \tag{3.51}$$

It then follows from (3.46) that the analogy to molecular transfers holds for

$$K_E = l^2\left|\frac{\partial \overline{u}}{\partial z}\right|, \tag{3.52}$$

with the eddy diffusivity K_E for moisture. This equation suggests that the magnitude of the turbulent-transfer coefficient K increases with increasing shear or increasing mixing length. There are some important limitations and notes to K-theory in the form described above which shall shortly be discussed:

- **Analogy to molecular viscosity**. This analogy is a bit dangerous (e.g. Tennekes and Lumley 1972) because K is a function of the flow (as turbulence is a property of the flow, see Subsection 2.1.1) whereas molecular viscosity ν is a function of the fluid. Therefore K should vary as turbulence varies and be parameterized for example in terms of the Richardson number (Subsection 5.2.4) (Stull 1988).

- **Limitations of mixing-length theory**. In the derivation of an expression for K using mixing-length theory it is assumed that w' is proportional to u'. (3.49) is only valid for mechanical generation of turbulence (Subsection 2.1.2), i.e. statically neutral situations (Subsection 5.2.2).
  The assumption of linear profiles of q' and u' in (3.48) is furthermore only valid for small eddies (over small distances) which underlines the "locality" in this theory.

- **Down-gradient constraint**. If analogy with viscosity is drawn, K is non-negative, implying that there is a down-gradient flux. In reality there are often large eddies found in the PBL "transporting heat from hot to cold regardless of the local gradient of the background environment" (Stull 1988). Thus the theory often fails when such big eddies (thermals) exist. Allowing negative values for K leads to fluxes from cold to hot, which is against the common understanding of the diffusion concept.

In order to account for large scale eddies sometimes a correction term is incorporated in the flux approximation (e.g Holtslag and Moeng 1991):

$$\overline{w'\theta'} = -K_H \left(\frac{\partial \overline{\theta}}{\partial z} - \gamma_\theta \right), \tag{3.53}$$

wherein K_H denotes the eddy viscosity of heat. γ_θ is a counter-gradient term (and usually a function of θ and w). Better results for large eddies are usually provided by non-local closures, discussed in the next section.[5]

3.9.2 Non-Local Closures

In non-local closures unknown variable at a grid point are estimated "using known quantities which are defined at locations that are a significant distance away in the vertical" (Warner 2011). From this definition follows that turbulence is pictured as a superposition of eddies (Stull 1988). A simple non-local closure is for example the mixed layer scheme in which potential temperature θ is constant with height and the layer is assumed horizontally homogeneous (Stensrud 2007):

$$\frac{\partial \overline{\theta}}{\partial t} = -\frac{\partial \overline{w'\theta'}}{\partial z}. \tag{3.54}$$

Due to θ being constant with height the only fluxes which change potential temperature in time occur at the bottom and the top of the mixed layer:

$$\frac{\partial \overline{\theta}}{\partial t} = \left[(\overline{w'\theta'})_S - (\overline{w'\theta'})_H \right] \frac{1}{H}, \tag{3.55}$$

with H the top height of the layer and S referring to a flux from the surface. An equation for the latter is obtained via the sensible heat flux at the surface and depends on the difference between the ground (sea surface) temperature and the temperature of the overlying atmosphere. $(\overline{w'\theta'})_H$ is determined by the turbulent entrainment[6] of θ at the top of the mixed layer which results in changes of the layer height. In order to keep the system of equations closed one can relate $(\overline{w'\theta'})_H$ and $(\overline{w'\theta'})_S$ by an entrainment coefficient which is for example obtained in laboratory measurements (Stensrud 2007).

Another framework for a first-order non-local closure is provided by Stull's *transilient turbulence theory* (1984, 1988, 1993). It allows non-local vertical mixing between pairs of grid points of a vertical column, even if the points are non-adjacent. If one focuses

[5] The deficiencies concerning larger eddies are also tried to overcome by using higher-order closures, such as presented in Chapter 4, where K becomes a function of TKE.

[6] a) "In meteorology, the mixing of environmental air into a preexisting organized air current so that the environmental air becomes part of the current"; b) "The process by which turbulent fluid within a mixed layer incorporates adjacent fluid that is nonturbulent, or much less turbulent"; (Glickman 2012)

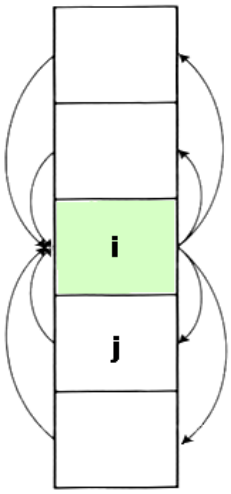

Figure 3.4: Transilient turbulence theory (Stull 1984): Non-local mixing across finite distances with eddies mixing air to and from grid box i.

on one reference grid box (the colored box in the middle of Figure 3.4) one can identify other boxes from which eddies mix air into the reference box. Similar the boxes which receive air from the reference box can be located. This process can be repeated for every grid box in the column serving as "reference box", so that superposition of several eddies can be imagined. Denoting the reference box by index i, the concentration of a passive tracer in i is given by $\overline{\xi}_i$. If c_{ij} gives the fraction of air in box i that was mixed into the cell coming from box j, the new concentration in box i can be found by summing all the mixing processes over N boxes of the column:

$$\overline{\xi}_i(t + \Delta t) = \sum_{j=1}^{N} c_{ij}(t, \Delta t)\overline{\xi}_j(t). \tag{3.56}$$

ξ_j is the initial value of the tracer in box j (source box) at time t and ξ_i its final value in box i after a time-step Δt. If c_{ij} is identified as $N \times N$ matrix (transilient matrix) containing the mixing coefficients (which indicate the fraction of air coming from a source cell j, ending in grid cell i), (3.56) gives a matrix equation. Note that c_{ij} is only a function of time and time-step. Even if $\overline{\xi}_j$ changes (denoting heat, moisture or momentum instead of a tracer) the matrix stays the same. Physical (e.g. conservation of air mass) and numerical constraints (stability) are discussed in Stull (e.g. 1988), describing the theory in more detail.

4 Turbulence Parameterization in COSMO-CLM

In the previous sections the general problems of turbulence closure were introduced, revealing the need for parameterization schemes which keep the set of fundamental equations closed. In the case studies following in the final chapter of this thesis (Chapter 5) I intercompare Consortium on Small Scale Modelling model in CLimate Mode (COSMO-CLM) simulations with varied turbulence parameterization and analyze their performance in reference to measured radiosounding data. The next section gives an introduction to COSMO-CLM, followed by a description of the turbulence parameterizations implemented in COSMO-CLM are presented.

4.1 The COSMO-Model

The Consortium on Small Scale Modelling model in CLimate Mode (CCLM) arose from the operational weather forecast Lokal-Modell (LM) of the german weather service Deutscher Wetterdienst (DWD). The model is developed, evaluated and maintained by the Consortium on Small Scale Modelling (COSMO) and used by several national weather services in Europe. In 2002 the first climate version of the LM (CLM) was completed (Rockel et al. 2008). In 2005 the CLM became the regional Community-Model for the german climate research. CLM and LM (already renamed to COSMO-Model) were unified in 2007 to a limited area model for operational weather forecast and regional climate modeling (Rockel et al. 2008). A lot of information about the model can be obtained at the website of the CLM-community[1], an open international network of scientists developing and working with CCLM. Furthermore Rockel et al. give a nice introduction in a special issue of the *Meteorologische Zeitschrift* focusing on CCLM (Rockel et al. 2008). The extensive model documentation (including Doms (2011) and Doms et al. (2011) on which the following section is based) can be downloaded from the website of the CLM-community.

The COSMO-Model is a nonhydrostatic model based on the primitive thermo-hydrodynamical equations presented in Section 3.3 and Section 3.4. Nonhydrostatic means that the hydrostatic approximation (hydrostatic equation: $\frac{\partial \overline{p}}{\partial z} = \overline{\rho} g$) is not applied and the vertical momentum equation is solved. The model equations, describing a compress-

[1] http://www.clm-community.eu/

ible flow in a moist atmosphere, are formulated in spherical coordinates with a rotated pole and a generalized terrain-following height coordinate (see Doms (2011) for a detailed description). There are several physical processes taken into account in parameterization schemes. Besides subgrid-scale turbulence whose parameterization will be presented in more detail in Section 4.2, CCLM parameterizations includes surface layer, grid-scale clouds and precipitation, subgrid-scale clouds, moist convection, and shallow convection and radiation.

The fundamental atmospheric equations were already presented in Section 3.3. They also form the basis of the COSMO-Model. Since the model considers the atmosphere as a multicomponent continuum consisting of an ideal mixture of dry air, water vapor, liquid water, and water in solid state, the water budget equation takes into account all these constituents. This also influences the equation of state due to an altered virtual temperature. Since the model is nonhydrostatic and uses a vertical coordinate based on geometrical height, a separate prognostic equation for the pressure is needed:

$$\frac{dp}{dt} = \frac{p}{\rho}\frac{d\rho}{dt} + \rho R_d T \frac{d\alpha}{dt} + \rho R_d (1+\alpha)\frac{dT}{dt}. \tag{4.1}$$

R_d is the gas constant for dry air and α denotes a moisture term including the mass fractions of water vapor, liquid water and ice. The thermodynamic model variables ψ are then $u, v, w, T, p', \rho, q^v, q^l$ and q^f, where p' is a perturbation pressure (the deviation of pressure from a reference state) and the indices v, l, f denote water in vaporized, liquid or frozen form. For a detailed derivation of the equations in rotated geographical coordinates the reader is referred to Doms (2011).

Analogous to what was shown in Section 3.4 averaging of the basic model equations results in additional terms—turbulent fluxes of momentum, moisture and heat:

$$\mathbf{F}_\psi = \overline{\rho \mathbf{v}' \psi'}, \tag{4.2}$$

with ψ denoting one of the prognostic thermodynamic variables of the model. Reynolds averaging is performed in the same way as in (3.22) ($\psi = \overline{\psi} + \psi'$)[2]. The bold symbols in (4.2) represent vectors. $\mathbf{v}$ is the barycentric velocity (relative to the rotating earth). Source terms due to turbulent mixing appearing in the prognostic equations for the thermodynamic variables $\left(\frac{\partial \psi}{\partial t} = \ldots + M_\psi\right)$ are then denoted by M_ψ:

$$M_\psi = -\frac{1}{\rho}\nabla \cdot \mathbf{F}_\psi \tag{4.3}$$

In CCLM4.0, the model version used for the simulations in this study (Subsection 5.1.1), several turbulence schemes are available. The next section describes the ones used in this thesis in more detail.

[2]Doms (2011) define furthermore a mass weighted average $\widehat{\psi}$ and the deviation ψ'' from the mass weighted mean value but this becomes obsolete with the help of the Boussinesq approximation in the treatment of turbulent fluxes.

4.2 Turbulence Closure in COSMO-CLM

The turbulence parameterization schemes used in the simulations of this thesis express the turbulent flux $\mathbf{F}_\psi$ on the basis of K-theory (Subsection 3.9.1):

$$\mathbf{F}_\psi = -\rho\, \mathbf{K}_\psi\, \nabla\psi, \tag{4.4}$$

so that subgrid scale fluxes are proportional to the gradient of the resolved quantity. $\mathbf{K}_\psi$ is a simply diagonally structured matrix in the form

$$\mathbf{K}_\psi = \begin{pmatrix} K_\psi^h & 0 & 0 \\ 0 & K_\psi^h & 0 \\ 0 & 0 & K_\psi^v \end{pmatrix}. \tag{4.5}$$

h and v denote horizontal and vertical components. For the scalar quantities (heat, water vapor, liquid water and ice) they are considered to be equal. Different values are taken for the diffusion coefficients of horizontal and vertical momentum exchange.

4.3 1D TKE-based Turbulence Scheme

For this turbulence scheme the set of model equations is extended by the use of an additional prognostic equation for Turbulence Kinetic Energy (TKE) (see Section 3.7), leading to additional terms like the buoyant heat flux $\mathbf{F}^{\theta_v}$ and the mixing term for turbulent kinetic energy M_e. The 1D TKE-based turbulence scheme imposes horizontal homogeneity of variables and fluxes. This is the so-called boundary layer approximation and results in neglecting all horizontal turbulent fluxes (Doms et al. 2011). The approximation can be applied for horizontal scales of motion much larger than the vertical scale. The contributions from the vertical transports are then dominant. In meso-β (20 km to 200 km) scale flow systems its application is usually justified (Doms et al. 2011). In the one dimensional TKE-based scheme a 1.5-order closure (level 2.5 in the notation of Mellor and Yamada 1982) is applied. A simplified set of basic equations is sufficient for the derivation of the second order budgets. Due to their negligible direct impact on turbulent fluxes, Coriolis forces, radiation and precipitation are not considered. Furthermore thermodynamically filtered (Doms et al. 2011) equations are applied. This leads to a transformation from the dependent variables θ, q_v (specific humidity), and q_c (specific cloud water content), which appeared in the additional prognostic equation for TKE, to θ_l and q_w as dependent variables. $\theta_l = \theta - \left(\frac{L_v}{c_{pd}}\right) q_c$ is the liquid water potential temperature, with the latent heat of vaporization L_v and the specific heat of dry air c_{pd}. $q_w = q_v + q_c$ denotes total water. Both variables are conserved in moist adiabatic displacements in the vertical. Since the original turbulent fluxes $\mathbf{F}^\theta$, $\mathbf{F}^{q_v}$ and $\mathbf{F}^{q_c}$ are required by the (non-simplified) model equations, a closure for phase transitions

is obtained from the statistical cloud scheme (CCLM uses a variant of Sommeria and Deardorff (1977), for further details see Doms et al. (2011)). In this way effects from subgrid scale condensation and evaporation are included in the turbulent fluxes of heat and moisture. The turbulence scheme parameterizes the vertical turbulent fluxes by:

$$\overline{w'\psi'} = -K^{\psi}\frac{\partial\overline{\psi}}{\partial z}. \tag{4.6}$$

As stated before the horizontal fluxes are neglected. For $\psi = \theta_l$,q_l the turbulent diffusion coefficients K^{ψ} have the form:

$$K^{\psi} = K^{H} = q\,l\,S^{H}, \tag{4.7}$$

whereas they are calculated by

$$K^{\psi} = K^{M} = q\,l\,S^{M} \tag{4.8}$$

for the velocity components u and v. The indices H and M stand for heat and momentum. $S^{H,M}$ denote stability functions dependent on buoyancy, vertical shear, the turbulent "master" length scale l, and the turbulent velocity scale q. For a detailed description of these terms see Mellor and Yamada (1982). The turbulent velocity scale $q = \sqrt{2\overline{e}}$ is obtained from the TKE-equation. For l, the characteristic length scale for vertical mixing, the *Blackadar mixing length* is assumed (Blackadar 1962):

$$l = \frac{kz}{1 + \frac{kz}{l_{\infty}}}, \tag{4.9}$$

where $k \cong 0.4$ denotes the *von Kármán's* constant and l_{∞} is the asymptotic mixing length. z is the height. l_{∞} is a limit reached by l in the free atmosphere. In a simplified framework one can picture this length as the maximum eddy size still part of the parameterized spectrum (cf. Baldauf et al. 2011; Koller 2007). l_{∞} has proven to be a sensitive parameter (e.g. Baldauf et al. 2011) and will take two different values in the case studies of Chapter 5. A reduction of l_{∞} results in less mixing in the vertical, larger vertical gradients and a less stable Planetary Boundary Layer (PBL) which can foster convection-initiation (Baldauf et al. 2011).

4.4 3D TKE-based Turbulence Scheme

With decreasing grid size (3 km are used in the case studies of Chapter 5) parameterization of turbulent processes is becoming increasingly important. Especially the boundary layer approximation (Section 4.3) seems not adequate anymore. Whether a three-dimensional treatment is already imperative at the resolution of 3 km is still open to be answered (Doms et al. 2011). The scheme implemented in version 4.0 of CCLM

was adopted from a Large Eddy Simulation (LES)-like model of Herzog et al. (2002). In the CCLM-documentation (Doms et al. 2011) the authors mention that no universal parameterization exists and the dependence on the specific grid resolution has to be taken into account. At the present time a new turbulence scheme is being developed (Machulskaya and Mironov 2013). The implementation of the scheme used in this thesis shall now be presented.

As the name implies in this closure the three-dimensional form of the turbulent flux terms is retained. In the notation of (Doms et al. 2011) these are the terms on the right-hand side of:

$$\left(\frac{\partial \overline{u_i}}{\partial t}\right) = \ldots - \frac{1}{\rho}\frac{\partial \tau_{ij}}{\partial x_j} \tag{4.10}$$

$$\left(\frac{\partial \overline{T}}{\partial t}\right) = \ldots - \frac{1}{c_{pd}\rho}\frac{\partial h_j}{\partial x_j} \tag{4.11}$$

$$\left(\frac{\partial \overline{q}^k}{\partial t}\right) = \ldots - \frac{1}{\rho}\frac{\partial f_j^{q_k}}{\partial x_j}, \tag{4.12}$$

with the momentum flux τ_{ij}, the heat flux h_j and the water flux $f_j^{q_k}$ in which $k = v, l$ stands for vapor and cloud liquid water. The momentum flux tensor is specified as:

$$\tau_{ij} = -\rho K_m^{ij}\left(\frac{\partial \overline{u_i}}{\partial x_j} + \frac{\partial \overline{u_j}}{\partial x_i}\right), \tag{4.13}$$

for which it is important to note that the upper indices ij in K_m^{ij} are not involved in the tensor summation convention. A distinction is made between horizontal and vertical momentum coefficients in a way that:

$$K_m^H := K_m^{11} = K_m^{12} = K_m^{22} \quad \text{“horizontal momentum”}, \tag{4.14}$$

$$K_m^V := K_m^{13} = K_m^{23} = K_m^{33} \quad \text{“vertical momentum”}. \tag{4.15}$$

Due to symmetry considerations there are only six components necessary, cf. Subsection 2.3.3. The scalar fluxes are expressed as:

$$h_j = -c_{pd}\rho\pi K_h^j \frac{\partial \overline{\theta}}{\partial x_j} \qquad \text{and} \tag{4.16}$$

$$f_j^{q^k} = -\rho K_h^j \frac{\partial \overline{q}^k}{\partial x_j}, \tag{4.17}$$

with the Exner function $\pi = \left(\frac{p}{p_0}\right)^{\frac{R}{c_p}}$. Again the diffusion coefficients are taken to be the same for heat and water, given by:

$$K_h^H := K_h^1 = K_h^2 \quad \text{“horizontal heat”}, \tag{4.18}$$

$$K_h^V := K_h^3 \quad \text{“vertical heat”}. \tag{4.19}$$

The horizontal coefficients for both, heat and momentum, are assumed to be proportional to the vertical coefficients by an anisotropy factor dependent on the grid sizes (in the model coordinate system $\Delta\lambda$, $\Delta\phi$, Δz):

$$K^H_{m,h} := r\frac{\sqrt{(a\cos\phi\Delta\lambda)^2 + (a\Delta\phi)^2}}{\Delta z}K^V_{m,h} \approx r\frac{\sqrt{2}\Delta}{\Delta z}K^V_{m,h}, \tag{4.20}$$

where a is a grid-related variable, $\Delta \approx 2.8$ (the LM-Kürzestfrist resolution at that time) and $r = 0.1$. The vertical coefficients are finally specified as follows:

$$K^V_m = \phi_m l\sqrt{\bar{e}} \tag{4.21}$$

$$K^V_h = \phi_h l\sqrt{\bar{e}} \tag{4.22}$$

with the mixing length l again in Blackadar form (4.9) and TKE being $\bar{e}$. The parameters $\phi_{n,m}$ are functions of stability (including the Richardson number, Subsection 5.2.4).

4.5 Additional Remarks on the Turbulence Schemes

There are several remarks on parameterization in general and the turbulence parameterization schemes discussed above, which shall briefly be noted. Firstly, it should be recognized, that the parameterizations have to be computationally efficient, i.e. a "compromise between physical realism and computational economy" (Mironov 2010) has to be found. Many parameterizations were originally developed for models with coarser grids and have to be adapted for continuously finer-meshed grids.

Deficiencies of the COSMO turbulence schemes described above regarding the PBL representation (Mironov and Raschendorfer 2010) are known and the scheme is under constant development. There are attempts to unify the parameterizations of boundary layer turbulence and shallow convection (Mironov 2010) and a TKE-scalar variance scheme, accounting for non-locality and turbulence anisotropy, is under development (Machulskaya and Mironov 2013).

Specific remarks concerning the schemes in Section 4.3 and Section 4.4 include the question if the master length scale could be chosen as a function of stability (as proposed by Mellor and Yamada 1982) and if the present implementation of three-dimensional treatment is adequate to realistically simulate the vertical structure of the PBL. Suklitsch et al. (2011) found in their study that the current 3D turbulence scheme did not notably lead to an improvement regarding the simulation of 2m air temperature and total precipitation amount. In his thesis Koller (2007) noticed that a proper implementation of the 3D scheme would be necessary for a full three-dimensional description of the turbulent exchange. The question arises whether a LES-like closure is already suitable at a grid spacing of 3 km since the postulation $\Delta x \approx \Delta y \approx \Delta z$ is not met yet. Several studies (e.g. Ament (2006), Koller (2007), Baldauf et al. (2011)) suggested that a reduction of

the asymptotic turbulence length l_∞ bears a potential improvement of convective precipitation forecasts in convective-scale Numerical Weather Prediction (NWP). In general a reduction of the asymptotic turbulence length (Section 4.3) leads to less vertical mixing, larger vertical gradients and a more unstable PBL (Baldauf et al. 2011). As was pointed out by Ament (2006) and Koller (2007) the improvement in convection-initiation stems from a shifting in the portion of parameterized and resolved heat fluxes and the thus intensified vertical movement.

If and how the schemes differ in the simulation of temperature, dew point temperature, and vertical wind profiles will be analyzed in the next chapter which compares CCLM hindcast simulations to radiosounding data.

5 Case Studies

For the case studies I compare CLM output with radiosounding data. Two events are chosen—one weak gradient situation in July 2007 and an inversion situation in January 2008—which are analyzed with respect to vertical profiles, stability parameters and varied simulation parameters (Section 5.3). In the following I will give a short overview over the analyzed model runs and the differences in their parameterization schemes. In order to get an idea what can be deduced from the atmospheric profiles Subsection 5.1.2 will deal with radiosondes and the common tool for presenting data gained from weather balloons—the Skew-T diagram. Afterwards the synoptic conditions and weather situations which are to be analyzed are presented.

5.1 Data

The data used in the case studies were on the one hand obtained by the COSMO-Model using different turbulence schemes and on the other hand provided by radiosonde measurements from the station Vienna Hohe Warte. The following sections will describe the data in more detail.

5.1.1 COSMO-CLM Data

The model output which I analyzed in my case studies stems from the project Non-Hydrostatic Climate Modelling 1 (NHCM-1) during which hindcast simulations with different resolutions and parameterizations were conducted. Detailed information about the experimental design, the model setting and domains can be found in the corresponding report (Suklitsch et al. 2011). Here I only present the key settings.

I analyzed simulations at a 3 km (0.03°) resolution with 32 vertical levels. The driving data for the 10 km simulations, which in turn provide the boundary data for the 3 km simulations (see Figure 5.1), were taken from the operational analysis and short term forecasts of European Centre for Medium-Range Weather Forecasts (ECMWF)'s Integrated Forecasting System (IFS) (Bechtold et al. 2008), with an update interval of three hours for the lateral boundary conditions. The model version used in the NHCM-1 study was Consortium on Small Scale Modelling model in CLimate Mode (CCLM) 4.0. General information about the model and its physics was already presented in Section 4.1. The 10 km "parent simulation" in which the 3 km for my analysis were nested has the following key settings:

- **10 km parent run:** 3rd order Runge-Kutta numerics (time step: 80 s); Kain-Fritsch moist convection (Kain and Fritsch (1993); Kain (2003)); cloud ice scheme with prognostic cloud water and cloud ice, prognostic rain and snow and transport of rain/snow; 1D Turbulence Kinetic Energy (TKE)-based turbulence scheme including sub-grid scale effects of condensation/evaporation (Section 4.3); lateral boundary conditions update every three hours

The three model runs whose output will be intercompared and checked against the radiosoundings were generated using the following settings:

- **reference run:** 3rd order Runge-Kutta numerics (time step: 30 s); no convection; cloud ice scheme with prognostic cloud water and cloud ice, prognostic rain and snow and transport of rain/snow; 1D TKE-based turbulence scheme including sub-grid scale effects of condensation/evaporation (Section 4.3); lateral boundary conditions update every hour

- **3D turbulence:** same as in reference run, but with 3D turbulence (Section 4.4)

- **tur_len=150 m:** same as in reference run but with an asymptotic turbulence length (Section 4.2) of tur_len=150 m (instead of tur_len=500 m); additional changes in the cloud scheme: q_crit=1.6 (critical value for normalized over-saturation) at clc_diag=0.5 (cloud cover at saturation)

Note that the other two runs differ from the reference run only by the specified settings. The vertical profiles presented in Section 5.3 were obtained by extracting the data for the model column in which the meteorological ground station Vienna-Hohe Warte is located. A further description will be given in the following.

5.1.2 Radiosounding Data

In addition to surface maps of temperature, pressure, wind and humidity, observational information in weather forecasting is commonly presented as vertical profiles of these parameters. The information about the vertical structure of the atmosphere is traditionally gained by radiosondes. These instrument packages are carried aloft by a weather balloon and communicate the data back to the ground via a radio transmitter. Radiosondes are released all over the world (mainly concentrated over land in the Northern Hemisphere) and the observations are usually taken at the same universal time each day (00:00 UTC/ 12:00 UTC). The University of Wyoming provides sounding data from stations all over the world[1]. The data used to plot the vertical profiles in Section 5.3 were downloaded from their homepage.

[1] Its website is http://weather.uwyo.edu/upperair/sounding.html.

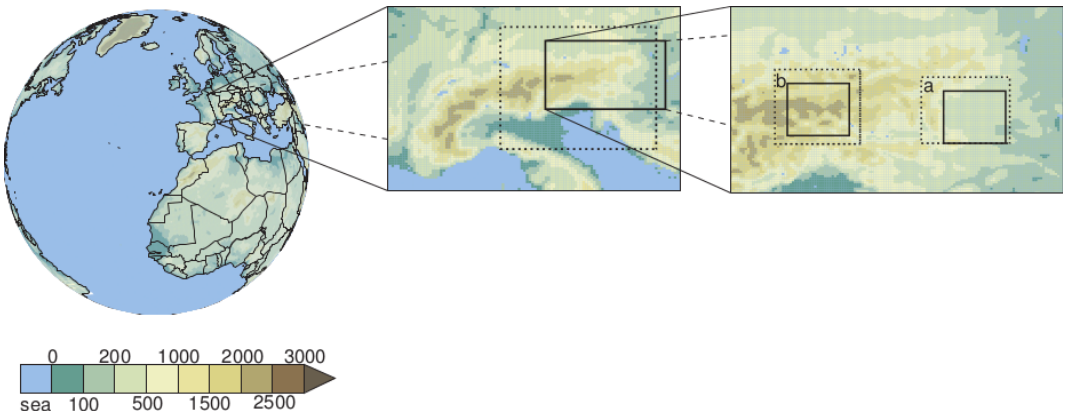

Figure 5.1: Model domains for the simulations conducted in the NHCM-1 study. The left panel shows the globe with IFS topograhpy and the 10 km domain with the 3 km resolution domain within (next panel from the left). The panels on the right also shows the 1 km domains (a),(b) not used in this thesis (Suklitsch et al. 2011).

Sounding data used in Section 5.3 of this thesis stem from radiosondes launched at the meteorological station Vienna-Hohe Warte. The WMO station number is 11035 and the elevation is 209 m. In order to compare the soundings with the CLM-data the grid column containing the station's latitude/longitude value (48-15N, 016-22E (dms)) was evaluated. By analyzing only this column the drift of the radiosonde was neglected.

5.2 Methods

In order to compare model and radiosounding data the vertical structure of the Planetary Boundary Layer (PBL) is investigated. A current method for the analysis is displaying the data in a Skew-T Log-P Diagram and deriving parameters to characterize the PBL. Two important boundary layer parameters used in this study are Convective Available Potential Energy (CAPE) and Bulk Richardson Number (BRN). They will be described in this section after introducing the Skew-T Log-P Diagram and some considerations about atmospheric stability.

5.2.1 Skew-T Log-P Diagram

This section is closely reliant on the lecture notes from Bart Geerts from the Atmospheric Science Department of the University of Wyoming (Geerts 2011). Further didactically useful information is provided at MetEd (2006b) with a special "Skew-T Mastery".

Instead of displaying the local vertical structure of the troposphere in a temperature-height diagram one uses pressure, which is proportional to air mass, as one of the coor-

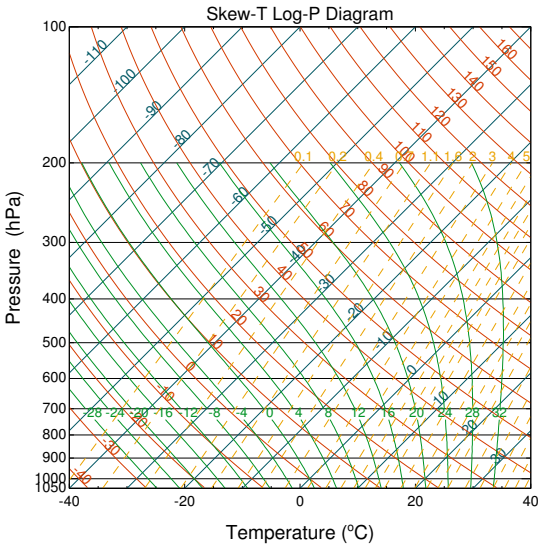

Figure 5.2: Plain Skew-T diagram.

dinates.

A Skew-T Log-P diagram (Skew-T for short) is hence so-called due to the log-p vertical coordinate (approximately height) and the slanted (skewed) isotherms. It is a pseudo-adiabatic diagram because it is derived from the assumption that latent heat of condensation is not taken into account and accumulated condensation/sublimation products fall out instantly. The diagram consists of two sets of straight lines, the horizontal isobars and the diagonal isotherms. The steeper diagonal saturation mixing ratio lines are slightly curved from the lower left to the upper right. In addition there are sets of dry adiabats (upward convex) and saturated adiabats (downward convex). The conventions for the coloring of those sets of lines varies—as can be seen in Figure 5.2 in our case we use black for the isobars, blue for the isotherms and dashed yellow mixing ratios. The dry adiabats are represented by red and the saturated adiabats by green lines. Many useful IDL-routines for atmospheric science applications of which some have served as templates for the plotting-routines in this work can be found in Brunner (2004). In addition to the above described set of fixed orientation lines two variable lines, a temperature and a dew point curve, are plotted in the Skew-T diagram. They are referred to as Environmental Lapse Rate (ELR) and Dew Point Lapse Rate (DLR). The term "environmental" relates to the fact that a parcel method is used. A hypothetical parcel of air[2] is moved upward or downward in the atmosphere and the resulting changes in its characteristics are compared to the conditions in the surrounding environment. One

[2]Per definition a dimensionless, non-entraining bubble of air, whose pressure adjusts instantaneously to that of the ambient air through which it rises or sinks (Geerts 2011).

assumes that no mixing of mass or heat takes place—the quantity of air moves in a dry or moist adiabatic fashion—a somewhat unrealistic but useful simplified concept. In the diagrams presented here the dew point curve is a solid blue line and the temperature is represented by a solid black curve. The curves connect data points from various atmospheric levels. Since the dew point is less or equal to the temperature, the DLR is always to the left of the ELR. Only in the case of saturated air, like for example in foggy conditions, the DLR and ELR coincide. For dry air there is a large difference between ELR and DLR—i.e. the dew point difference is large. One aspect that argues in favor of Skew-T diagrams is the simple determination of moisture or stability parameters whose values can be either read/interpolated from intersections of ELR/DLR and the specific humidity lines at the required pressure, or gained from simple calculations with these values. For further information on how this is done see the above mentioned lecture notes (Geerts 2011).

5.2.2 Stability

As far as the atmosphere is concerned, stability refers to a tendency of encouraging or inhibiting vertical motions. When a parcel of air, which is displaced vertically, returns to its original position the atmosphere is said to be stable. Neutrality refers to a parcel remaining still after being displaced. In unstable conditions lifting will occur because the air parcels can maintain their upward motion. To put it simply, a stable boundary layer is found when the surface is colder than the air above, for example during clear nights. An unstable boundary layer is found during sunny days with surfaces warmer than the air above (Wallace and Hobbs 2006). The layer is then in a state of free convection (see also Subsection 2.1.2). One way to determine stability for unsaturated air, is to study the lapse rate of virtual potential temperature[3] $\frac{\partial \theta_v}{\partial z}$ with the stability criteria (e.g. Jacobson 1999):

$$\frac{\partial \theta_v}{\partial z} \begin{cases} < 0 & \text{unsaturated unstable} \\ = 0 & \text{unsaturated neutral} \\ > 0 & \text{unsaturated stable} \end{cases} \tag{5.1}$$

Conditional instability refers to instability depending on whether or not the ascending parcel is saturated (air being unstable if it is saturated)—usually the normal state of the atmosphere. According to Stull (1991) this traditional approach should be discarded in favor of a non-local approach accounting for both "the local lapse rate and convective air parcels moving across finite distances." (see also Section 3.9). The atmospheric stability in this study will be assessed following Leuenberger et al. (2010) and will be explained in Subsection 5.2.4.

[3] The virtual potential temperature "is found by bringing a moist parcel to a pressure of 1000 mbar, then converting all moisture in the parcel to dry air and determining the parcel's temperature" (Jacobson 1999).

5.2.3 Convective Available Potential Energy

CAPE is the maximum available amount of buoyant energy which can accelerate air vertically. Convection feeds from the energy being inherent in thermal stratification. CAPE is an indicator for the potential of severe weather since deep convection can not occur unless CAPE > 0. "The environmental CAPE for convective storms is often in the range of $1000\,\mathrm{J\,kg^{-1}}$ to $2000\,\mathrm{J\,kg^{-1}}$" (MetEd 2006a). For a reference parcel CAPE is calculated by (e.g. Leuenberger et al. 2010):

$$\mathrm{CAPE}(z) = \int_{z_{LFC}}^{z_{EL}} \frac{T_v^p - T_v^e}{T_v^e} dz. \tag{5.2}$$

Indices p and e denote parcel and environment, T_v the virtual temperature. The integration is performed from the Level of free convection (LFC), where the parcel first becomes warmer than its surroundings, to the Equilibrium Level (EL), where it is no longer warmer than the environment. CAPE differs for different air parcels. Surface-based CAPE is calculated for an air parcel with the corresponding $2m$ temperature and dew point temperature. Alternatively, a parcel possessing the average mixing ratio and potential temperature of the air e.g. in the lowest 50 hPa or 500 m-thick layer above the ground can be used for computing the CAPE. In this work CAPE has been calculated using surface values for the radiosondes and the first level values of the CLM-data respectively.

5.2.4 Bulk Richardson Number

The BRN, which is an approximation to the gradient Richardson Number by using finite differences across layers instead of gradients, quantifies the ratio of buoyancy to mechanical shear. The BRN serves as a stability parameter and is usually calculated with respect to the ground values (cf. Leuenberger et al. (2010)):

$$\mathrm{BRN}(z) = \frac{g(\theta_v(z) - \theta_{v2\mathrm{m}})(z - z_{\mathrm{ground}})}{\overline{\theta_v(z)}[u^2(z) + v^2(z)]}. \tag{5.3}$$

Table 5.1 suggests an interpretation for the BRN (Jacobson 1999). When the virtual potential temperature decreases with increasing height (BRN < 0) the atmosphere is buoyantly unstable and turbulent. For small negative values of BRN, wind is dominating and turbulence is primarily produced mechanically. If the value is negative and large, free convection is the ruling process. When BRN becomes positive, wind shear compared to buoyant stability is large and turbulence arises from forced convection. For large positive BRNs one assumes the flow to become laminar. As the terms "small" and "large" in connection with the Bulk Richardson Number indicate (Table 5.1) there is no exact interpretation for BRN-values. As far as the positive BRN values are concerned

BRN	Type of Flow	Level of Turbulence Due to Buoyancy	Level of Turbulence Due to Shear
< 0, large	turbulent	large	small
< 0, small	turbulent	small	large
> 0, small	turbulent	none (weakly stable)	large
> 0, large	laminar	none (strongly stable)	small

Table 5.1: Interpretation of the Bulk Richardson Number (Jacobson 1999).

Richardson himself proposed a value of +1 of the (flux) Richardson number[4] (Stull 1988) as critical value where the flow becomes laminar (dynamically stable) because shear and buoyant suppression balance each other. The *critical Richardson number*, for which literature gives a range of different values, is hence the number below which flows with decreasing positive BRNs become turbulent. According to Lee et al. (1984) the problem of finite differences across layers, which is due to the sometimes large vertical spacing between sounding points, can be met by using an empirical approximation for the relationship of BRN over a layer and the turbulence within that layer. In this empirical relationship the probability for turbulence becomes zero at a value of BRN < 10.25. For the negative branch (BRN < 0), always predicting turbulence, Priestley (1957) states a value of Richardson number RN $= -0.011$ "as indicative of that at which free convection should begin to compete with forced convection as an effective agent of heat transfer, and it should become dominant at a value not many times greater." Later works suggest a range $-0.02 >$ RN > -0.05 for the transition zone between forced and free convection (e.g. Hansen 1966).

Following Leuenberger et al. (2010) I chose a value of $\mathrm{BRN}_{cr} = 0.22$ for convective and $\mathrm{BRN}_{cr} = 0.33$ for stable conditions. The stability assessment is (also in accordance with Leuenberger et al. (2010)) achieved by the calculation of a linear regression coefficient β ((5.4)) between the virtual potential temperature and the height in the four lowest model levels. A positive coefficient indicates stable, a negative β convective conditions.

$$\beta = \frac{\sum_{i=1}^{4} z\theta_v - 1/4 \sum_{i=1}^{4} z \sum_{i=1}^{4} \theta_v}{\sum_{i=1}^{4} z^2 - 1/4 \sum_{i=1}^{4} z \sum_{i=1}^{4} z} \tag{5.4}$$

From BRN-profiles the height of the PBL can be deduced. It is given by the level at which the BRN reaches the critical value (Sørensen et al. 1996). This method will be used in Subsection 5.3.1.

[4] "A dimensionless number defined as the ratio of the buoyancy term of the turbulence kinetic energy budget equation and the negative of the shear terms of that same equation" (Glickman 2012). Following K-theory Subsection 3.9.1 the fluxes can be replaced with gradients, leading to the gradient Richardson number to which the BRN is an approximation.

5.3 Test Cases

In order to analyze the effect of varied turbulence parameterization schemes I choose a typical summer and a typical winter situation as test cases. For the summer case a weak pressure gradient should bring forward a situation in which the local character and not the synoptic conditions take the dominant position. In the winter setting a sub-inversion fog/stratus situation, a frequent phenomenon in the Vienna basin, is explored.

In the following sections the atmospheric conditions of the analyzed days are introduced and the corresponding model output will be presented.

5.3.1 Test Case 1: July 8, 2007

In 2007 the days from July 7 to July 9 were characterized by a low pressure gradient. Figure 5.3 gives an overview of the synoptic situation on the day of interest. Global radiation, temperature, and wind speed data from the meteorological ground station (Figure 5.4) serve as supplementary information, giving an impression on the weather conditions in the analyzed period. On July 9, 2007 a cold front crossed Austria from west, reaching Vienna in the evening, leading to a heavy decrease in temperature, strengthened wind, and partly heavy precipitation. In Figure 5.4 the presence of clouds can be inferred from indentations in the global radiation curves, especially distinct on July 9. The cold front appears as rapid drop of the temperature curve connected with a rash increase of wind speed. The characterization of the general weather situation (low pressure gradient) follows the classification given in the weather monthly weather review of Zentralanstalt für Meteorologie und Geodynamik (ZAMG) (Derka 2007). In Figure 5.7 and Figure 5.8 it can be seen that the winds are not too weak. Steinacker (2000) for example gives a limiting value of 15 kn ($\hat{=}$ 7.72 m s^{-1}) in 850 hPa for low gradient situations, a condition not met, as Figure 5.7 and Figure 5.8 show.

The Skew-T diagrams from 00Z (Figure 5.5) and 12Z (Figure 5.6) compare the radiosounding to the CLM data. They show that the model generally captures the vertical structure of the atmosphere. Since the vertical temperature and humidity profile contain many details and the number of model levels (32 in our case, see Subsection 5.1.1) is restricted, CLM profiles generally show a smoother development than the radiosoundings which comprise measurements at a higher number of levels. At 00Z (Figure 5.5), all of the models underpredict the temperature as well as the dew point difference in the lowest tropospheric layers (up to approx. 830 hPa). The 3D run highly overestimates the nocturnal inversion.

At 12Z (Figure 5.6) the troposphere presents itself conditionally unstable with present surface-based CAPE (Subsection 5.2.3). In the model runs the lowest layers show a greater dew point difference than the radiosounding. The reference run pronounces a small inversion at 850 hPa which cannot be found in the sounding or the other CLM-runs, whereas the sounding gives two small inversions at 600 hPa and 460 hPa which are

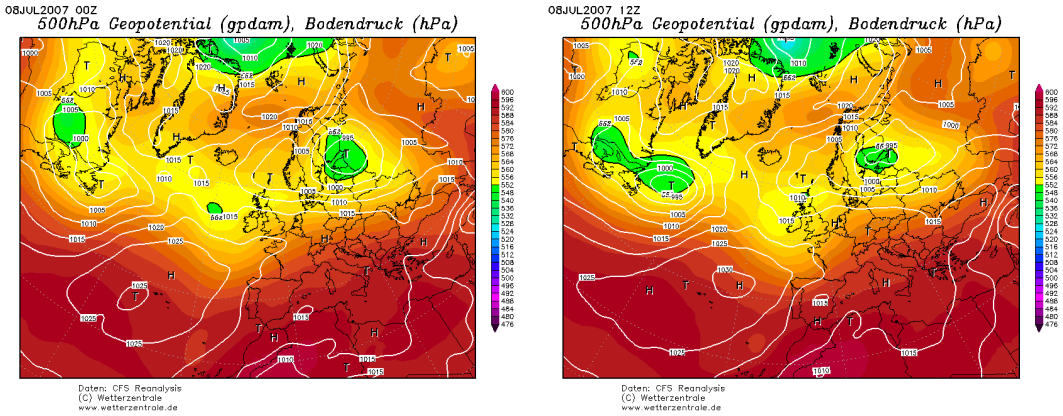

Figure 5.3: Weak pressure gradient synoptic situation on July 8, 2007 at 00Z and 12Z (www.wetterzentrale.de).

smoothed out in the CLM simulations.

As can be seen in Figure 5.7, the CLM-simulations are also capable of reproducing the measured wind profile, even though with confinements and varying quality. The 3D and the tur_len run both underestimate the windspeed at the lowest level. The reference run gives too large values from 970 hPa to 880 hPa; above that it displays a decrease in wind speed over a depth of 50 hPa which is not shown in the radiosounding. Also the decline in wind speed around 700 hPa in the 3D and the tur_len run are not confirmed by the measurements.

The 12Z comparisons (Figure 5.8) agree in the broad picture but show larger deviations, especially for the 3D and the tur_len simulation. The tur_len run shows a wind speed decline in the lowest layers which is neither shown by the measurement (but note there are only two measurements in that height range; a decline is still improbable) nor by the other simulations. The 12Z run also exhibits quite deviating values for the wind direction in the lowest part of the boundary layer. Figure 5.9 and Figure 5.10 show the BRN for the vertical profiles obtained from radiosonde and CLM simulations. The BRN (Subsection 5.2.4) quantifies the ratio of buoyancy to mechanical shear. Usually it is calculated with respect to the ground values (5.3). The left panel in Figure 5.10 shows BRNs calculated according to (5.3). The right panel gives the BRNs computed by using the height and potential temperature values from the first level instead of $\theta_{v2\mathrm{m}}$ and z_{ground}. I have performed this comparison because the relative humidity values at 2m (which are diagnostic not prognostic values) seem too low in many cases. A comparison with semi-automatic meteorological station (TAWES) data showed an underestimation of the $\mathrm{RELHUM}_{2\mathrm{m}}$-values in more than two thirds of the values in the grid column of interest (Vienna Hohe Warte) for all of the model runs. For the BRN-computation with θ_v at the lowest model level the accordance of model with the measured data is

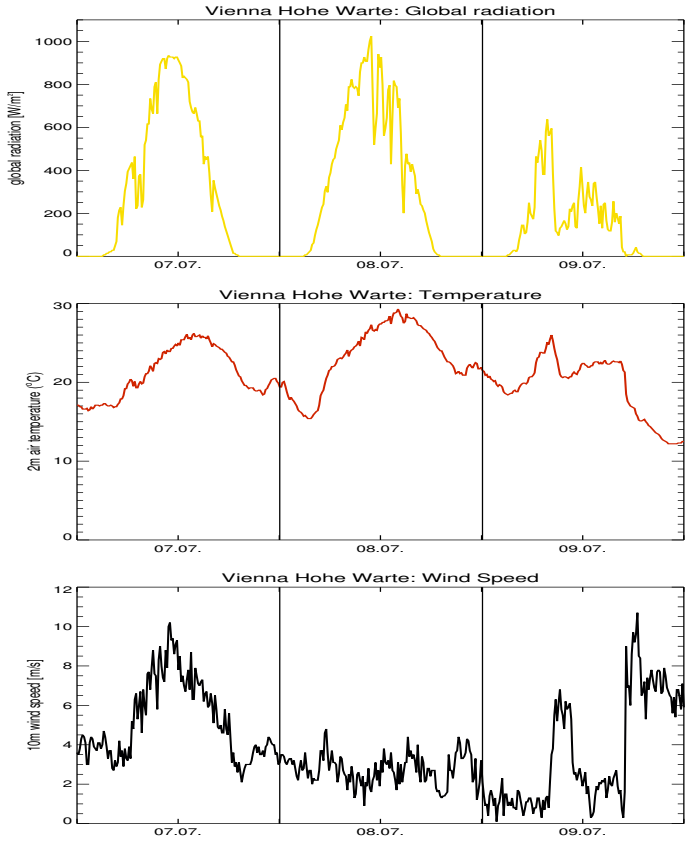

Figure 5.4: Development of global radiation, 2m temperature and wind speed at the meteorological ground station Vienna Hohe Warte from July 7 to July 9, 2007.

substantially better.

From Figure 5.9 and Figure 5.10 the height of the PBL can be deduced. The height is given by the level at which the BRN reaches the critical value (Sørensen et al. 1996). In general this diagnostic determination works better under convective conditions. Under stable conditions the ability to predict the PBL-height is poorer (Seibert et al. 2000). From the radiosounding (Figure 5.9) the top of the boundary layer can be obtained at 725 hPa. The heights computed with $\theta_{v2\mathrm{m}}$ are too large. For the "θ_v-at first model level" runs (Figure 5.10 right panel) the PBL-height is predicted too low. The best agreement with the sounding as far as the PBL-height is concerned is given by the tur_len run, even if it is also in this case slightly underestimated. The tur_len run features too large values of the BRN between 930 hPa and 900 hPa. This is due to the underestimated wind speed in these levels (Figure 5.8) and wrongly suggests a higher degree of turbulence

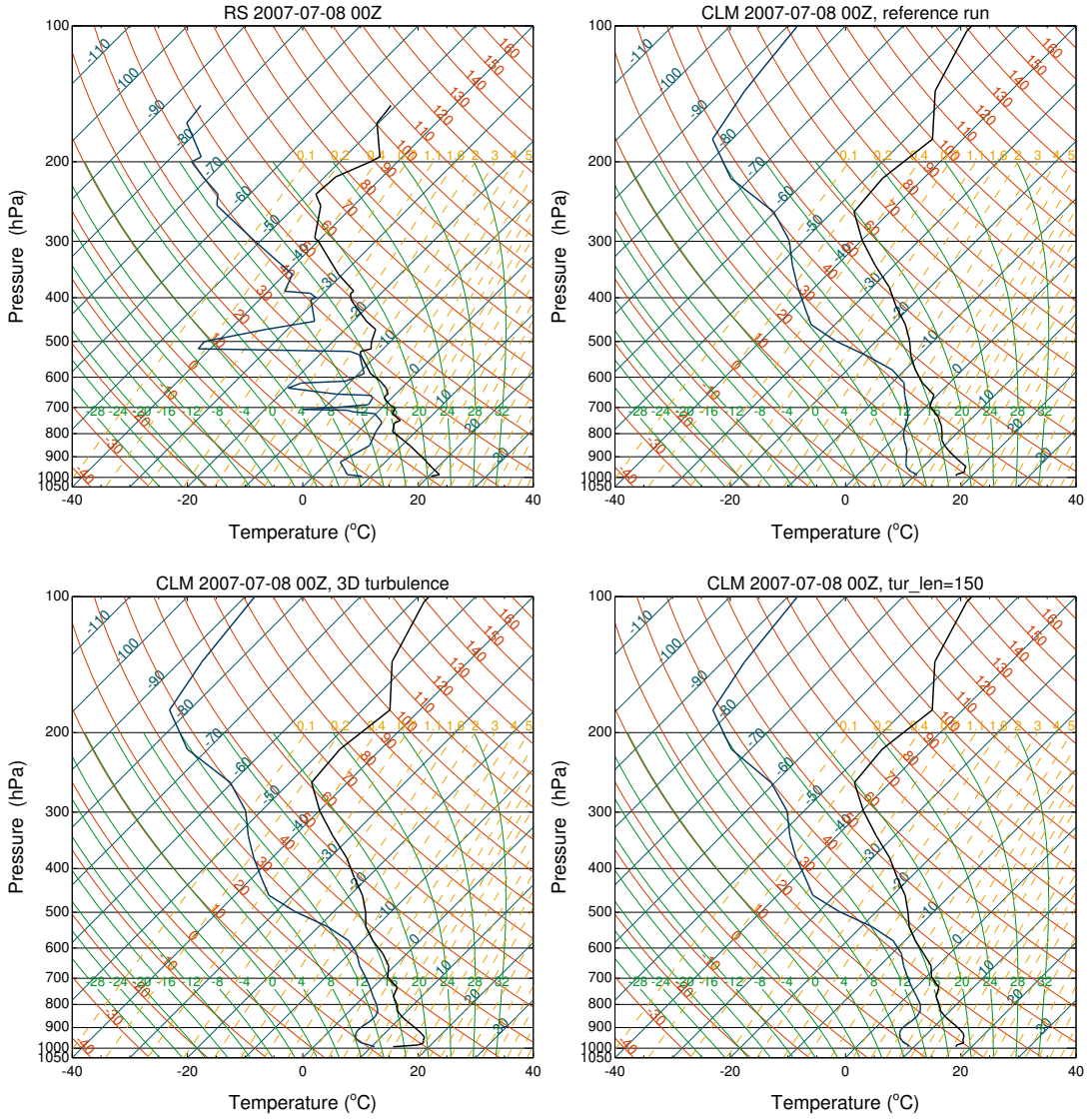

Figure 5.5: Skew-T diagrams of the radiosounding and the corresponding model runs on July 8, 2007 at 00Z.

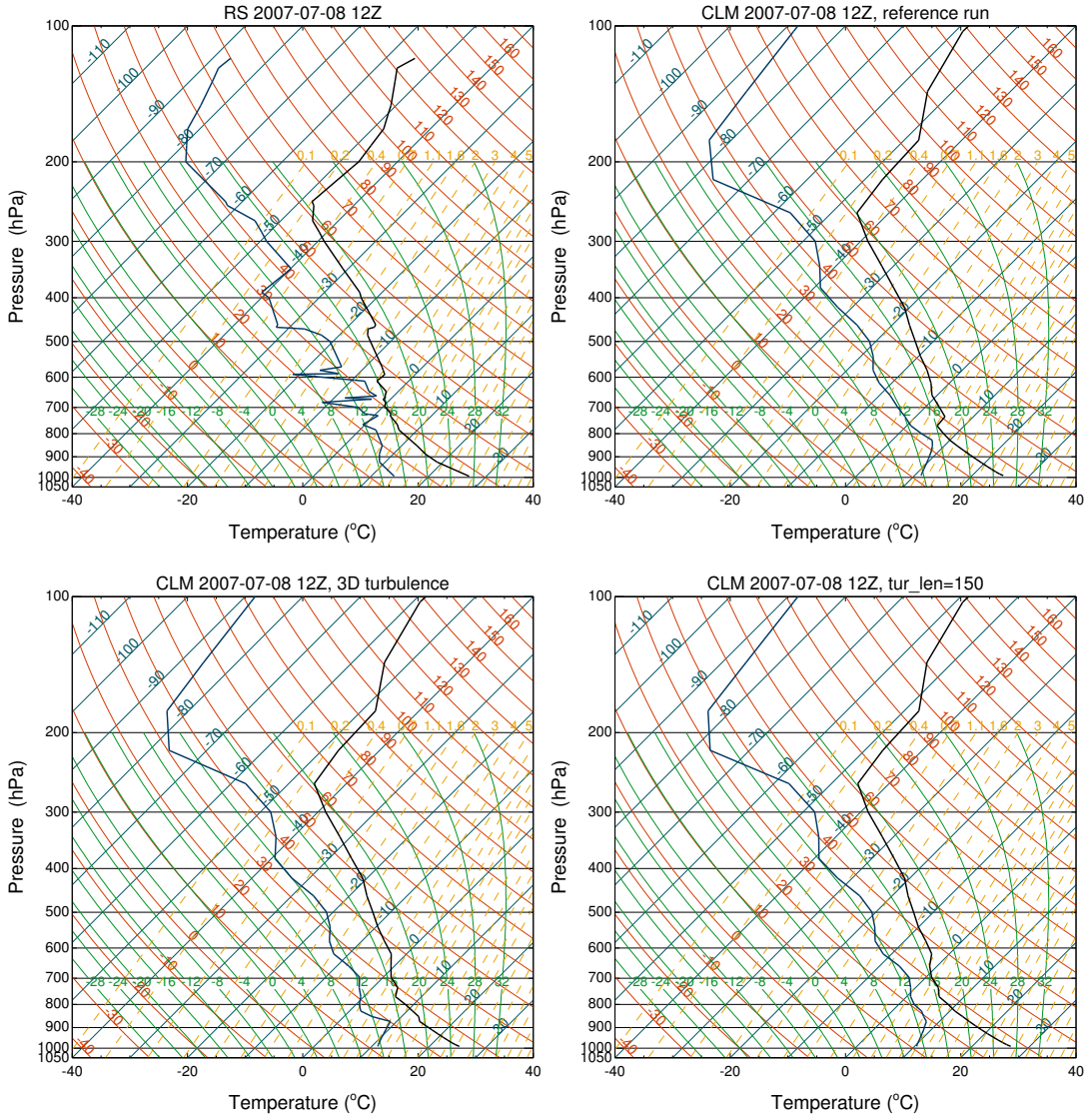

Figure 5.6: Skew-T diagrams of the radiosounding and the corresponding model runs on July 8, 2007 at 12Z.

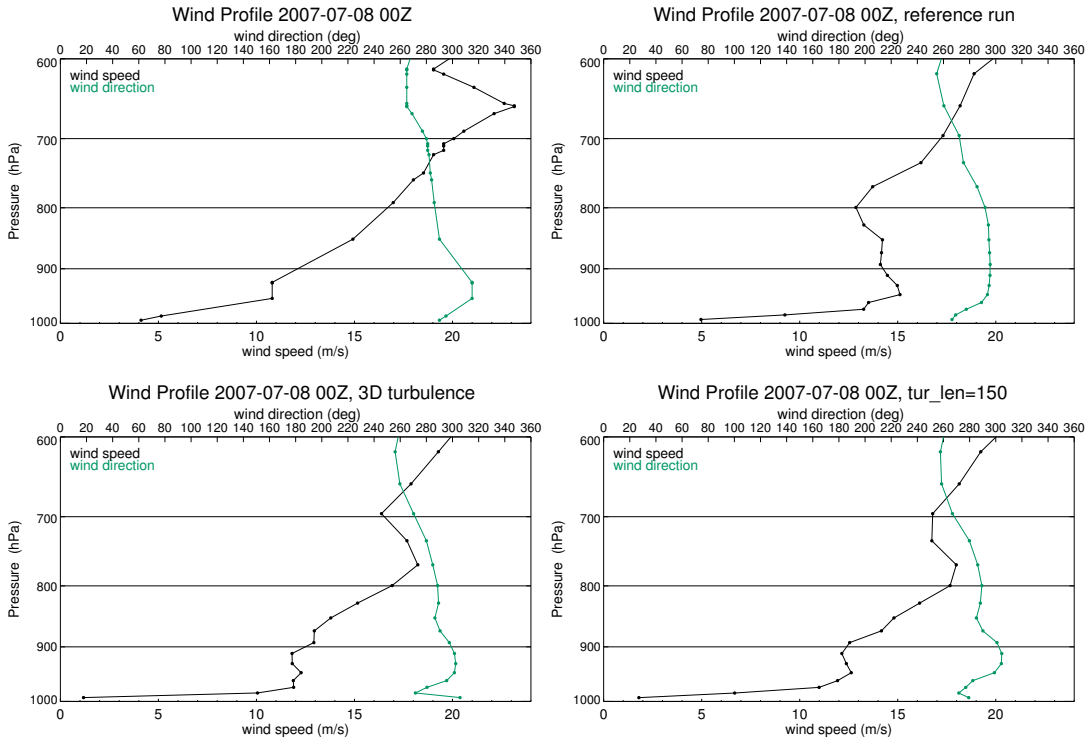

Figure 5.7: Comparison of radiosounding and CLM wind profiles from July 8, 2007 00Z.

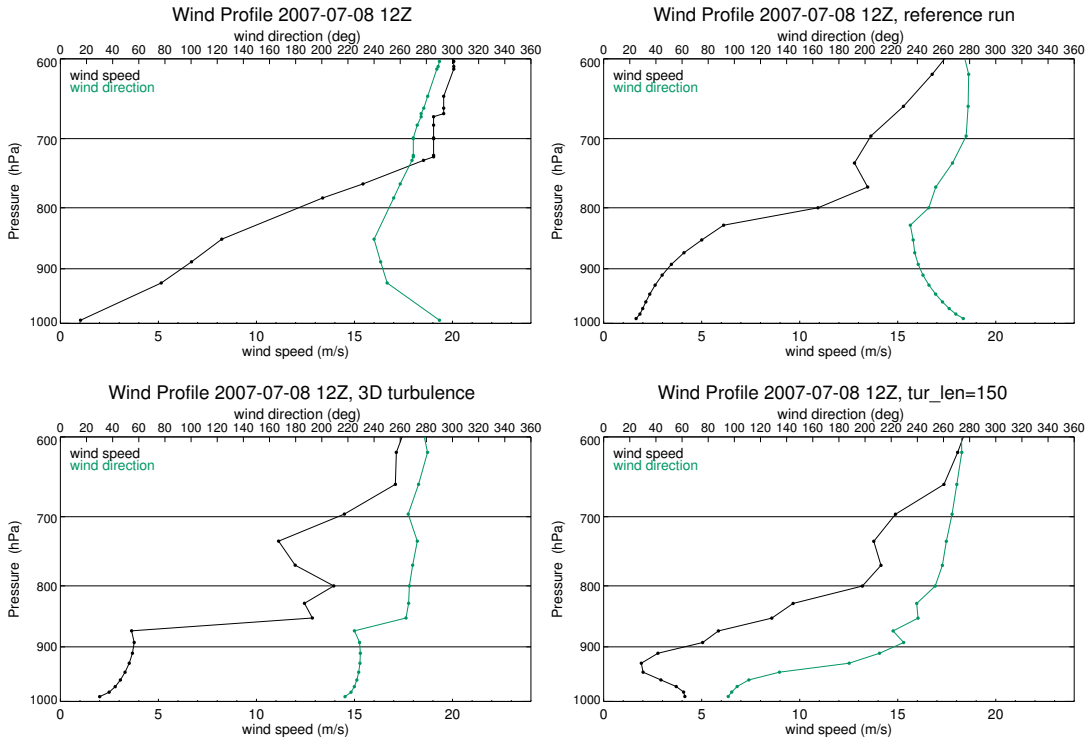

Figure 5.8: Comparison of radiosounding and CLM wind profiles from July 8, 2007 12Z.

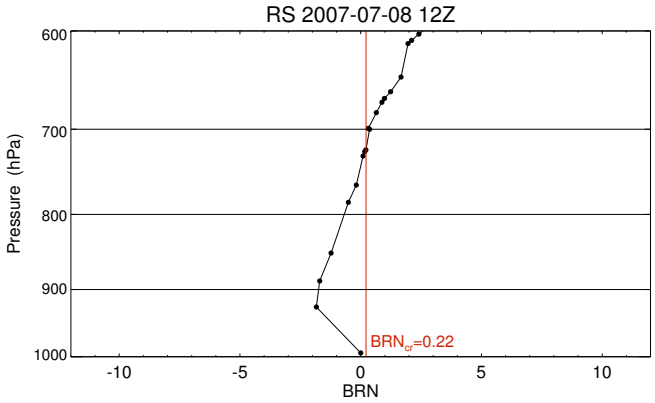

Figure 5.9: Profile of the Bulk Richardson Number for the radiosounding at 12Z on July 8, 2007.

due to shear. Maximum CAPE[5] is underpredicted in all of the model runs (presumably due to the overestimated dew point difference in the lowest atmospheric levels). The highest CAPE-value is is observed for the tur_len run. The lower vertical resolution (the fewer vertical levels in the model runs), could lead to a misestimation of vertical gradients and, as a consequence, to an over- or underestimation of CAPE. Furthermore for the model runs the values at the lowest levels above the ground and not the ground values were used for its calculation.

5.3.2 Test Case 2: July 9, 2007

Following the suggestions that a reduced asymptotic turbulence length in combination with an adapted subgrid cloudiness scheme (Subsection 5.1.1) could lead to improved results in operational convective-scale numerical weather prediction with COSMO (Koller (2007) and Baldauf et al. (2011)), July 9, 2007 is also investigated. The synoptic situation for this day was presented in Test Case 1 (Subsection 5.3.1). In the course of July 9, 2007 a low pressure system passed with an associated cold front the alps from west. Figure 5.11 shows a comparison of the 12Z vertical profiles. The tur_len run shows indeed the best consistency with the radiosonde profile. It only exhibits a small inversion at 840 hPa not measured by the radiosonde.

With regard to BRN the "θ_v-at first model level" 3D run (Figure 5.12) shows the best agreement with the radiosonde. The tur_len-run gives a more accurate PBL-height but due to an underestimation of wind speed at 860 hPa a too large BRN in this level.

In order to analyze the effect of the varied turbulence parameterization schemes on convective precipitation I compared the total precipitation amounts of the three model

[5]CAPE calculated with the parcel method is an upper bound of the available potential energy because it does not account for the reaction of the environment on the parcel displacement (Emanuel 1994).

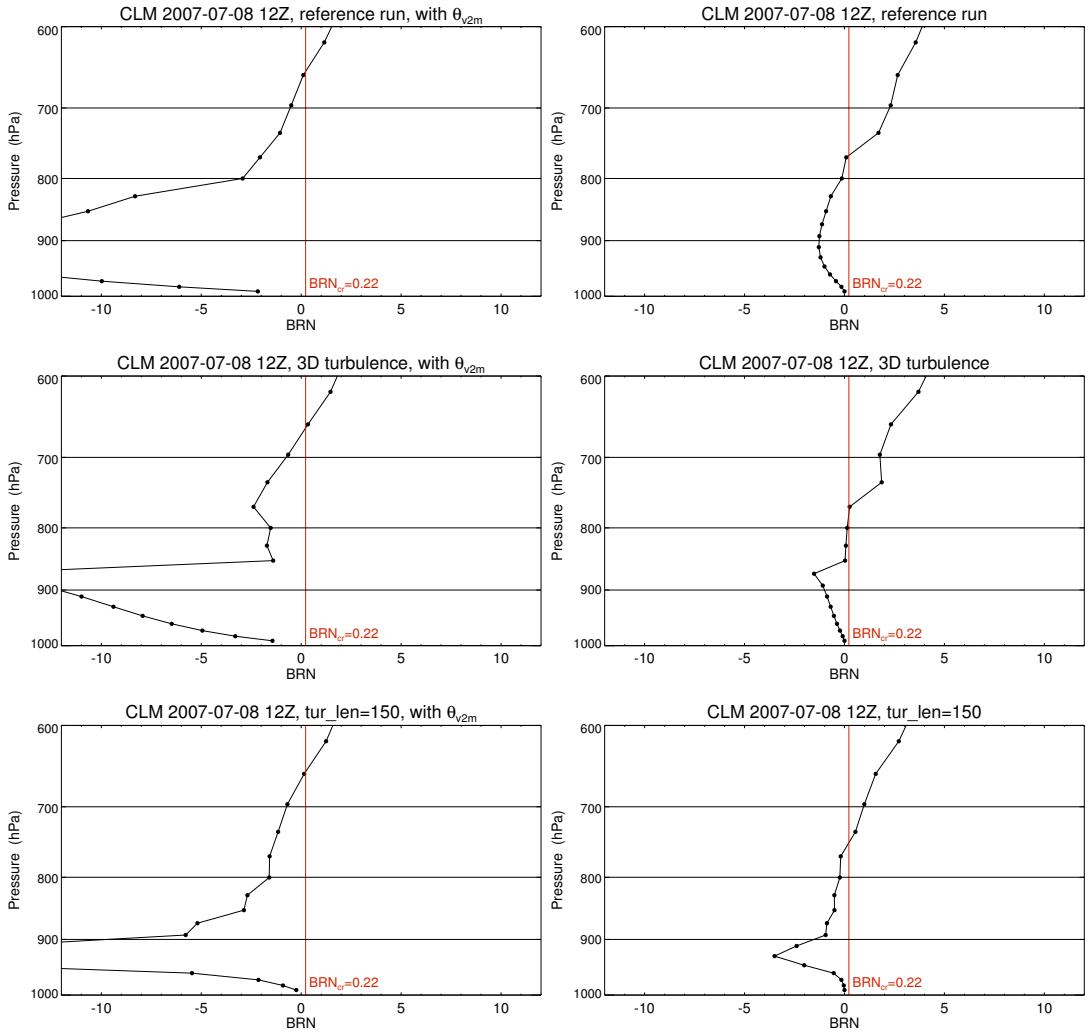

Figure 5.10: Comparison of simulated Bulk Richardson Numbers calculated with $\theta_{v2\mathrm{m}}$ (left) and θ_v (right) at the lowest model level for July 8, 2007 at 12Z.

runs to the measured values at the ground station. Koller (2007) found in his thesis that a reduction of the asymptotic turbulence length tends to result in an overestimation of convective precipitation and too early triggering of convection. This tendency is reflected in Figure 5.13. The tur_len run gives a larger value than measured and simulates the heavy rain an hour too early. The 3D turbulence run highly overestimates the precipitation amount by producing more than 24 mm instead of the measured 7 mm in the 18th hour. The best agreement with the measurement is in this case given for the reference run.

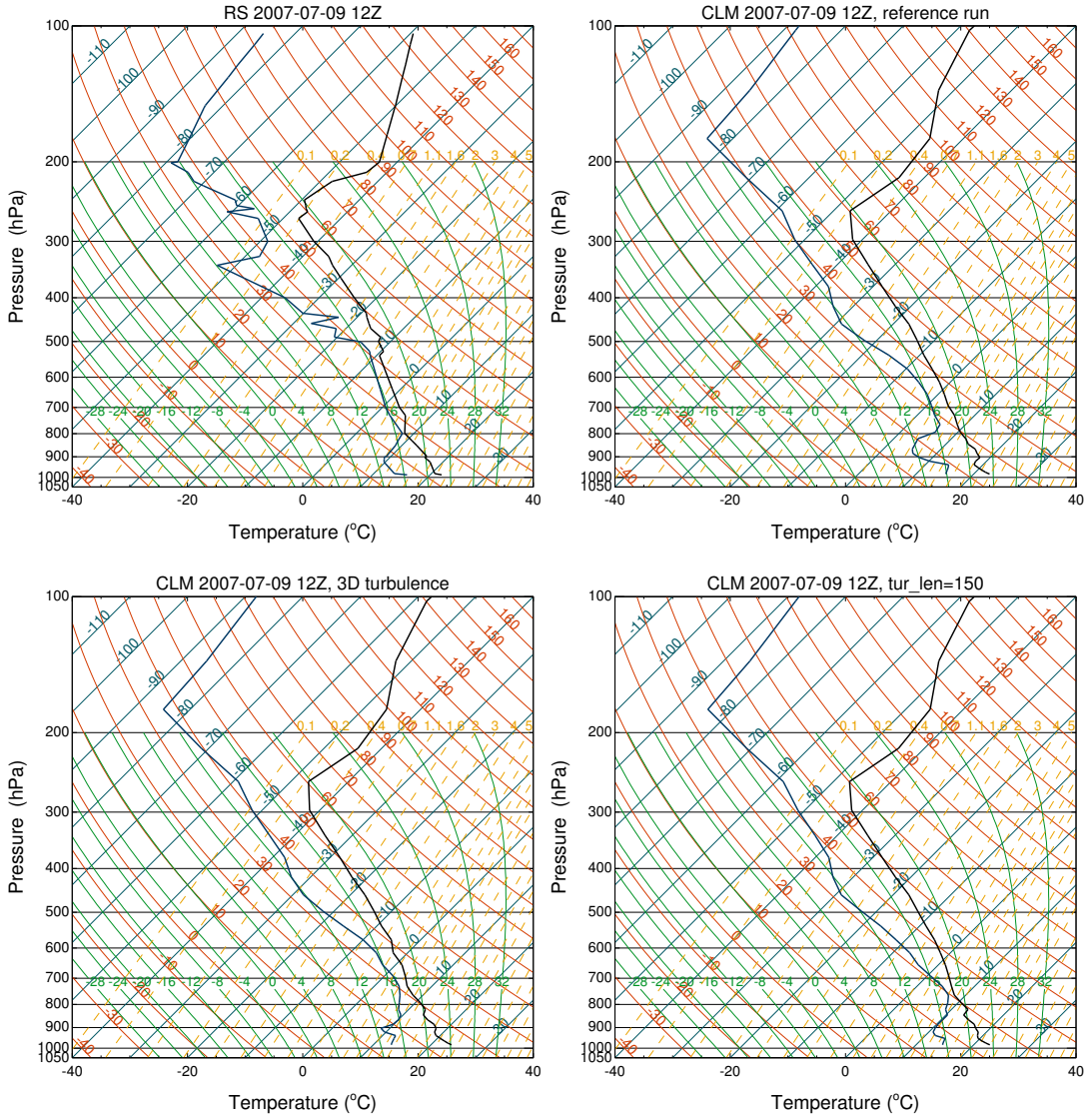

Figure 5.11: Skew-T diagrams of the radiosounding and the corresponding model runs on July 9, 2007 at 12Z.

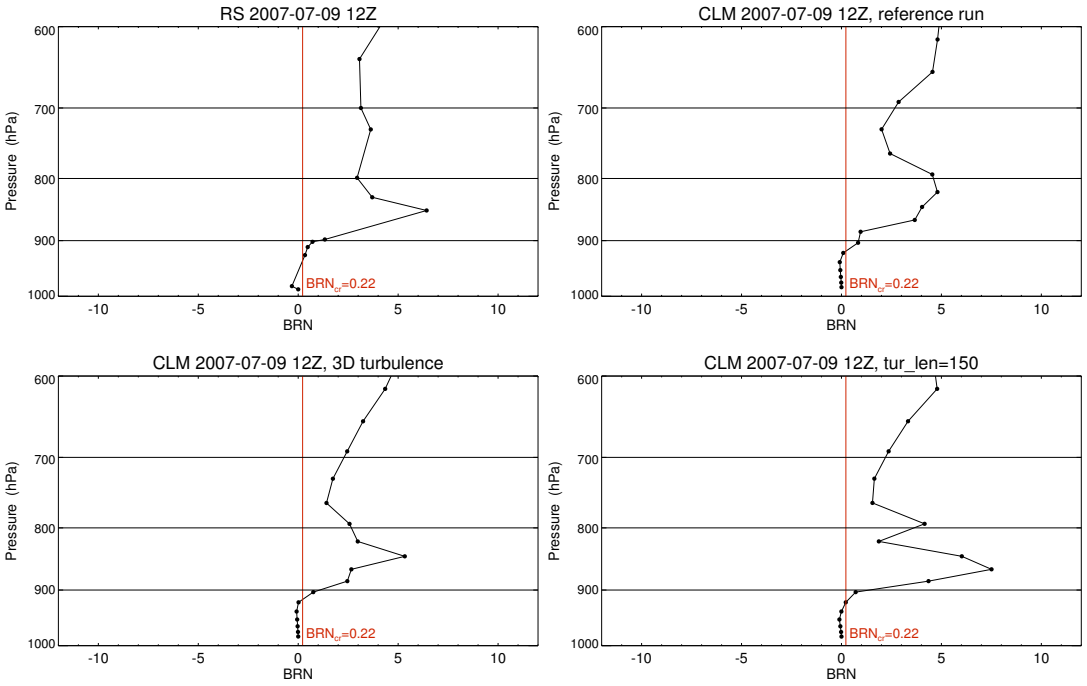

Figure 5.12: Comparison of measured and simulated Bulk Richardson Numbers (calculated with θ_v at the lowest model level) for July 9, 2007 at 12Z.

5.3.3 Test Case 3: January 11, 2008

The 10th and 11th of January in 2008 were characterized by south-western conditions (Figure 5.14). Due to the supply with mild air from south, Foehn established in western Austria. A high-pressure area can be seen over eastern Europe and the winds at the station Vienna Hohe Warte showed mainly a south-eastern direction—a situation which favors high fog or low stratus in Vienna (cf. Lichtenauer 2004). Figure 5.15 shows the fog layer in the lowest 100 hPa for the radiosounding and the corresponding model output. This layer is indicated by the overlap of ELR and DLR. Whereas reaching up to 900 hPa in the sounding, the fog layer shown by the model runs reaches only up to 940 hPa. Furthermore the sounding shows a larger dew point difference above the fog layer. While exhibited too low, the temperature inversion is captured by all of the simulations. A closer look at the wind profiles (Figure 5.16) might give a possible explanation for the underestimation of the fog-layer height. All the simulations show, with differing intensity and level number, a decrease in wind speed in the range of approx. 920 hPa to 840 hPa. As far as the wind direction is concerned, the 3D run gives an unplausable turn of the wind direction of almost 150 degrees from the first to the second level, whereas the other simulations capture the direction more accurately.

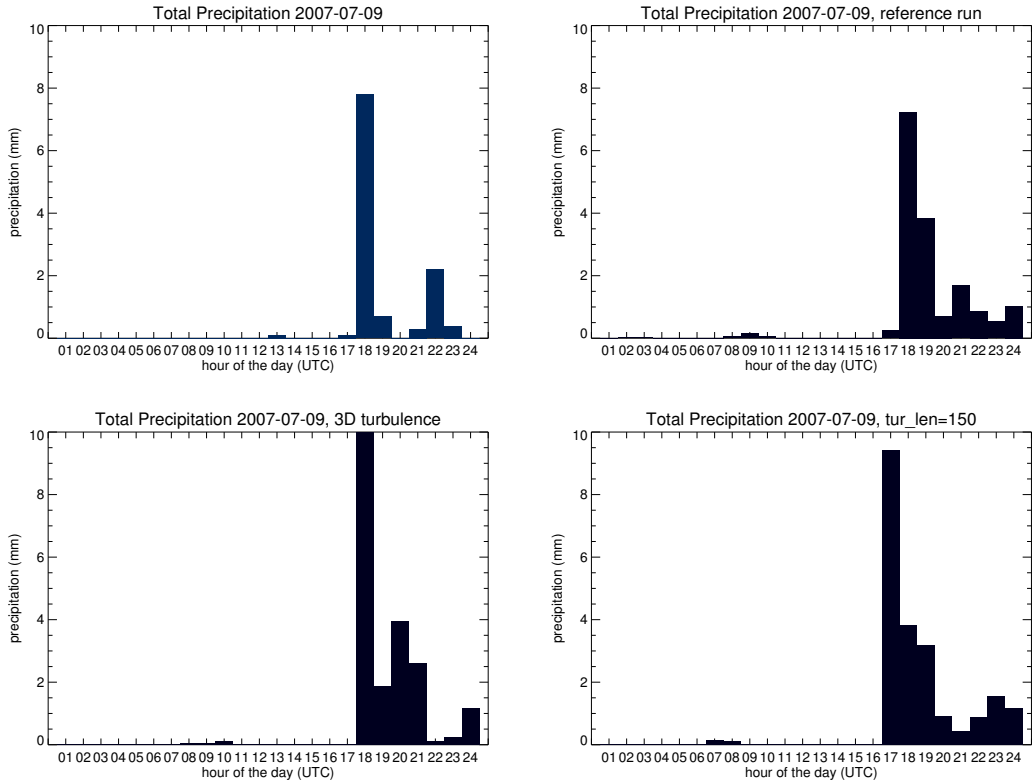

Figure 5.13: Comparison of measured precipitation (climate station) and CLM precipitation amounts for July 9, 2007.

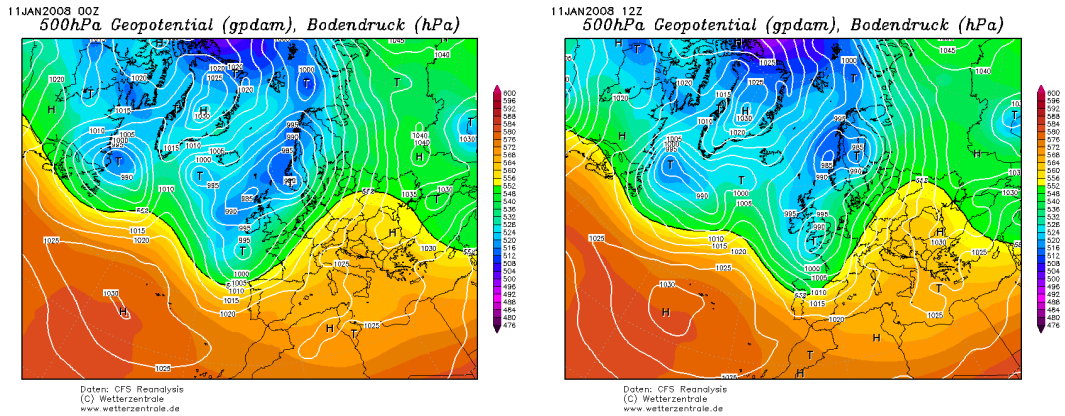

Figure 5.14: Synoptic situation on January 11, 2008 at 00Z and 12Z (www.wetterzentrale.de).

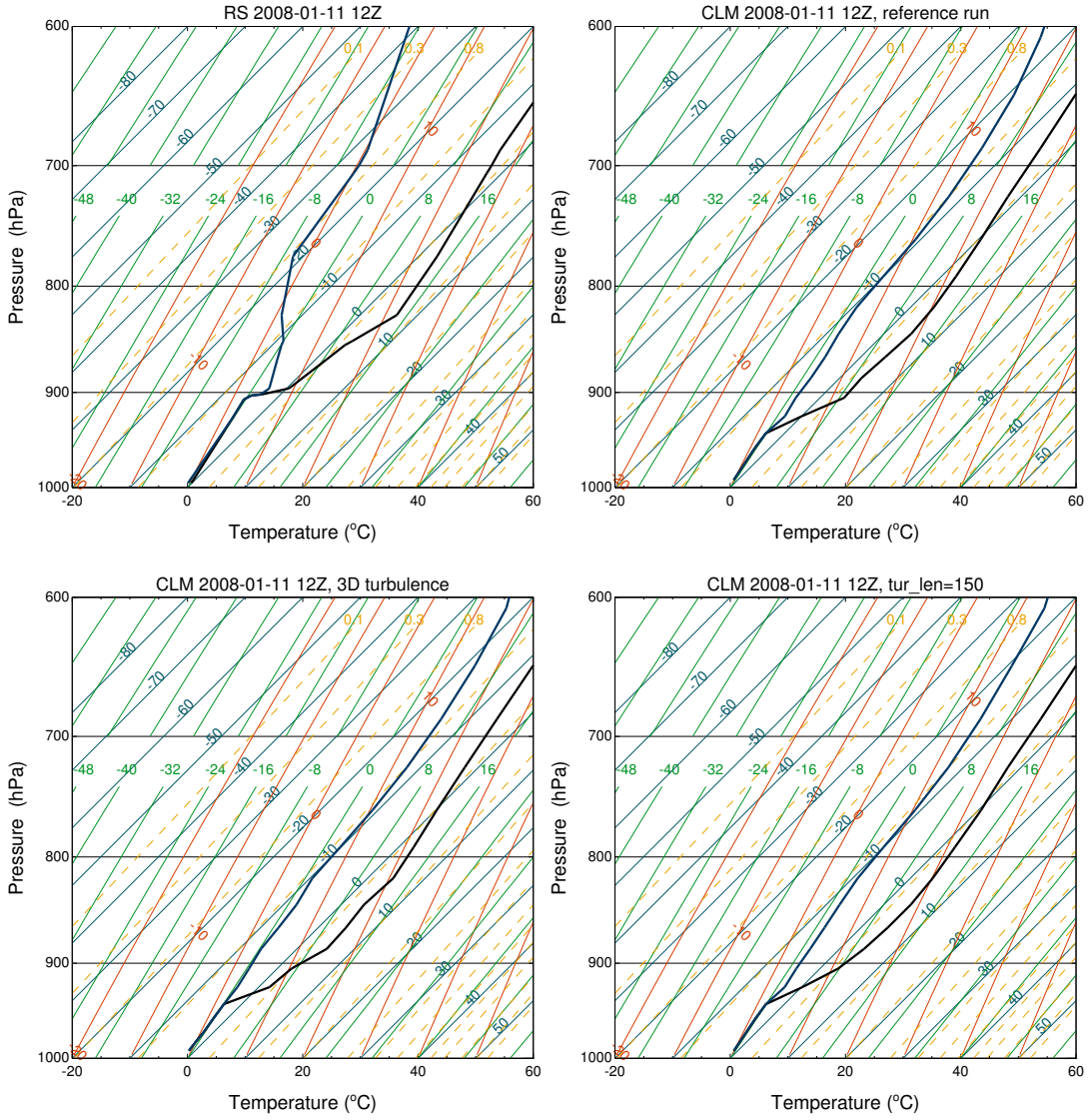

Figure 5.15: Fog layer in a zoomed-in skewed temperature profile for January 11, 2008.

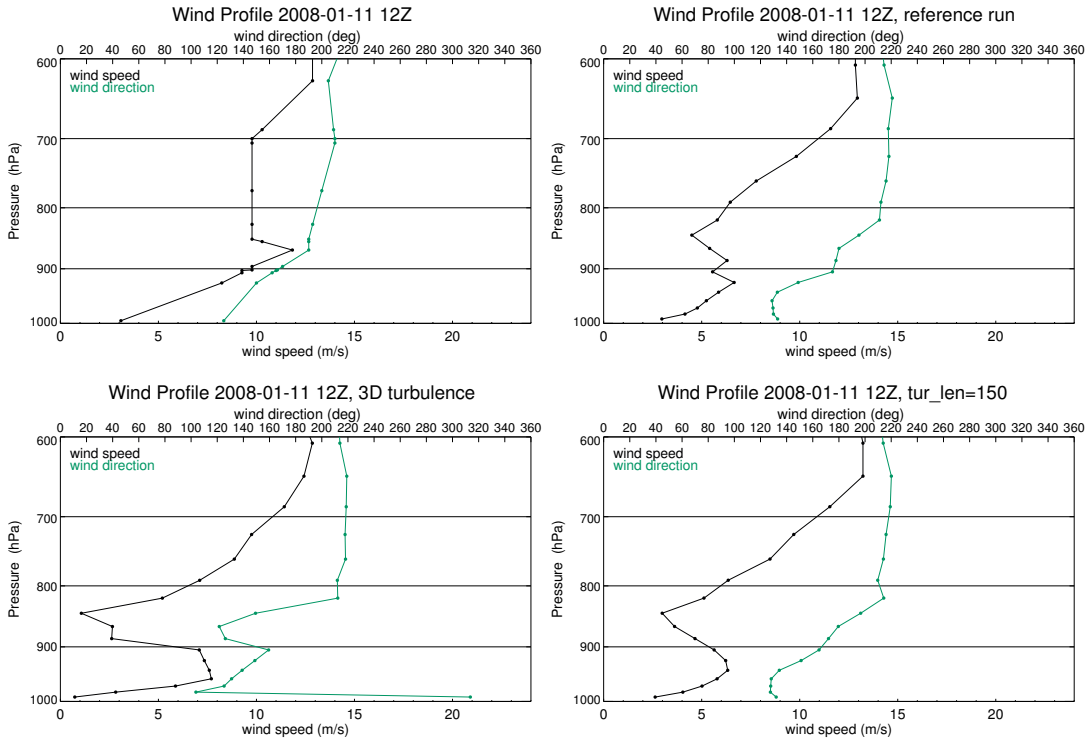

Figure 5.16: Comparison of radiosounding and CLM wind profiles on January 11, 2008 12Z.

6 Discussion and Outlook

After giving an introduction to the Planetary Boundary Layer (PBL), where turbulence is one of the determining processes, this thesis approached the question of "what is turbulence?" on a phenomenological basis. The mathematical concept of Reynolds decomposition was presented, and the attention was directed towards the importance of turbulent fluxes in the PBL. The concept of eddy fluxes gave a first impression of an analogy which should be evoked in a later section—the analogy between eddy fluxes and molecular diffusion. The scales of turbulent motion and the energy cascade, in which Turbulence Kinetic Energy (TKE) is transferred continuously to smaller scales before being converted into heat, were shortly described at the end of this primary chapter on turbulence. After defining the components of the climate system and some of their important interactions, a brief introduction to climate modeling was given. The fundamental equations, describing the temporal evolution of the primary meteorological variables, and the physical concepts behind them were presented. Applying Reynolds averaging to these equations to account for turbulent processes not explicitly resolved, led to unknown variables. By trying to derive these unknown quantities using prognostic equations, more unknowns entered the set of equations. This is the problem of turbulence closure which needs to be approached by parameterization. Several closure techniques were presented in the subsequent sections. The turbulence parameterizations implemented in the Regional Climate Model (RCM) COSMO were then described. The last section of this thesis presented three case studies in which the performance of the varied COSMO-CLM turbulence parameterizations was compared to radiosounding measurements. The results from this section demonstrate the general ability of the model to reproduce the prevailing atmospheric conditions. As far as the temperature and humidity vertical profiles are concerned, all of the simulations deliver a similarly satisfactory performance. Regarding the wind speed profiles the model runs partly exhibit greater deviations from the measurements. The presumption that a reduced asymptotic turbulence length would improve the model performance in the convective case could only be confirmed to small extents in this study. However, as was shown by Koller (2007), the main improvements from a l_∞-reduction did not stem from extensive changes in the atmospheric stratification, but rather from enhanced convection-initiation. Particularly over areas with weak synoptic or orographic forcing the potential for model refinement through the thus altered ratios of parameterized heat fluxes could be shown (Koller 2007). The investigation of such flux profiles could be content of future work. In addition to such analyses consideration could be given to an investigation of the energy

balance at the surface, for example with regard to soil moisture content. Furthermore profiles of TKE for different grid resolutions could be analyzed in order to gain better understanding of the turbulence schemes. It should also be noted, that on July 9, 2007 the low pressure system passing the alps and the associated cold front were the dominating atmospheric conditions. As for example (Baldauf et al. 2011) state, convective events in synoptically driven situations were already satisfactorily simulated by the operational COSMO-Model. Therefore the expectations for an improvement due to the tur_len scheme (Subsection 5.3.2) should probably not be as high as in an airmass convection situation. The simulations of the 3D run did not show more realistic profiles than that of the two other runs. This might be due to the premature implementation of the scheme at the time of the study (NHCM-1). The question about the causes of the 24 mm precipitation (Figure 5.13) remains open. Baldauf (2006) found in a case study that the 3D-turbulence does not seem to alter the total amount of precipitation but could cause a spatial shift of the precipitation areas of 40 km or more. If this explanation applies to the situation of July 9, 2007 could be subject of analysis in future studies. As far as the fog event (Subsection 5.3.3) is concerned all of the simulations displayed fog in the lowest atmospheric layers. Since the vertical extent of a fog layer tends to rise with wind speed, one possible explanation for its underestimation (Figure 5.15) could be the decrease in wind speed in the range of approx. 920 hPa to 840 hPa (Figure 5.16). The formation of fog is a complex process. In addition to considerations regarding the turbulence scheme, surface and radiation processes and the interaction of their parameterization schemes should also be investigated.

Acronyms

A

ABL Atmospheric Boundary Layer [synonym to PBL]. 1, 70

B

BRN Bulk Richardson Number. 50, 52, 54, 57, 58, 60

C

CAPE Convective Available Potential Energy. 50, 52, 55, 58

CCLM COSMO-CLM [short form]. 34, 41–44, 47, 48

CLM Climate Limited-Area Modelling. 41, 47, 49, 52, 54, 55, 57

COSMO Consortium on Small Scale Modelling. 41, 42, 46, 63, 69, 70

COSMO-CLM COSMO model in CLimate Mode. 41, 69

D

DLR Dew Point Lapse Rate. 50, 61

DWD Deutscher Wetterdienst [German Weather Service]. 41, 70

E

ECMWF European Centre for Medium-Range Weather Forecasts. 47

EL Equilibrium Level [the level of neutral buoyancy]. 52

ELR Environmental Lapse Rate. 50, 61

G

GCM General Circulation Model. 19

I

IFS Integrated Forecasting System. 47

L

LES Large Eddy Simulation. 26, 44

LFC Level of free convection. 52

LM Lokal-Modell [operational weather forecast model of the DWD; former name of the COSMO-Model]. 41, 46

N

NHCM-1 Non-Hydrostatic Climate Modelling 1. 47, 48, 63

NWP Numerical Weather Prediction. 48

P

PBL Planetary Boundary Layer [synonym to ABL]. 1, 6, 11, 12, 14, 25, 26, 28, 32, 34, 37, 44, 46, 48, 54, 58, 60, 69

R

RCM Regional Climate Model. 19

S

SODAR SOnic Detection And Ranging [a remote measurement technique]. 9

T

TAWES TeilAutomatisches WetterErfassungsSystem. 57

TKE Turbulence Kinetic Energy. 14, 15, 27, 32–34, 38, 43, 44, 46–48, 63

Z

ZAMG Zentralanstalt für Meteorologie und Geodynamik [Austrian Weather Service]. 54

Bibliography

Ament, F. (2006). "Energy and moisture exchange processes over heterogeneous land-surfaces in a weather prediction model." Master Thesis. Universität Bonn: Mathematisch Naturwissenschaftlichen Fakultät (cit. on pp. 46, 47).

Arya, S. P. (2001). *Introduction to Micrometeorology*. San Diego, CA: Academic Press, p. 420 (cit. on pp. 2, 5, 7, 15, 18, 36).

Baldauf, M. (2006). *Implementation of the 3D-Turbulence Metric Terms in LMK*. COSMO Newsletter No.6. Consortium for Small-Scale Modelling, p. 7 (cit. on p. 72).

Baldauf, M., A. Seifert, J. Förstner, D. Majewski, M. Raschendorfer, and T. Reinhardt (2011). "Operational Convective-Scale Numerical Weather Prediction with the COSMO Model: Description and Sensitivities." In: *Monthly Weather Review* 139, pp. 3887–3905. DOI: 10.1175/MWR-D-10-05013.1 (cit. on pp. 44, 46, 47, 63, 72).

Bechtold, P., M. Köhler, T. Jung, F. Doblas-Reyes, M. Leutbecher, M. J. Rodwell, F. Vitart, and G. Balsamo (2008). "Advances in simulating atmospheric variability with the ECMWF model: From synoptic to decadal time-scales." In: *Quarterly Journal of the Royal Meteorological Society* 134 (634), 1337–1351. DOI: 10.1002/qj.289 (cit. on p. 49).

Blackadar, A. K. (1962). "The Vertical Distribution of Wind and Turbulent Exchange in a Neutral Atmosphere." In: *Journal of Geophysical Research* 67, 3095–3102 (cit. on p. 44).

Brunner, D. (2004). *Basic IDL routines for atmospheric science applications*. URL: http://www.iac.ethz.ch/staff/dominik/idltools/idl_atmosphys.html (visited on 09/17/2012) (cit. on p. 52).

Davidson, P. A. (2004). *Turbulence: An Introduction for Scientists and Engineers*. Oxford: Oxford University Press, p. 657 (cit. on pp. 5, 7).

Davidson, P. A., Y. Kaneda, K. Moffatt, and K. R.Sreenivasan (2011). *A Voyage Through Turbulence*. Cambridge: Cambridge University Press, p. 434 (cit. on p. 5).

Derka, H. (2007). *Witterungsverlauf*. URL: http://www.zamg.ac.at/fix/klima/wetterlagen07-07.pdf (visited on 03/05/2013) (cit. on p. 56).

Doms, G., ed. (2011). *A Description of the Nonhydrostatic Regional COSMO-Model, Part I: Dynamics and Numerics*. Consortium for Small-Scale Modelling. URL: http://www.cosmo-model.org/content/model/documentation/core/default.htm (cit. on pp. 41, 42).

Doms, G., J. Förstner, H.-J. H. E. Heise, D. Mironov, M. Raschendorfer, T. Reinhardt, B. Ritter, R. Schrodin, J.-P. Schulz, and G. Vogel, eds. (2011). *A Description of the Nonhydrostatic Regional COSMO-Model, Part II: Physical Parameterization*. Consortium for Small-Scale Modelling. URL: http://www.cosmo-model.org/content/model/documentation/core/default.htm (cit. on pp. 41, 43–45).

Emanuel, K. A. (1994). *Atmospheric Convection*. Oxford: Oxford University Press, p. 580 (cit. on p. 63).

Encyclopaedia Britannica (2007). *Earth's atmosphere*. URL: http://media-3.web.britannica.com/eb-media/56/97256-004-E3540AD9.jpg (visited on 03/17/2013) (cit. on p. 2).

Garratt, J. R. (1992). *The Atmospheric Boundary Layer*. Cambridge: Cambridge University Press, p. 316 (cit. on p. 1).

Geerts, B. (2011). *Lecture Notes: ATSC 3032, Weather Analysis and Forecasting*. URL: http://www-das.uwyo.edu/~geerts/bart/ (visited on 02/07/2013) (cit. on pp. 51–53).

Giorgi, F. and L. O. Mearns (1999). "Introduction to special section: Regional Climate Modeling Revisited." In: *Journal of Geophysical Research* 104, 6335–6352. DOI: 10.1029/98JD02072 (cit. on p. 21).

Glickman, T. S., ed. (2012). *Glossary of Meteorology*. URL: http://glossary.ametsoc.org/wiki/ (visited on 03/05/2013) (cit. on pp. 12, 15, 25, 38, 55).

Hansen, F. (1966). *The Richardson Number in the Planetary Boundary Layer*. Report. New Mexico: Atmospheric Sciences Laboratory, p. 33 (cit. on p. 55).

Herzog, H.-J., U. Schubert, G. Vogel, A. Fiedler, and R. Kirchner (2002). *LLM—the High−Resolving Nonhydrostatic Simulation Model in the DWD—Project LITFASS Part I: Modelling Technique and Simulation Method*. Technical Report No.4. Consortium for Small-Scale Modelling, p. 70 (cit. on p. 45).

Hillebrandt, W. and F. Kupka, eds. (2009). *Interdisciplinary Aspects of Turbulence*. Lecture Notes in Physics. Heidelberg: Springer, p. 344 (cit. on p. 5).

Holtslag, A. A. M. and C. H. Moeng (1991). "Eddy Diffusivity and Countergradient Transport in the Convective Atmospheric Boundary Layer." In: *Journal of the Atmospheric Sciences* 48, 1690–1698 (cit. on p. 38).

Jacobson, M. Z. (1999). *Fundamentals of atmospheric modeling*. Cambridge: Cambridge University Press, p. 656 (cit. on pp. 8, 22, 24, 25, 53–55).

Kain, J. S. (2003). "The Kain-Fritsch convection parameterization: an update." In: *J. Appl. Meteor.* 43, pp. 170–181 (cit. on p. 50).

Kain, J. S. and J. M. Fritsch (1993). "Convective parameterization for mesoscale models: the Kain-Fritsch scheme." In: *Meteorol. Monogr.* 24, pp. 165–170 (cit. on p. 50).

Koller, M. (2007). "Die Rolle von numerischen Verfahren und Parametrisierungen in atmosphärischen Simulationen mit expliziter Konvektion." Master Thesis. ETH Zürich: Rechnergestützte Wissenschaften (cit. on pp. 44, 46, 47, 63, 64, 71).

Kolmogorov, A. N. (1941a). "Dissipation of energy in isotropic turbulence." In: *Dokl. Akad. Nauk. SSSR* 32, pp. 19–21 (cit. on p. 16).

– (1941b). "The local structure of turbulence in incompressible viscous fluids at very large Reynolds numbers." In: *Dokl. Akad. Nauk. SSSR* 30, pp. 299–303 (cit. on p. 16).

Kraus, H. (2008). *Grundlagen der Grenzschicht-Meteorologie*. Berlin Heidelberg: Springer, p. 214 (cit. on p. 21).

Lee, D. R., R. B.Stull, and W. S. Irvine (1984). *Clear Air Turbulence Forecasting Techniques*. Technical note. Air Force Global Weather Central, Offutt AFB, NE 68113 (cit. on p. 55).

Lee, G. (1996). *Lecture Notes: Air Quality Meteorology, The Planetary Boundary Layer*. URL: http://san.hufs.ac.kr/~gwlee/session7/whatis.html (visited on 02/20/2013) (cit. on p. 2).

Leuenberger, D., M. Stoll, and A. Roches (2010). *Description of some convective indices implemented in the COSMO model*. Technical Report No.17. Consortium for Small-Scale Modelling, p. 18 (cit. on pp. 53–55).

Lichtenauer, S. (2004). "Ortsbezogene Hochnebelvorhersage mit Hilfe eines Limited Area Modells." Master Thesis. Universität Wien: Fakultät für Naturwissenschaften und Mathematik (cit. on p. 66).

Machulskaya, E. and D. Mironov (2013). "A TKE-Scalar Variance Mixing Scheme for COSMO." Presentation at the COSMO User Seminar March 5, 2013 (cit. on pp. 45, 46).

Mathieu, J. and J. Scott (2000). *An Introduction to Turbulent Flow*. Cambridge: Cambridge University Press, p. 375 (cit. on p. 16).

McDonough, J. M. (2007). *Lecture Notes: Introductory Lectures on Turbulence*. URL: http://www.engr.uky.edu/~acfd/lctr-notes634.pdf (visited on 05/03/2012) (cit. on p. 9).

Mellor, G. L. and T. Yamada (1982). "Developent of a Turbulence Closure Model for Geophysical Fluid Problems." In: *Rev. Geophys. Space Phys.* 20, pp. 851–875 (cit. on pp. 43, 44, 46).

MetEd (2006a). *CAPE*. URL: http://www.meted.ucar.edu/mesoprim/cape/print.htm (visited on 02/07/2013) (cit. on p. 54).

– (2006b). *Skew-T Mastery*. URL: http://www.meted.ucar.edu/mesoprim/skewt/ (visited on 02/07/2013) (cit. on p. 51).

Hillebrandt, W. and F. Kupka, eds. (2010). *Lecture Notes in Physics 756. Interdisciplinary Aspects of Turbulence*. Springer (cit. on p. 46).

Mironov, D. and M. Raschendorfer (2010). *COSMO Science Plan 2010–2014, Physics: Parameterisation of turbulence and of PBL processes*. Consortium for Small-Scale Modelling, p. 6 (cit. on p. 46).

Pielke Sr., R. A. (2002). *Mesoscale Meteorological Modeling*. San Diego, CA: Academic Press, p. 676 (cit. on pp. 22, 23, 25, 27).

Pope, S. B. (2000). *Turbulent Flows*. Cambridge: Cambridge University Press, p. 806 (cit. on pp. 16, 18).

Prandtl, L. (1925). "Bericht über Untersuchungen zur ausgebildeten Turbulenz." In: *Zeitschrift für angewandte Mathematik und Mechanik* 5 (cit. on p. 36).

Priestley, C. H. (1957). "Convection from the Earth's surface." In: *Proceedings of the Royal Society of London* 238, pp. 287–304 (cit. on p. 55).

Randall, D. (2009). *Reynolds Averaging*. URL: http://kiwi.atmos.colostate.edu/group/dave/pdf/Reynolds_Averaging.pdf (visited on 02/25/2013) (cit. on p. 10).

Richardson, L. F. (1922). *Weather Prediction by Numerical Process*. London: Cambridge University Press, p. 236 (cit. on p. 15).

Rockel, B., A. Will, and A. Hense (2008). "The Regional Climate Model COSMO-CLM (CCLM)." In: *Meteorologische Zeitschrift* 17, pp. 347–348 (cit. on p. 41).

Françoise, J. P., G. L. Naber, and T. S. Tsun, eds. (2006). *Encyclopedia of Mathematical Physics. Turbulence Theories*. Elsevier (cit. on p. 16).

Rotach, M. and J. Schmidli (2011). *Lecture Notes: Boundary Layer Meteorology and Air Pollution Modeling*. URL: http://www.iac.ethz.ch/edu/courses/master/modules/boundary_layer_meteorology (visited on 03/20/2012) (cit. on pp. 6, 7, 11–14, 21).

Roth, M. (1991). "Turbulent transfer characteristics over a suburban surface." PhD Thesis. University of British Columbia: Department of Geography (cit. on p. 9).

Rummukainen, M. (2010). "State-of-the-art with regional climate models." In: *Wiley Interdisciplinary Reviews: Climate Change* 1, pp. 82–96. DOI: 10.1002/wcc.8 (cit. on p. 20).

Seibert, P., F. Beyrich, S. E. Gryning, S. Joffre, A. Rasmussen, and P. Tercier (2000). "Review and intercomparison of operational methods for the determination of the mixing height." In: *Atmospheric Environment* 34, pp. 1001–1027. DOI: 10.1016/S1352-2310(99)00349-0 (cit. on p. 58).

Somerville, R., H. Le Treut, U. Cubasch, Y. Ding, C. Mauritzen, A. Mokssit, T. Peterson, and M. Prather (2007). "Historical Overview of Climate Change Science." In: *Climate Change 2007: The Physical Science Basis*. Ed. by S. Solomon et al. Cambridge, UK and New York, NY, USA: Cambridge Univ Press, pp. 93–127 (cit. on p. 20).

Sommeria, G. and J. W. Deardorff (1977). "Subgrid-Scale Condensation in Models of Nonprecipitating Clouds." In: *Journal of the Atmospheric Sciences* 34, pp. 344–355 (cit. on p. 44).

Sørensen, J. H., A. Rasmussen, and H. Svensmark (1996). "Forecast of Atmospheric Boundary-Layer Height Utilised for ETEX Real-Time Dispersion Modelling." In: *Phys. Chem. Earth* 21.5-6, pp. 435–439. DOI: 10.1016/S0079-1946(97)81138-X (cit. on pp. 55, 58).

Steinacker, R. (2000). *Eine ostalpine Strömungslagenklassifikation*. Interner Bericht. Universität Wien: Institut für Meteorologie und Geophysik, p. 8 (cit. on p. 56).

Stensrud, D. J. (2007). *Parameterization Schemes: Keys to Understanding Numerical Weather Prediction Models*. Cambridge: Cambridge University Press, p. 459 (cit. on pp. 36, 38).

Stull, R. B. (1984). "Transilient Turbulence Theory. Part I: The Concept of Eddy-Mixing across Finite Distances." In: *Journal of the Atmospheric Sciences* 41.10, pp. 3351–3367 (cit. on pp. 38, 39).

– (1988). *An Introduction to Boundary Layer Meteorology*. Dordrecht Boston London: Kluwer Academic Publishers, p. 666 (cit. on pp. 1–3, 10–13, 22–25, 27, 30, 32–35, 37–39, 55).

– (1991). "Static Stability—An Update." In: *Bulletin of the American Meteorological Society* 72.10, pp. 1521–1529 (cit. on p. 53).

– (1993). "Review of non-local mixing in turbulent atmospheres: Transilient turbulence theory." In: *Bound.-Lay. Meteorol.* 62, pp. 21–96 (cit. on p. 38).

Suklitsch, M., H. Truhetz, A. Prein, and A. Gobiet (2011). *NHCM-1: Non-Hydrostatic Climate Modelling Part II, Current state of selected cloud-resolving regional climate models and their error characteristics*. Scientific Report. University of Graz, Austria: Wegener Center for Climate and Global Change, p. 115 (cit. on pp. 20, 46, 49, 51).

Tennekes, H. and J. L. Lumley (1972). *A First Course in Turbulence*. Cambridge, Massachusetts, and London, England: The MIT Press, p. 300 (cit. on pp. 5, 7, 17, 37).

Wagner, A., S. Altherr, B. Eckert, and H. J. Jodl (2002). *Multimedia in Physics Education: A video for the quantitative analysis of the Reynolds number*. URL: http://pen-physik.de/medien/MM_Videos/index.html?/medien/MM_Videos/reynolds/reynolds.html (visited on 04/15/2012) (cit. on p. 6).

Wallace, J. M. and P. V. Hobbs (2006). *Atmospheric Science: An Introductory Survey*. Burlington: Academic Press, Elsevier, p. 504 (cit. on pp. 8, 53).

Ware, M. O. C. (2002). *Lecture Notes: Transport Processes in the Environment, Fall 2002*. URL: http://dspace.mit.edu/bitstream/handle/1721.1/37147/1-061Fall-2002/OcwWeb/Civil-and-Environmental-Engineering/1-061Transport-Processes-in-the-EnvironmentFall2002/LectureNotes/detail/7-lec.htm (visited on 04/15/2012) (cit. on p. 6).

Warner, T. T. (2011). *Numerical weather and climate prediction*. Cambridge: Cambridge University Press, p. 526 (cit. on pp. 34, 38).

Weisstein, E. (1996–2007). *Wolfram Research. Eric Weisstein's world of biography: Werner Heisenberg*. URL: http://scienceworld.wolfram.com/biography/Heisenberg.html (visited on 02/24/2013) (cit. on p. 5).

Wyngaard, J. C. (2010). *Turbulence in the Atmosphere*. Cambridge: Cambridge University Press, p. 393 (cit. on p. 5).

Abstract:
The planetary boundary layer (PBL) sets the stage to various weather phenomena and its evolution is closely related to severe weather events. Accurate forecasts and climate projections of the PBL are therefore of great interest. As turbulence is the dominant mechanism of the PBL, its representation presents a crucial task in climate modeling. Particularly regarding smaller-scale atmospheric processes, turbulence parameterization is of increasing importance and its accurate implementation raises expectations of improved model performance.

After giving an introduction to the PBL, this thesis approaches the question of "what is turbulence?" on a phenomenological basis. Mathematical treatment of turbulence is discussed and the fundamental equations of climate models, describing the temporal evolution of meteorological variables, are presented. Applying Reynolds averaging to these equations to account for turbulent processes not explicitly resolved leads to unknown variables. The appearance of these unknown quantities is known as turbulence closure problem which needs to be approached by parameterization. This thesis presents several closure techniques and describes turbulence parameterization schemes implemented in the COSMO climate model. To evaluate the performance of these schemes at 3 km horizontal resolution with respect to their ability to represent the vertical structure of the PBL, simulations are compared to radiosounding measurements. Two typical meteorological conditions—a gentle pressure gradient situation in July 2007 and a fog/stratus situation in January 2008—serve as case studies. The results indicate the ability of the model to generally capture the PBL conditions. Whereas the fog layer height is underestimated in the analyzed model setups, improvements from a decreased asymptotic turbulence length in the convective situation, as suggested by other studies, are to some extent confirmed in this work.

Zum Inhalt:
Die planetare Grenzschicht (PGS) bildet die Voraussetzung für verschiedenste Wetterphänomene und Unwetterereignisse sind eng an ihre Entwicklung im Tagesgang gekoppelt. Präzise Voraussagen und Klimaprojektionen der PGS sind daher von großer Bedeutung. Die Abbildung von Turbulenz als dominanter Prozess der PGS stellt eine wichtige Aufgabe in der Klimamodellierung dar. Besonders kleinskalige atmosphärische Prozesse betreffend, gewinnt Turbulenzparametrisierung an Bedeutung. Ihre angemessene Implementierung in Modellen verspricht verbesserte Klimasimulationen.

Nach einer Einführung in die PGS nähert sich diese Diplomarbeit der Frage "Was ist Turbulenz?" zunächst phänomenologisch. Möglichkeiten zur mathematischen Beschreibung von Turbulenz werden erläutert und die fundamentalen Gleichungen, welche die zeitliche Entwicklung von meteorologischen Größen in Klimamodellen beschreiben, werden präsentiert. Die Anwendung der Reynoldsmittelung, die dazu dient auch nicht explizit aufgelöste turbulente Prozesse zu berücksichtigen, führt zum Auftreten unbekannter Terme in den Grundgleichungen. Das Auftauchen unbekannter Größen ist als Turbulenzschließungsproblem bekannt und erfordert Parametrisierungsansätze. In dieser Arbeit werden einige solcher Schließungsansätze vorgestellt und die Implementierung der Turbulenzparametrisierung im regionalen Klimamodell COSMO präsentiert. Um die Leistung der verschiedenen Parametrisierungen zu analysieren, werden Modellsimulationen mit Radiosondenmessungen verglichen. Dabei dienen eine gradientschwache Wetterlage im Juli 2007 und eine Nebelsituation im Januar 2008 als Fallbeispiele. Die Ergebnisse zeigen, dass das Modell in der Lage ist, die vorherrschenden Zustände in der PGS zu erfassen. Während die Höhe der Nebelschicht in den analysierten Modellkonfigurationen unterschätzt wird, bestätigt die vorliegende Arbeit nur in gewissem Ausmaß die in anderen Studien erzielte Verbesserung durch Reduzierung der asymptotischen Turbulenzlänge.

Wegener Center for Climate and Global Change
University of Graz
Brandhofgasse 5
A-8010 Graz, Austria
www.wegcenter.at
ISBN 978-3-9503112-9-7